A NOVEL ENGINE HEAD DESIGN USING A ROTARY VALVE SYSTEM IN TRADITIONAL FOUR-STROKE INTERNAL COMBUSTION ENGINES

A thesis presented to the faculty of the Graduate School of Western Carolina University in partial fulfillment of the requirements for the degree of Master of Science in Technology

By

Erik Paul Myers

Director: Dr. Paul Yanik
Associate Professor and Graduate Program Director
School of Engineering and Technology

Advisor: Dr. Tony Rizk

Committee Members:
Dr. Martin Tanaka, School of Engineering and Technology
Dr. Yusef Fahmy, School of Engineering and Technology
Dr. Hayri Sezer, School of Engineering and Technology

Acknowledgments

I would like to acknowledge the part that God has played in my life and the blessing that it has been to be able to pursue higher education in research. I extend a special thanks to Dr. Tony Rizk, whose support in my ambitions helped me realize what I could accomplish through this thesis. I would also like to thank Dr. Tanaka, Dr. Fahmy, and Dr. Sezer, who's presence on my thesis committee gave me the confidence and support to make this possible.

My family and friends have played a major role in giving me constant support and encouragement during this time. I would like to thank my parents, and my sister and brother-in-law, and all those close to me for everything that they have done for me in life. I would also like to personally thank all of those in the graduate program with me, whose friendship made the impossible possible.

Finally, I would like to give thanks to Western Carolina and the opportunity that was provided for me here to excel in my research.

TABLE OF CONTENTS

LIST OF TABLES

LIST OF FIGURES

LIST OF EQUATIONS

ABSTRACT

A NOVEL ENGINE HEAD DESIGN USING A ROTARY VALVE SYSTEM IN TRADITIONAL FOUR-STROKE INTERNAL COMBUSTION ENGINES

Erik Paul Myers, M.S.T.

Western Carolina University (May 2019)

Director: Dr. Paul Yanik

Internal combustion engines are an integral part of society today. Their efficient operation and function are paramount to their design. By improving the function of the engine, it may be possible to increase the potential available power output to the flywheel. By redesigning the engine head and replacing the traditional poppet valve system with a novel rotary valve system, the incoming fuel and air mixture can more easily flow into the cylinder. In turn, this will increase the amount of fuel and air present during combustion, and more evenly distribute the pressure of the fluid throughout the cylinder. The resulting combustion process will then burn more consistently and produce more power at the piston face. It was found that not only does the rotor valve system increase the available pressure at the piston face, but also the internal energy in the working fluid during combustion. The rotor valve system also alleviated flow restriction issues during the intake and exhaust stroke.

CHAPTER ONE: INTRODUCTION

1.1 Internal Combustion Engine Design

The internal combustion engine must be engineered to withstand problems such as system overheating and timing lag. To improve engine performance, additions are continually added to the engine until it becomes a complicated assembly, which can place undue stress on the system. A prime example of this is the poppet valve intake/exhaust system. This system has undergone many changes through the years, including variable valve timing, variable lift, and numerous cluttering additions that can have both a positive and negative effect on performance, all depending on how these valve trains are implemented.

1.2 Improvements Made

While most changes to the traditional poppet valve assembly have helped improve combustion efficiency, a system can easily become overly complicated if care is not exercised in its design. For example, Honda's patented V-TEC system allows for variable timing using an eccentric camshaft. While this can help performance and efficiency, the fragile composure of the camshaft components can prohibit use with high compression applications, and a higher-octane fuel must be used to prevent function loss from exhaust deposits. Similar modifications have been made through the years, and yet many designs focus more on small component redesign. A large inhibiting part of the valve train could be improved or replaced if dissected appropriately – the poppet valves.

1.3 The Poppet Valve

The poppet valve is an essential part of any traditional engine head design. The valve serves as the operating component which seals/unseals the cylinder at appropriate times to certain strokes during the cycle. As basic as the valve design is – Close in geometry to a flat mushroom or plunger– it can create certain flow inhibitions that are inherent from its function.

The protruding geometry of the valve head means that even with the valve in the fully open/closed position, gas must first flow around the head before moving down the appropriate channel. This causes erratic turbulent mixing and can lead to stagnant fluid flow around the edge of the valve head. Additionally, the valve's movement profile involves velocity reversal, leading to long periods of slow operating velocities for the valve, even at high RPMs. This can eventually lead to a phenomenon known as valve lag and can be a hard to address issue for performance engineers.

1.4 Design and Function of Poppet Valve systems

The design of poppet valve systems involves three basic assemblies. Firstly, the poppet valve creates separation between external channels and cylinders of the engine block. The head itself contains the channels and mounts for both the camshaft and valves. Finally, the camshaft creates the necessary timing and movement of the poppet valves. In this sense, the valvetrain serves one major purpose – Manage engine exhaust and intake. This system, while functional, can be redesigned to perform the same task without loss to complexities.

1.5 Rotor Valve Design

The Rotor Valve System (RVS) is designed to perform the exact same task of the traditional poppet valve system. The Rotor Valve does the same thing that a poppet valve does. It manages the intake and exhaust strokes, and seals off the engine during compression and combustion. The RVS has two main components: Spinning disks (rotors) and a head that holds the rotors. Each cylinder has one rotor overhead.

The basic geometric design of the rotor is a flat, rotating disk with a single port. During engine operation, this rotor rotates over a cylinder head, and the port aligns with either the intake or exhaust channel at the appropriate time. While both the poppet valve and rotor do the same thing, the rotor is different in that there is no obstruction to flow when the rotor is open.

These rotors can be rotated above the cylinder side-by-side using mating teeth on the outsides of the rotor faces. In this fashion, the rotors are driven without the assistance of a camshaft. Their moment of inertia can be increased without affecting the motion of the system, allowing for an even larger port to be cut out, increasing airflow. Laying the rotors on their side also allow for an incredibly low-profile head, decreasing overall engine size.

1.6 Areas of improvement in the Rotor Valve Design

While the Rotor Valve System (RVS) allows for many potential areas of design improvements, there are still characteristics that can inhibit system function, and will need to be addressed during design to keep the application practical. The rotor valve faces a challenge which traditional poppet valves do not; high pressure and temperature are exerted on the rotor valve face during rotation in the combustion stroke. Normal valve systems are static during the combustion stroke, held firmly against the valve seat while combustion occurs. The rotor valve

system must be able to resist significant flexion while rotating. This suggests that the rotor valve must be made from a high tensile strength material.

The rotor valve system is also affected by a problem with friction forces acting on the rotor valve face. The rotor faces must be kept lubricated during rotation, without allowing oil into the system otherwise. This leads to a design which must be structurally robust yet intricate to properly oil the rotor faces.

1.7 Purpose and Potential Gains

The main purpose of the Rotor Valve System is to perform what a traditional valve system does, only more efficiently. By eliminating extra moving components, the system becomes simple to operate, as well as produce. The performance benefits inherent with better flow include increased efficiency, response to throttle opening, and better power output. A lower profile engine will also lead to an increase in potential stroke length and increased torque output.

1.8 Automotive Manufacturing

The automotive manufacturing industry could benefit from RVS technology. The ability to construct a smaller, more durable engine at a lower cost holds the potential to make automobiles more cost effective, as well as performance cars more attractive at a consumer level. This also holds intrinsic value for consumers, as lower manufacturing costs translate to lower purchasing and maintenance costs.

1.9 Performance and Efficiency Evaluation

The fundamental purpose of this thesis is to evaluate the plausibility of the Rotor Valve System. This system will be evaluated to assess if it is not only capable, but also comparable to a traditional valve system., this question will be addressed Using Computational Fluid Dynamics. The flow structure, possible efficiency differences and performance characteristics of the RVS will also be analyzed. In this modeling, fluid/heat transfer features and the Navier-Stokes equations (as well as the k-ε turbulence model) will be used in conjunction with SolidWorks to determine these characteristics. The goal of this research is to show an increase in both power output and improvement of fluid flow capabilities over a traditional system.

CHAPTER TWO: LITERATURE REVIEW AND COMPARISON

The available literature suggests that an integrated cam/port system has been significantly analyzed in a four-stroke system. There are many journal articles that shed light on the advantages and disadvantages of such a system, the feasibility of manufacturing, and the potential outcomes of design implementation. There have also been several renditions of the traditional valvetrain, the most prevalent being solenoid-actuated valves and the elimination of the camshaft altogether.

2.1 Camless Valve Control

The most relevant example of camless valve control is the theoretical DigitalAir™ camless valve system, designed at the University of Bath by Stephen J. Charlton. The DigitalAir™ design features a four-stroke engine head with valves that are mounted horizontally to the cylinders, instead of over-head. This method prevents valve-piston overlap and moves the intake/exhaust openings closer to the cylinder center. The valve stroke has been completely modified to feature 25% of the original valve stroke length, while maintaining an almost identical flow area around the valve seat. The intake/exhaust channels have also been designed to promote flow efficiency and reduce flow resistance when the valves are open, and the traditional camshaft has been replaced with solenoid-controlled electromagnets. (Charlton, et al., Digitalair™ Camless FVVA System – Part 1, Valve Train Design, Capability and Performance., 2017)

As revolutionary as the DigitalAir™ design is, it still fails to address issues related to flow around the valve head, timing delay due to rapid solenoid switching, magneto overheating,

and potential gaps in compression related to valve seating delay. Following suit, most abstracts and journal entries are limited to experiments or designs that replace the camshaft entirely, failing to look at the valves as possibly the largest obstruction to stable fluid intake and timing advancement. In a proceeding of the Joint Fluids Engineering Division in 2014, the design of a piezo-driven micropump was introduced. While this pump does not feature internal combustion, fluid flow through its chambers can still be used to draw references about the behavior of fluid in other designs (Such as internal combustion flow). This design, featuring three alternating fluid chambers, used electrically controlled piezo disks to induce the Coanda effect and prompt flow laterally between two opposed chambers. (He, Yang, Yuan, Zhu, & Zhang, 2014)

The Coanda effect eliminated the need for valves in the micro pump and demonstrated how sensitive fluid flow can be to abrupt changes in geometry, not unlike a valve head interrupting intake/exhaust flow into a combustion cylinder. Removing the valve from the intake port could help reduce the vortices and subsequent boundary layer separation resistance caused by fluid flow around the stagnation point of the valve head and incite easier flow into the entire cylinder before compression. Such a change in flow geometry would be ideal in facilitating high-speed intake and exhaust strokes, potentially increasing the available power band width in traditional engines.

2.2 Swirl Generation and Control

In fact, internal combustion engines are so sensitive to fluid flow parameters that changing the flow characteristics of the fluid can have a significant effect on the performance of combustion. In a 2007 study, various engine inlet angles were experimentally tested to see how the angle of incoming combustion fluid could increase engine performance. Overall, the research

suggested that an increased angle of intake (Twenty degrees or higher) could help the propagation of swirls in the intake stroke, resulting in better mixing of combustion gases and a better lean operation of the engine. This induced swirl formation was achieved using an additional "Swirl Control Value" which varies the geometry of the intake port, giving the gas certain flow characteristics. While this method was effective in increasing engine performance, it adds yet another component to the valve-train to be considered. (Lee, Bae, & Kang, 2007)

A recent paper involving the study of geometry of intake ports acknowledged that, with the proper air-fuel mixture and encouraging port incline, a swirl could easily be generated which could decrease the emission of NO_x exhaust gases by increasing the lean burning efficiency of a four-stroke engine. However, this publication fails to address the interference caused by additional "swirl plates" used to help propagate swirl. It was found that when an additional plate was added around the brim of the intake valve, it could help swirl formation. The flow restriction caused by this addition was not addressed in the publication, and it can be reasonably inferred that the flow area suffered due to this addition. (Xu & Choa, 2016)

Simulations involving swirl generation are backed further by experimental testing, and numerous researches have begun studying the impact of Large Eddy Simulations (LES) in performance. In a thesis presented in 2015, swirl formation was experimentally found to be drastically changed by the geometry of the intake port, specifically swirl homogeneity. This flow change characterizes the implied results from CFD simulations and shows that prescribed geometry can be especially beneficial to flow generation by using the tilt from intake ports to naturally form vortices. (Soder, 2015)

Flow swirl mixing has been found both experimentally and through simulation to be a dominant factor when considering engine efficiency and the formation of combustion gases.

While this is certainly an important research topic, little investigation has been done to study the effect of valve size and displacement on flow characterization, outside of variable valve timing. Extensive research has been performed to show how improvements in efficiency can come from adjusting valve displacement durations through eccentric camshaft profile changes. This research, if coupled with valve interference evaluation, could produce an incredibly effective solution to mixing problems caused by the absence of a flow generation orifice.

2.3 Combination of Valve, Port, and Swirl Design

Many available sources thoroughly consider the effect of timing change during operation on combustion efficiency and power output. Dual overhead cams have been undergoing extensive testing and design iterations to minimize losses caused by static valve timing. This eccentric timing is widely adopted in industry, especially to increase the performance output of smaller four-cylinder inline engines. (Albatlan & Mohamed, 2014) Valve timing itself has also been analyzed, and the effect of increasing the valve overlap and stroke durations has been considered. The trade-off behind lengthening the overlap is an increase in exhaust/intake fume mixtures as well as a destabilized vortex profile. This overlap increase affects the performance of the engine, but again does not address the effect of valve heads in flow interruption. (Lanzanova, Dalla Nora, & Zhao, 2017)

In combination, the effect of swirl generation on valve lifting has also been analyzed. In a past report in the *Experimental Thermal and Fluid Science* Journal, a direct injection diesel engine was set up experimentally to have two heads; one with symmetric intake ports and one with intake ports slanted at approximately 12° towards the cylinder center. (Kang & Reitz, 1999) The results suggested that while a symmetric port setup created more prominent vortices, the

slanted design allowed for increased swirl generation, granted that the valves were still allowed to lift a certain amount to prevent flow restrictions.

2.4 Engine Performance Affected by Engineering

The effects of additional swirl generating orifices, aligned intake ports, and manifold geometry on engine efficiency can be described well by research into acoustic noise reduction. Noise reduction is a close companion to research into fluid flow of an operating cylinder and employs principles to analyze the effect of noise reducing components (Such as a muffler or manifold) on fluid flow within the system. (Davies, 1995) In a 1995 research article, the effects of such imposed sound dampening devices were analyzed and their interference in intake/exhaust were determined.

Overall, the installation of a noise reduction device pulls pressure away from a working fluid, and the result can negatively affect the flow of the fluid to/from the chamber as a pressure drop reduces potential movement energy across a control volume. In a similar fashion, obstructions to flow (Such as an extended valve head) can cause pressure loss, and eventually lead to flow restriction if the culminative losses are not accounted for. The prospect for flow potential to be increased by removing obstructions is straight forward and achievable, given the correct approach and methodology.

Novel approaches to intake and exhaust design showcase the efficiency increase that can be gained by optimizing fluid passage to the cylinder. A recent article in the *Energy Conservation and Management* journal describes a variable plenum (used to optimize efficiency at variable engine speeds. By increasing the plenum at lower speeds, the fluid can be encouraged to flow into the cylinder, but this change must be retroacted at higher RPM's to prevent a

performance decrease, since the fluid will be travelling at a higher speed. In a similar fashion, modification to both the head channel and manifold can facilitate a productive mixture of available gases for combustion and an efficient transport sequence. (Ceviz & Akın, 2010)

2.5 Patent Approaches to Rotary Valve Design

Many patent designs have tried to address timing efficiency through the incorporation of rotary valves in the system. While most designs appropriately re-configure the valve train, they require a complete re-design of the engine assembly as well, which can lead to costly manufacturing issues in practical application.

Few patent designs approach the valve train with a horizontal rotary valve, However Barry Muth's design in his patent application utilizes this concept quite well. In his patent, the engine is managed by a single large rotary valve assembly, which is placed atop the engine block. This system uses one rotary valve to control all strokes of all four cylinders, and employs similar design features to this design, including seals a fore and aft of the rotary valve. However, this design requires a square four-cylinder engine block, which is not commonly available in industry and would require special manufacturing. (United States Patent No. 0152983, 2002)

Many patent designs emulate a traditional camshaft valve head, featuring camshafts with built in rotary valves which rotate in-plane with the camshaft axis. This feature more appropriately resembles a typical system and could be more easily retrofitted to an existing system. Donald Duve, in his patent application, proposes a dual camshaft design, devoting one to intake and the other to exhaust. This design mimics poppet valve function very closely, but features a Geneva machine to quickly accelerate the rotary valves to their open and closed

position. While this quick stroke duration is an advantage, the Geneva gearing presents added components to the system. (United States Patent No. 5711265, 1998)

Ronald Conklin presents a very similar design in his rotary valve head. The function of the rotating camshafts is to move the rotary valves to their respective positions. This design closely resembles Duve's patent, but offers a more robust valve design. This patent also features a complicated gear train to properly interact with the valves, but will remove valve interference initially associated with the poppet valve head blockage. (United States Patent No. 5205251, 1993)

Keith Lawes' patent design features a complete re-design of the entire internal combustion engine, utilizing an opposed piston design in tandem with rotary valves. These valves are low profile, but again require a redesign of the block to accept the new heads. Among available rotary head designs, Lawes' is one of the more developed, offering even coolant passageway design and the proposed heat sink flanges required to cool the rotary valves during operation. (United States Patent No. 0308491, 2011)

Two patents by Leon Bachelier propose a combination of previous patents. Each cylinder is governed by a single, vertical rotary valve, all connected with a driveshaft. These valves hold a single large passageway to connect the intake and exhaust plenums to the cylinder at appropriate times. This design is simple, applicable to most engines, and satisfies the elimination of flow interference from poppet valves. However, there is a problem with extended channel size causing primary head loss during intake and exhaust strokes, as well as exhaust gases being trapped within the valve between exhaust and intake strokes. (United States Patent No. 0187831, 2004) In Bachelier's later patent, the design is re-designed to feature curved rotor channels, thus helping alleviate flow resistance to the cylinder. This poses a manufacturing challenge though, as

boring a curved hole through a cylindrical valve would be difficult, unless included in casting. (United States Patent No. 0102130, 2006)

Andrew Thomas presents a rather unique rotor design in his patent, using a long cylinder to create either an intake or exhaust channel. This design is very effective in creating a high-area flow path for the fluid, which will drastically reduce head loss. The design's rotor holds little mass and balancing for a proper resultant moment of inertia during manufacturing would be difficult. This piece will no doubt have to be cast, given its complex geometry, and this could result in improper grain formation to withstand combustion pressures during stroke operation, especially given the thin-walled nature of the rotor valve. If this rotor valve could be manufactured to withstand the combustion pressures, it could be successfully applied to a traditional combustion engine. The design also requires the implementation of dual spark plugs to properly combust all the mixing fluid, which results in additional machining and component inclusion. (United States Patent No. 0266983, 2007)

Caterpillar offers a well-developed patent through Martin Dirker, featuring both a head and valve cover design, as well as a rotary valve train to be inserted within the head. Again, this patent approaches the design using rotary valves as direct substitutes for a cam and poppet valve, retaining the rotating shaft within the valve train. The resulting head shape very closely resembles a traditional head and could be readily retrofitted to an existing engine. The rotor valves themselves will require extensive machining, and their thin walled nature means that combustion pressure could be of a concern, especially when used in a diesel engine application. (United States Patent No. 0210190, 2008)

CHAPTER THREE: DESIGN SPECIFICATION AND APPROACH

Based on generally accepted engine head designs and functionality, the design of the Rotor Valve System (RVS) involves three major assembly components: The rotor valves, the head block, and the valve cover. The model of the RVS will be based on a traditional engine head design and will include relevant functions such as four full strokes with overlapped timing.

3.1 Engine Design Selection

Before design of the RVS can be evaluated, a comparable system needs to be selected to model the traditional poppet valve setup. A system with enough data is desired, since the simulation will need to be calibrated against known parameters to ensure accuracy. Such systems include Toyota's AZ engine series (Used in the Toyota Camry) or Toyota's JZ engine series (Used in Toyota's Supra and Lexus vehicles). Another alternative design is the MV Agusta F4 series engine (a compact four-cylinder engine used in MV Agusta's motorcycles). The purpose behind the selection of such engines is that they all use conventional poppet valve/camshaft stroke management. These will provide an excellent baseline to compare the RVS to. The Toyota JZ engine series is renowned for its simplistic duel overhead camshaft design, as well as using a lightweight aluminum head. As well, the Agusta M4 features an incredibly compact four-cylinder engine, which features all the major operating components of a standard DOHC engine with four valves per cylinder. These engine variants, among others, offer relatively new (less than 20 years old) technology, but have been in service long enough to provide adequate information for efficiency and power output. For this thesis, the 2010 Agusta M4 1000cc four-stroke motorcycle engine has been selected, due in part to the readily available information

regarding various geometric properties (Such as inlet/exhaust port sizes, valve travel, and piston face clearance at Top Dead Center).

To appropriately compare such characteristics as thermal efficiency and pressure profiles, normalized tables of data must be readily available for the selected engine. As is the case for most engines, information regarding geometric layout is easily found, however finding information relating to thermal efficiency or inlet conditions is more difficult. In some cases, it may be necessary to draw assumptions based on a general case for modern four-stroke engines. Knowing these characteristics, logical assumptions can be calculated knowing data such as inlet pressure, temperature, etc.

After selection of the appropriate baseline engine (The Agusta M4) and its performance values, the poppet valve train profile and the respecting geometric properties are derived, and the engine dimensions and performance specifics will be used to properly model the engine in SolidWorks (Complete with the traditional valve head). This is the base by which the retrofitting of the RVS is performed for comparative analysis.

3.2 Basic System Modeling for the RVS

The rotor valve will follow the general design function of a poppet valve. For a four-cylinder engine, the assembly will feature four rotors, with each rotor containing an oil passage, radial seal, and an appropriately sized port. The purpose of the rotor valve is to provide seals to the cylinder during the compression and combustion strokes, and appropriately open the cylinder to intake and exhaust channels at the proper time, exactly as a traditional valvetrain is designed to function. One of the most difficult design characteristics of the rotor valve is addressing the axial stresses induced during the combustion stroke. The rotor will need to rotate under

combustion pressure during all four strokes, unlike traditional poppet valves. The rotor could be supplemented with two radial seals, much like the side seals in a Wankel rotary engine, to facilitate smoother rotation under pressure and allow space for flexion.

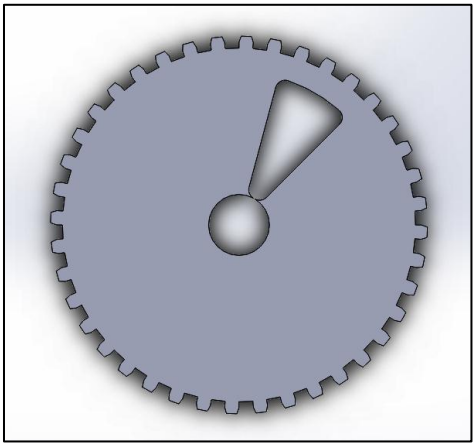

Figure 3.1 A proposed rotary valve with a port to allow fluid flow between the head and cylinder

The head block will contain the intake and exhaust channels, oil and coolant passageways, cylinder ports and mounting seats for the rotor valve component. The head block will hold the rotors mounted within the proper channels and be pre-drilled to accept the valve cover after installation. The primary purpose of the head block is to provide a stable reciprocal in which the rotor valve assembly can operate while keeping the system cooled and lubricated.

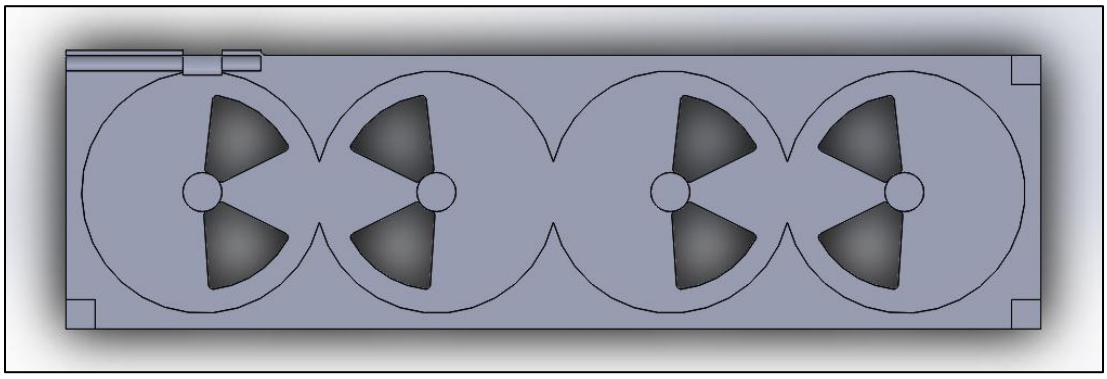

Figure 3.2 An above view of the rotary valve head

The valve cover will provide a sealing surface over the rotor valves following installation. This will keep the rotor valves seated within the head block, as well as provide appropriate lubrication and coolant return channels. The valve cover will also function as a timing cover to prevent interference with rotor valve timing.

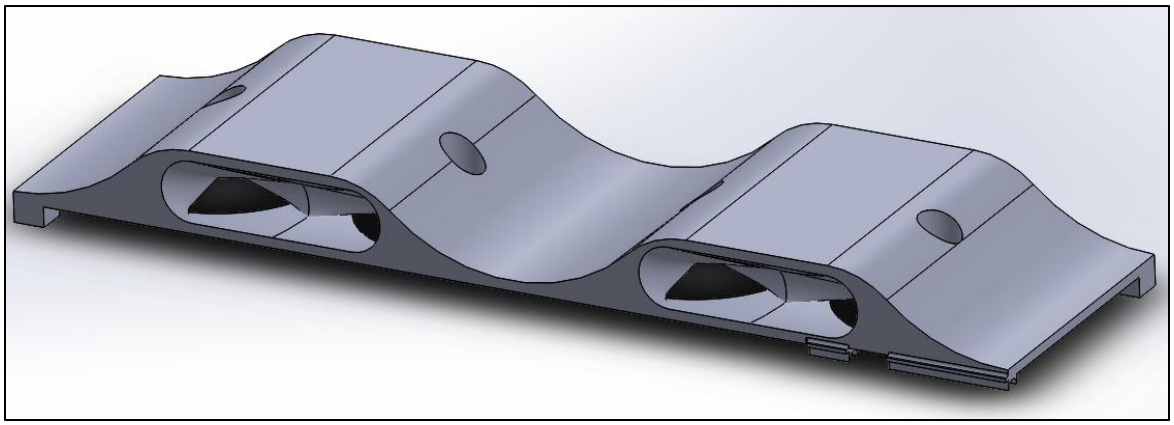

Figure 3.3 A low-profile valve cover, which incorporates the manifold mounting points

The rotor valves can be machined using an end mill after being turned to the proper radius. An appropriately sized port can then be added with optimal tangential geometry to promote smooth stroke transitions. This presents a straightforward manufacturing procedure for the rotor valves, which can be easily replicated or adjusted.

The head block and rotor valve cover could be manufactured in similar fashion, cast from a mold and machined to hold the proper fluid channels and passageways. The head block can be mirrored from an original poppet head valve design, to be properly mated with a pre-existing

engine block for future experimental testing. During machining, the head block and cover geometry would need to be designed to reduce the potential for crack propagation due to shear stress distribution. The mating surface of the rotors and the head block must be smooth; this may encourage a rounded-corner rotor design to prevent a right-angled head lobe profile (A 90-degree angle is an ideal profile for crack formation under stress).

3.3 Geometric Parameters of the Head Components

The RVS will be designed using available engine parameters for the Agusta M4, as well as known profiles of the camshaft and desired operation characteristics to closely resemble a traditional system. Parameters such as the following will be sourced directly from the traditional engine dimensions for the 2010 M4 (MV Agusta, 2017):

M4 Four Cylinder Engine Properties	
Cylinder Bore	76mm
Cylinder Stroke Length	75mm
Connecting Rod Length	107.3mm
Crank Arm Length	37.5mm
Inlet Valve Diameter	30mm
Exhaust Valve Diameter	25mm
Intake Valve Angle	10.25°
Exhaust Valve Angle	12.5°
Clearance at TDC (Referenced from Combustion Chamber Volume of 11.6cc)	2.557mm
Maximum Intake Valve Travel	10.3mm
Maximum Exhaust Value Travel	9mm
Intake Valve Opens	16° BTDC (-16° = 704° Cycle)
Intake Valve Closes	60°ABDC (240° Cycle)
Intake Valve Duration	256°
Exhaust Valve Opens	48° BBDC (492° Cycle)
Exhaust Valve Closes	18° ATDC (738° = 18° Cycle)
Exhaust Valve Duration	246°

Table 3.1 Table of Geometric Properties for the Agusta M4 Engine

Using these as well as other geometric measurements of the system, a baseline can be drawn, and it is possible to construct the traditional system outright. In order to highlight the difference of flow during the stroke length, the initial connecting rod length has been changed from 27.5mm to 37.5mm. The timing duration and poppet valve profiles will come directly from measured values. The RVS will share many components with the traditional system, such as stroke length and bore. The RVS will also share exact timing values, to further remove outside influence for deviations in results. The profiles for the traditional (And RVS) timing can be seen in Figure 3.4:

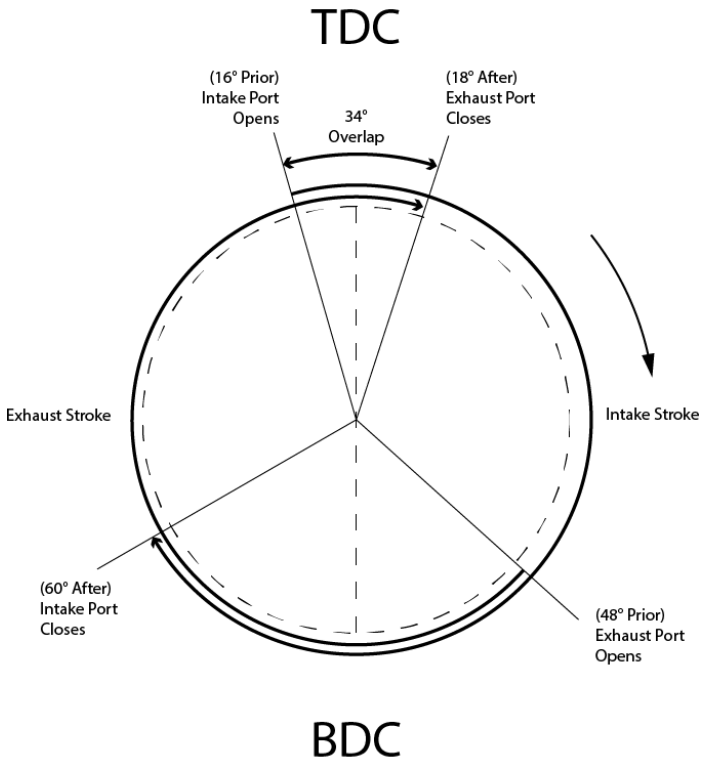

Figure 3.4 A timing diagram for the Agusta M4 engine, including valve overlap

Using these stroke durations, it is possible to derive the necessary rotor port edge locations for the RVS timing to accurately match that of the traditional system:

3.1) $$\theta = \frac{\theta_t \pm \frac{1}{2} G_r \theta_l}{G_r}$$

Where, in Equation *3.1*, θ is the desired angle conversion for the rotor head geometry, θ_t is the angle in the traditional system, and θ_l is the angular displacement of the rotor lobe. For this simulation, θ_l has been set at 60° for ease of calculations. The gear ratio of crankshaft to camshaft (G_r) is 2:1 for conventional four-stroke engines (In order to keep the intake and exhaust values closed for two of the four strokes a half gear ratio is necessary). The negative and positive forms of Equation *3.1* are used depending on the necessary timing conversion. For a system with a desired intake stroke of 128° (256° of the crankshaft rotation), an exhaust stroke of 123° (246° of the crankshaft rotation), and a desired overlap of 17° (34° of the crankshaft rotation), the corresponding values for the rotor head can be calculated, as seen below in Table 3.2:

Rotor Valve Engine Properties	
Intake Opening Angle	22° ATDC (44° BTDC Crankshaft Reference)
Intake Closure Angle	0° BDC (0° BDC)
Exhaust Opening Angle	6° ABDC (12° ABDC Crankshaft Reference)
Exhaust Closure Angle	21° BTDC (42° BTDC Crankshaft Reference)
Overlap Degrees	43° (86° Crankshaft Reference)
Lobe Opening Angle	60°

Table 3.2 Rotor Valve Timing Angles

After the part geometries have been determined, CFD simulations in SolidWorks (For basic pressure profile calculations) is used to analyze the systems behavior under standard four-

stroke cycle operation at all crankshaft positions. SolidWorks is a graphical CAD program which can be used to quickly draft 3-D models. It offers a basic fluid simulation tool, Flow Simulation, which can be used to justify certain design choices

3.4 Selecting the Appropriate Modeling Environment

Originally, the intent of the simulation processing was to use SolidWorks CAD to construct the Traditional and RVS systems, and then export this geometry into a more robust CFD software, such as OpenFoam or Fluent. OpenFoam is an opensource Linux based CFD program which can be used to construct complex systems with varying boundary conditions, including moving boundaries. Fluent is a commercially available CFD program which features a GUI and the ability to specifically analyze a full internal combustion engine cycle. Due to limitations in time, and to reduce scope creep during the thesis testing, the decision was made to forgo learning an entire new simulation software and its application. Instead, SolidWorks Flow simulation was used exclusively to analyze the systems. In part, this was due to both the familiarity of Flow Simulation processing and of the simplifications that could be made to significantly reduce processing time. The sacrifice of the ability to process moving boundary conditions and fuel/air mixing was compensated with the use of two simulation processes: Firstly, a cold flow simulation was used to analyze the pure geometric effect of the RVS on fluid flow into the system. Secondly, a full combustion cycle was approximated by calculating the adiabatic flame temperature at the end of the compression stroke and assuming consistency during the expansion. This also required that a fully pre-mixed gas was necessary as the working fluid, as SolidWorks does not support fluid mixing or atomization of fuels.

The heart of the system evaluation comes from modeling of the composed assembly using a computational fluid dynamics software. The overarching variables to be determined are the available pressure at the piston face during the power stroke, and pressure plots within the cylinder volume. By analyzing the pressure available of the design, a baseline comparison can be made between the two types of valve trains to suggest an overall performance difference. A pressure plot of the average pressures throughout the cylinder centerline over all crankshaft angles can give insight into pressure variance and mixing efficiency during operation.

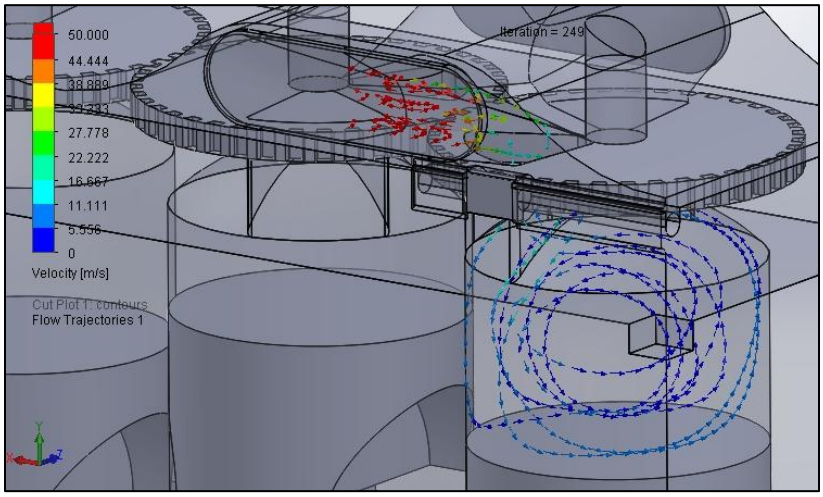

Figure 3.5 Swirl formation proof-of-concept in the RVS

SolidWorks Flow Simulation is used as a preliminary guide to justify the research by using cold flow assumptions, as it can be easily used to construct a detailed 3-D profile before moving on to a more rigorous combustion evaluation. As seen above in Figure 3.5, SolidWorks provides a proof of concept for analyzing the RVS response, as the system can be constructed and analyzed in program without having to export the file for mesh generation or boundary condition setup. SolidWorks is a useful precursor for testing since the system geometry can be

quickly edited in-program to see the effect of minute changes on simulation behavior. After certain geometric properties have been validated, the system can then be analyzed. These results will be the main supporting data for the conclusions drawn from the research.

The computer simulations will be ultimately based on the k-ε turbulence model, along with boundary conditions of the inlet and walls, as seen below in Equations *3.2* and *3.3*.

3.2) $$\rho u \frac{\delta k}{\delta x} + \rho v \frac{\delta k}{\delta x} = \frac{\delta}{\delta y}\left(\left[\mu + \frac{\mu_t}{\sigma_k}\right]\frac{\delta k}{\delta y}\right) + \mu_t \left(\frac{\delta u}{\delta y}\right)^2 - \epsilon - 2\mu\left(\frac{\delta \sqrt{k}}{\delta y}\right)^2$$

3.3) $$\rho u \frac{\delta \epsilon}{\delta x} + \rho v \frac{\delta \epsilon}{\delta y} = \frac{\delta}{\delta y}\left(\left[\mu + \frac{\mu_t}{\sigma_e}\right]\frac{\delta \epsilon}{\delta y}\right) + \frac{c_{\epsilon 1}\epsilon}{k}\mu_t \left(\frac{\delta u}{\delta y}\right)^2 - \frac{c_{\epsilon 2}\epsilon^2}{k} + 2\mu\mu_t \left(\frac{\delta^2 u}{\delta y^2}\right)$$

Where ρ is the density of the flowing fluid, u and v are the velocity components in the x and y direction, respectively, μ is the dynamic viscosity of the fluid, and the C and σ coefficients are pre-determined constants. The turbulent kinetic energy is represented by k, and the dissipation energy is represented by ε. These two equations can be used to represent the energy flow in turbulent fluid, i.e. the rate of incoming k or ε related to the creation or destruction of k and ε. Normally, these equations are difficult to iterate by hand, but modern software such as SolidWorks is suited for heavy iterative calculations of these functions. The k- ε model is incredibly robust and will provide concrete foundations for the simulations. The function itself is based on a derivation of the Naiver-Stokes equations, which help explain the behavior of flowing fluid.

After the equations have been properly defined, the boundary conditions for the system must be set to properly observe the respective behavior through the cylinder. The inlet boundary will be defined from data gathered regarding nominal engine inlet behaviors, including such characteristics as: Inlet pressure, inlet mass flow rate, wall temperature, heat flux, or other

conditions. Similarly, the outlet (exhaust) conditions will be similarly defined. Ideally, such boundary conditions could be defined from a system whose thermal efficiency and behavior was already known. This will allow calibration of the inlet/outlet conditions to produce the most accurate response before implementing the new system. Using such a system will provide an excellent comparison for the potential thermal efficiency change associated with the RVS, as well as more basic comparisons of pressure profile distributions in the SolidWorks cold flow analysis.

In each case, the thermal efficiency of both the RVS and the traditional set-up will be analyzed at all crankshaft angles throughout the four-stroke operation. The set-up boundary conditions have been derived from existing data and assembled into the tabulated set below (Gundmalm, 2009):

Simulation Boundary Conditions	
Cylinder Wall Temperature	480K
Piston Face Pressure	1bar 540K
Head Temperature	380K
Inlet/Outlet Temperature	375K
Valve (Rotor) Temperature	600K
Inlet Fluid	1.5bar 293.15K 34 m/s Maximum Magnitude
Outlet Fluid	38 m/s Maximum Magnitude
Working Fluid (Air)	STP unless otherwise defined

Table 3.3 Simulation Boundary Conditions

The values for temperature will allow SolidWorks to treat each declared face as a real wall, and the heat flux through those walls can be set to negligible, thus promoting a cold flow scenario. For the RVS, the Rotor temperature is based on the valve head temperature, to

accurately model those surfaces which are contacting the fluid as it enters the chamber. The working fluid for the cold flow simulations is air at STP unless dictated otherwise, such as in the inlet. For the inlet and outlet flow velocities, a special relationship had to be developed to prevent valve geometry pinch on the flow conditions. Initially, a constant value of 38 m/s and 34 m/s, for the outlet and inlet respectively, was used throughout the entire simulation. This resulted in simulation issues, which will be addressed in Chapter CHAPTER Four:.

3.5 SolidWorks Drafting Specifics

SolidWorks offers comprehensive graphical solutions to present the data of the CFD analysis. Of interest is displaying the plots for velocity in cross-sections of the engine cylinder, as well as using pressure data to draw conclusions about the efficiency of air mixing. By incorporating a cut plot of the cross sections of these parameters, the effectiveness of the engine can be compared to a traditional set-up. The graphs will also allow for visual representation of the CFD values. The combustion model will also be analyzed and displayed using SolidWorks Flow Simulation.

To ease the workload of the simulations, the bodies to be analyzed will be a single piston and head assembly. The following components on the single cylinder engine are created directly in SolidWorks:

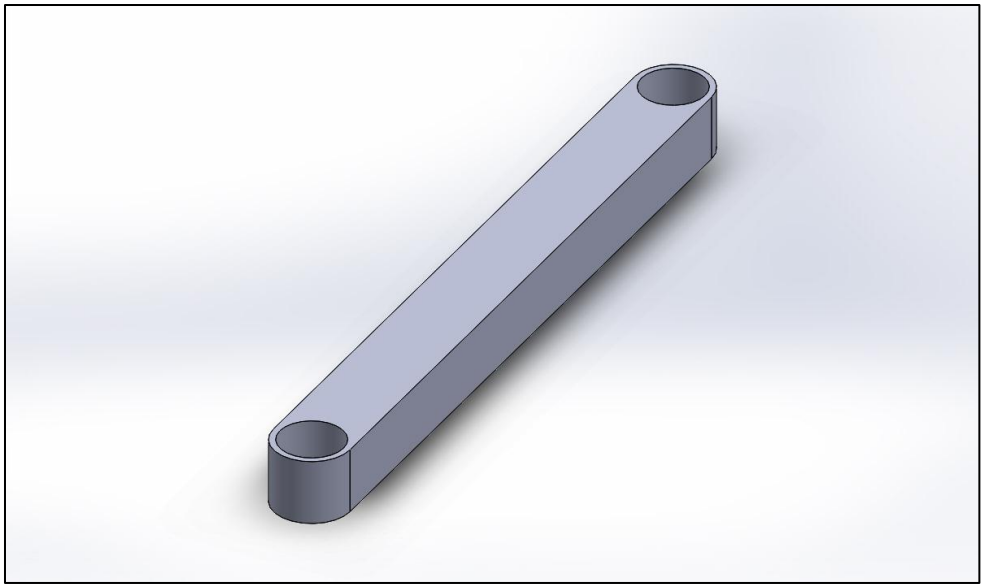

Figure 3.6 A simplified connecting rod

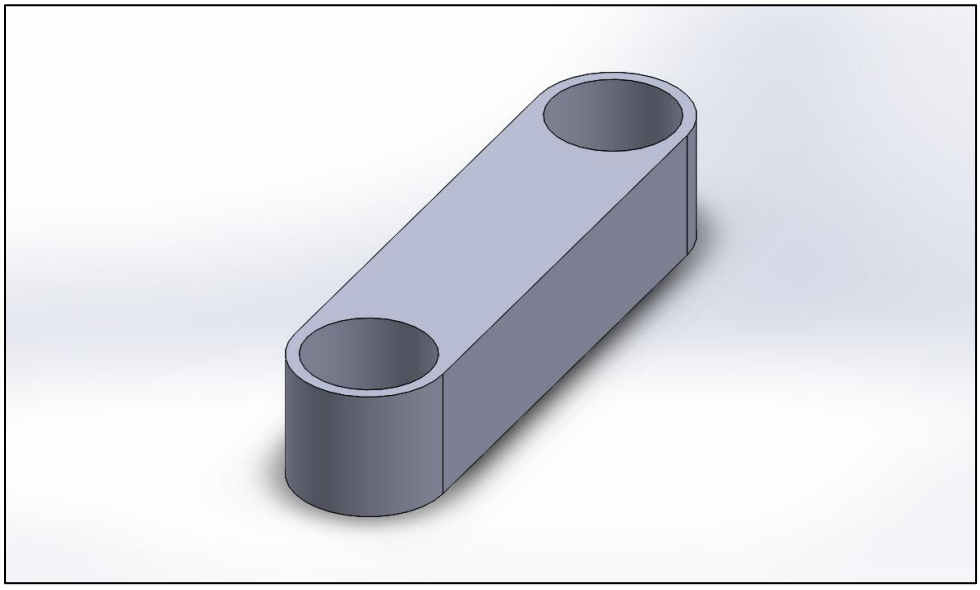

Figure 3.7 A simplified crank arm

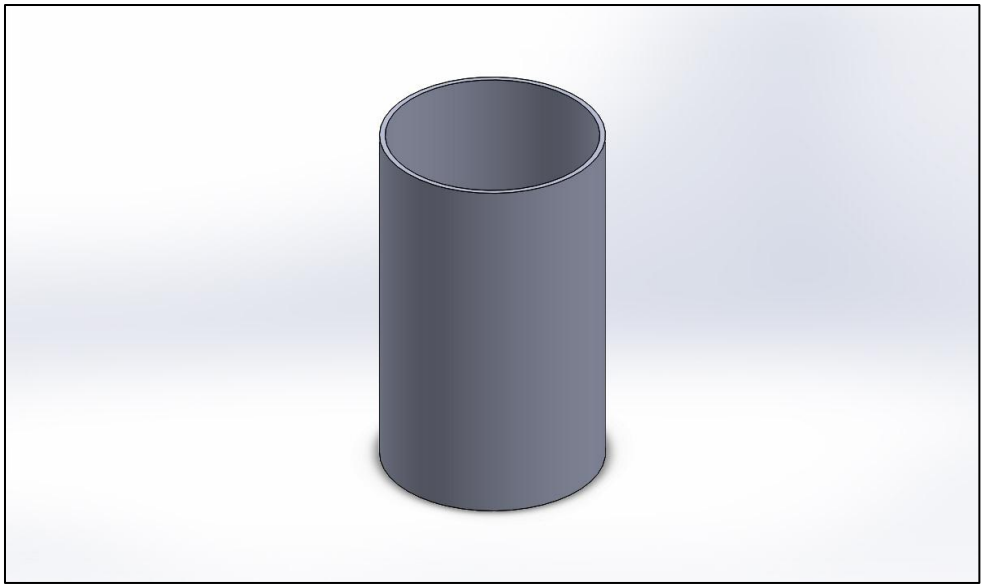

Figure 3.8 A basic cylinder sleeve

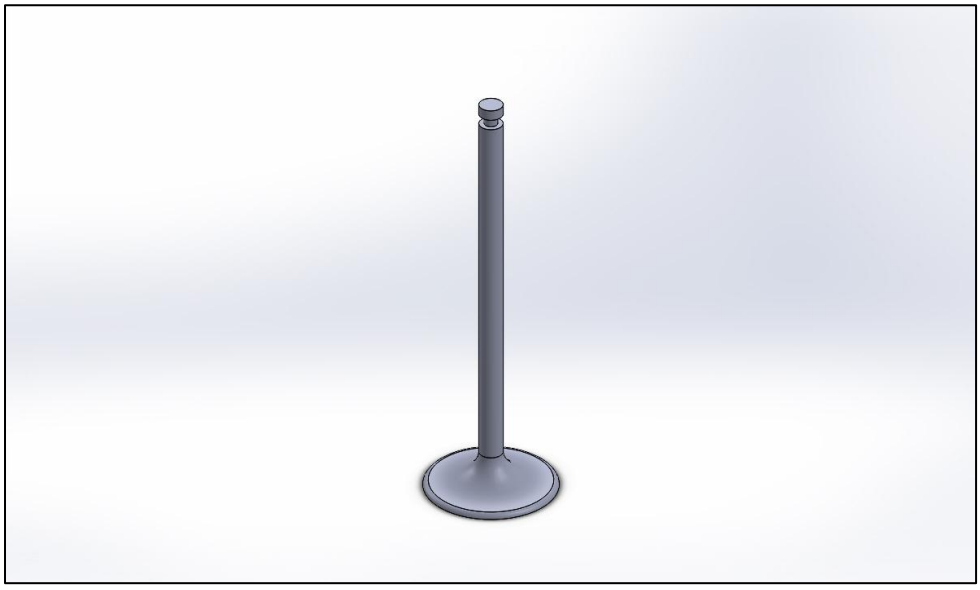

Figure 3.9 A simple poppet valve

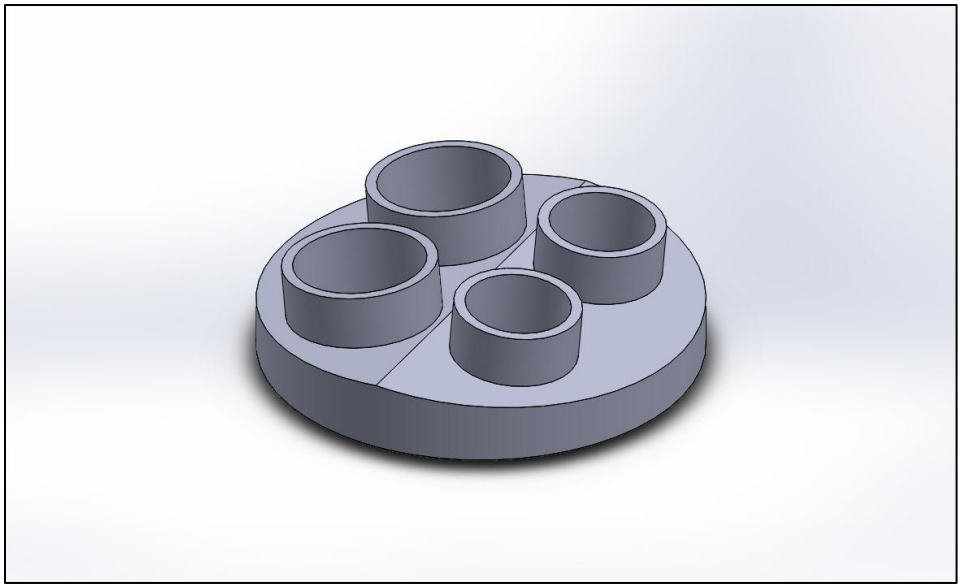

Figure 3.10 A basic head for the traditional design

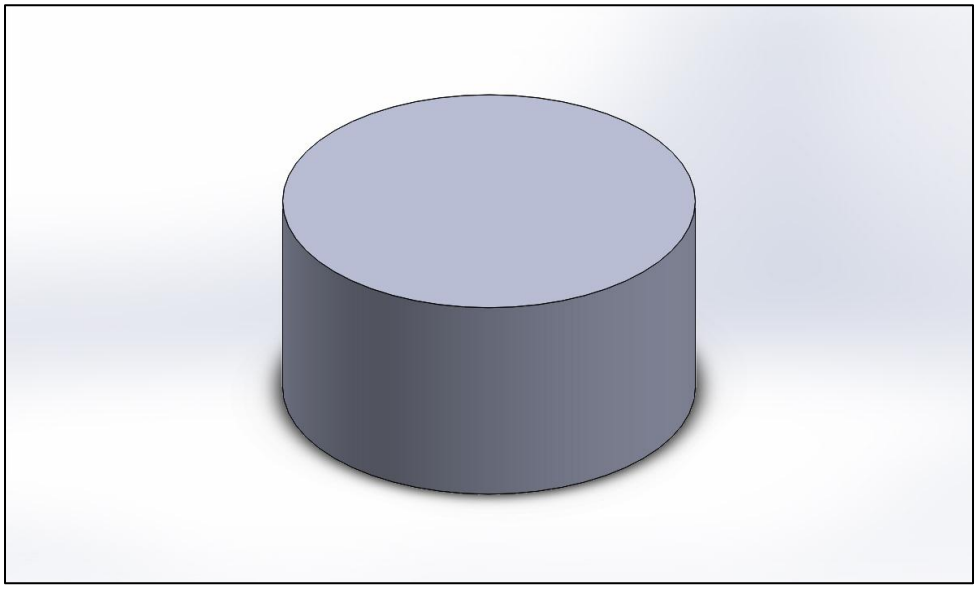

Figure 3.11 A simple cylinder used to represent the piston head

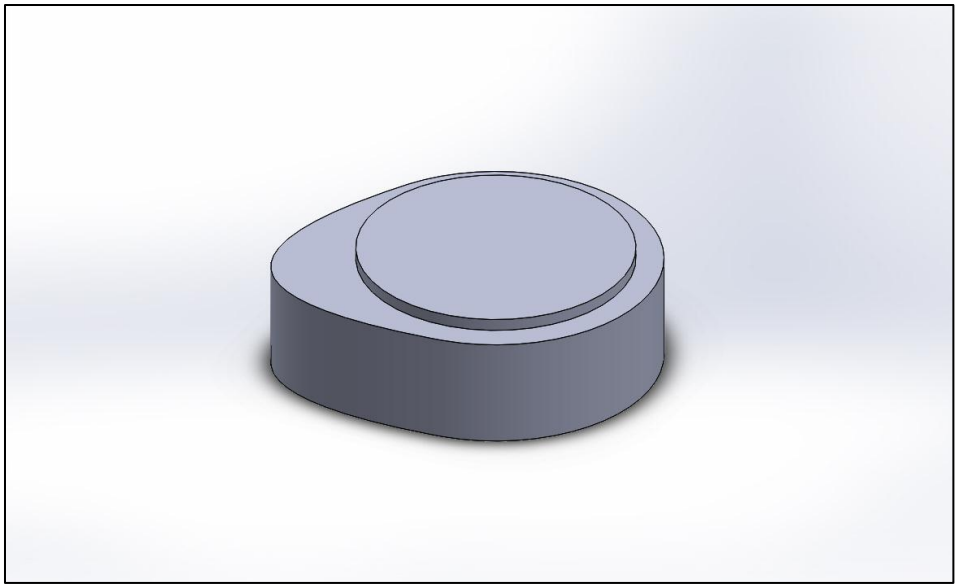

Figure 3.12 A simple representation of the cam profile

The geometric properties for such components of the traditional system are drawn from Table 3.1, including bore, stroke length, etc. When completely assembled, the traditional system is seen below:

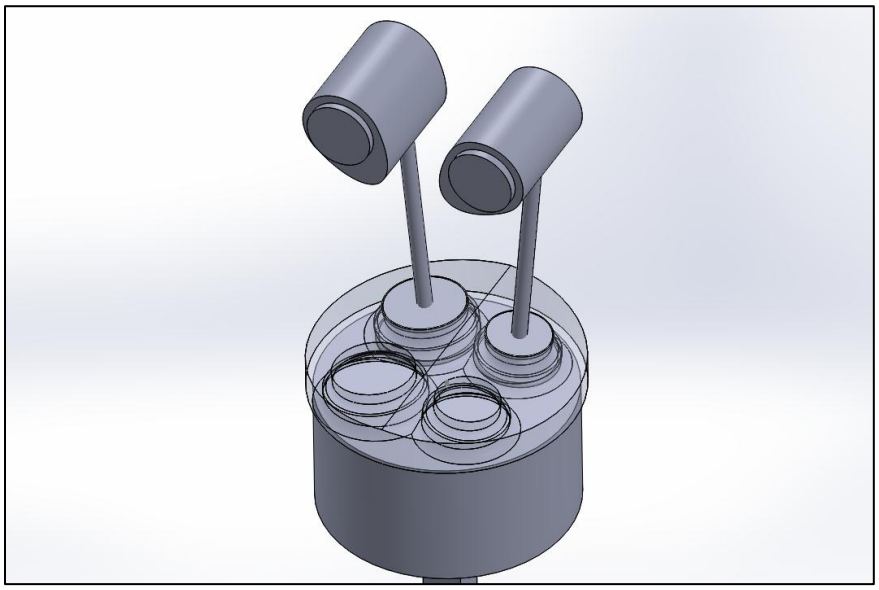

Figure 3.13 The assembled camshaft system and cylinder

For ease of reference the forward cams, intake valve, and exhaust valve have been hidden from view in Figure 3.13. The cam profiles resultant in Figure 3.12 were derived from the relationship between the starting/ending angles and the maximum valve displacement from Table 3.1. Using this, it is possible to construct a basic spline representation of these timing characteristics:

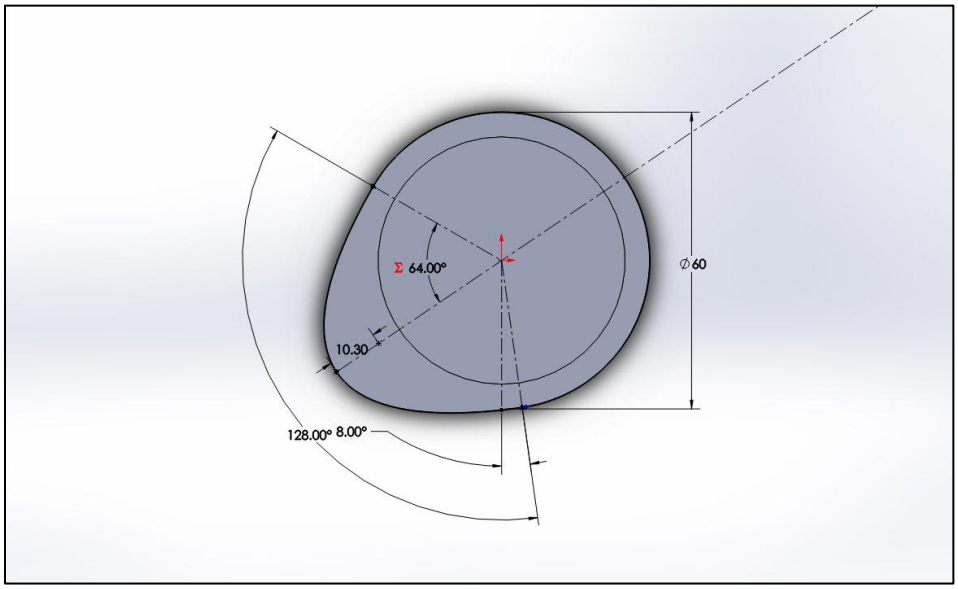

Figure 3.14 The geometry behind a cam profile

In Figure 3.14, the profile is defined by three basic measurements: The overall length of the intake/exhaust stroke, the maximum displacement for that stroke's valve, and the point at which the stroke begins relative to either TDC or BDC. Using these three values, it is possible to construct a rough approximation of the profile. Afterwards, the geometry of the spline can be

forced to a smooth, tangential transition to the rest of the cam profile, thus ensuring a smooth transition from start to finish.

The RVS system is inherently very similar to the traditional system, using the same cylinder, piston, crank arm, and connecting rod. However, both the head and valve system are different:

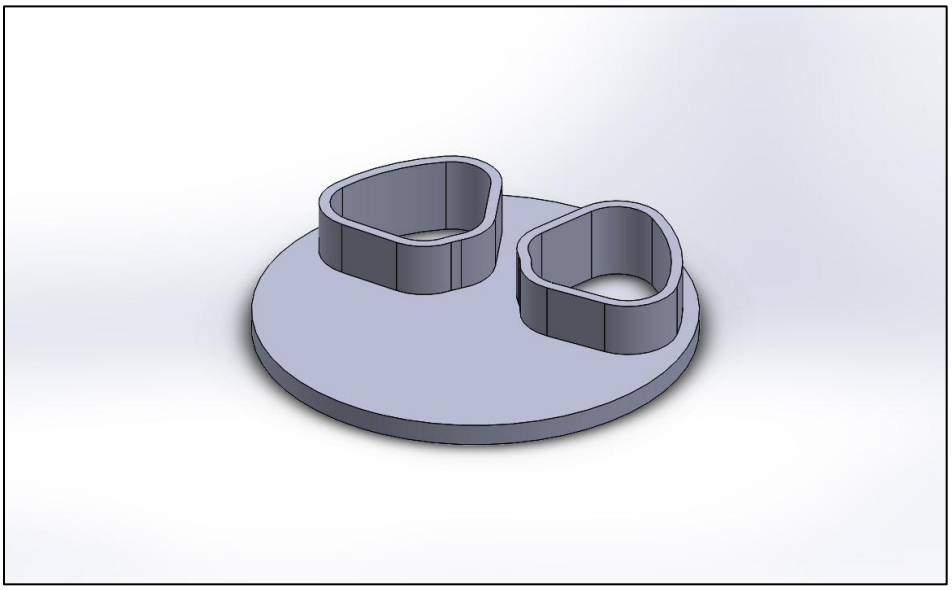

Figure 3.15 The rotor head cover

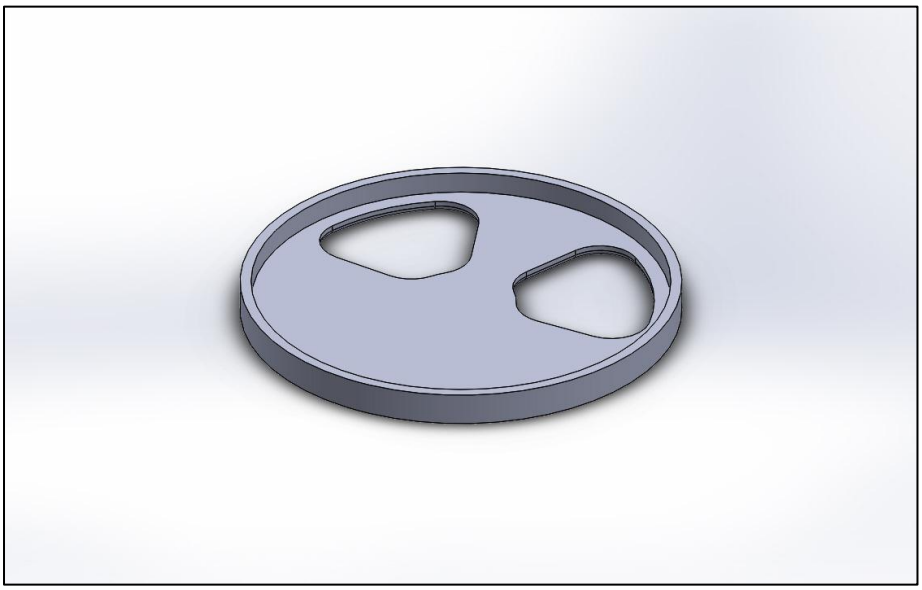

Figure 3.16 The rotor head itself

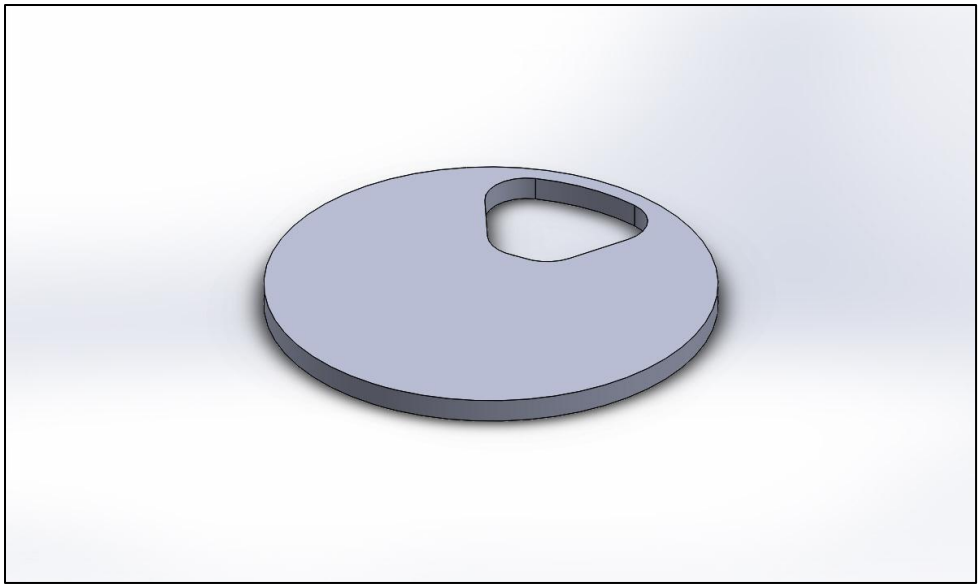

Figure 3.17 The rotor, serving as both the intake and exhaust valve

As seen from the figures above, the RVS model is a basic representation of the function of the rotor valve- manage the strokes of the engine as a valve train. The geometric layout for both the rotor head in Figure 3.16 and the actual rotor in Figure 3.17 are sourced from Table 3.2, which gets these calculations using an appropriate transformation Equation *3.1*.

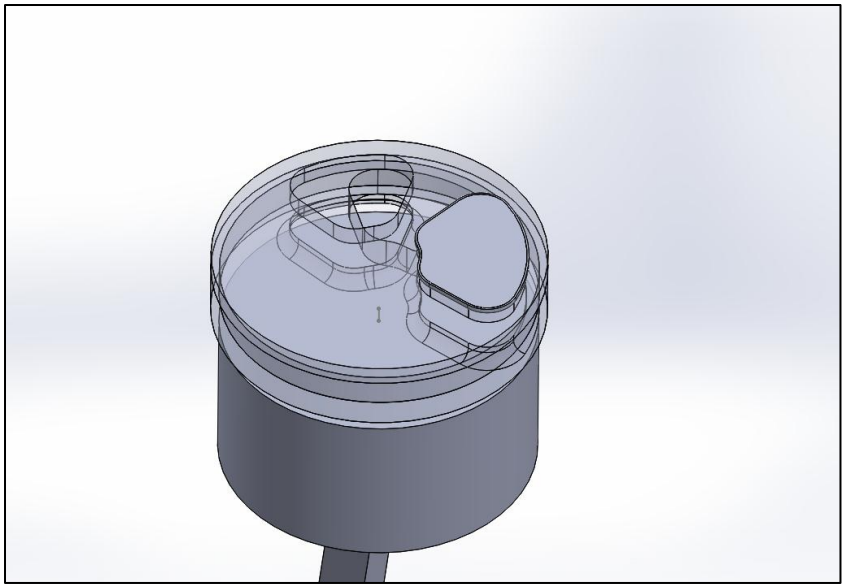

Figure 3.18 The completed RVS system

When completed, the RVS system closely resembled that of the traditional system, although it held a lower profile and had a different method of operation. It should be noted that both the traditional head in Figure 3.10 and the rotor head cover in Figure 3.15 included an additional 10mm inlet/outlet channel during the cold flow simulations, as well as a redesigned intake/exhaust plenum during the full combustion simulations. This was intended to help address an issue of vortices crossing the inlet face during simulation, which will be discussed in more detail in ChapterCHAPTER Four:.

3.6 SolidWorks Cold Flow Simulation

Of key importance in comparing the two systems is maintaining the same boundary and wall conditions for both the traditional and RVS setups. This will be done initially using a cold flow simulation. In cold flow, it will be assumed that the fluid flowing into the cylinder is air,

and there is no reaction between the working fluid and the boundaries. The focus of the cold flow simulation is to prove that, with similar operating conditions, the RVS shows a difference in fluid flow characteristics over the poppet valve system (Which will translate to a difference in fluid flow behavior and power output). Therefore, boundary conditions should remain constant after they have been properly defined for the traditional system. Defining boundary conditions in SolidWorks Flow Simulation is simple and requires little input besides the desired characteristics of the body. For all walls, including the piston face, cylinder lining, head and intake channels, a real wall assumption with negligible conduction was used, and values from Table 3.3 provided the physical temperatures measured previously (Gundmalm, 2009). The only other governing boundary conditions were those of an initial pressure at the piston face (Defined at 1bar) and the inlet/outlet velocities. The velocities themselves were not actually constant throughout the simulation but were represented by a polynomial equation to encourage a smoother transition between stroke start and termination, as described below in Table 3.4. Below, the inlet/outlet flow values are defined for all relevant Crank Angle Degrees in the cycle:

Crank Angle Degree (CAD) [°]	Inlet Velocity [m/s]	Outlet Velocity [m/s]	Crank Angle Degree (CAD) [°]	Inlet Velocity [m/s]	Outlet Velocity [m/s]
0	7.97	10.31	380	0.00	0.00
20	16.44	0.00	400	0.00	0.00
40	23.24	0.00	420	0.00	0.00
60	28.39	0.00	440	0.00	0.00
80	31.88	0.00	460	0.00	0.00
100	33.70	0.00	480	0.00	0.00
120	33.87	0.00	500	0.00	4.78
140	32.37	0.00	520	0.00	15.33
160	29.22	0.00	540	0.00	23.87
180	24.40	0.00	560	0.00	30.40
200	17.93	0.00	580	0.00	34.92
220	9.79	0.00	600	0.00	37.43
240	0.00	0.00	620	0.00	37.94
260	0.00	0.00	640	0.00	36.43
280	0.00	0.00	660	0.00	32.91
300	0.00	0.00	680	0.00	27.39
320	0.00	0.00	700	0.00	19.85
340	0.00	0.00	720	7.97	10.31
360	0.00	0.00			

Table 3.4 Inlet and Outlet flow velocities for various CAD

For flow conditions, the inlet/outlet velocity was suppressed when the valve was "closed", this was to simplify simulations with a single flow condition. Due to the low resolution of the testing CAD (Simulations were run discretely at every 20° CAD), only one stage in the simulation featured overlap between the two strokes – 0° CAD. This provides limited information about the effectiveness of the crossflow stage, as discussed in Chapter CHAPTER Four:. During simulations, the main area of interest of the cold flow analysis was the pressure

profile along the centerline of the cylinder. To accurately measure this, a centerline was drawn between the center of the piston face and the center of the head face, as seen below:

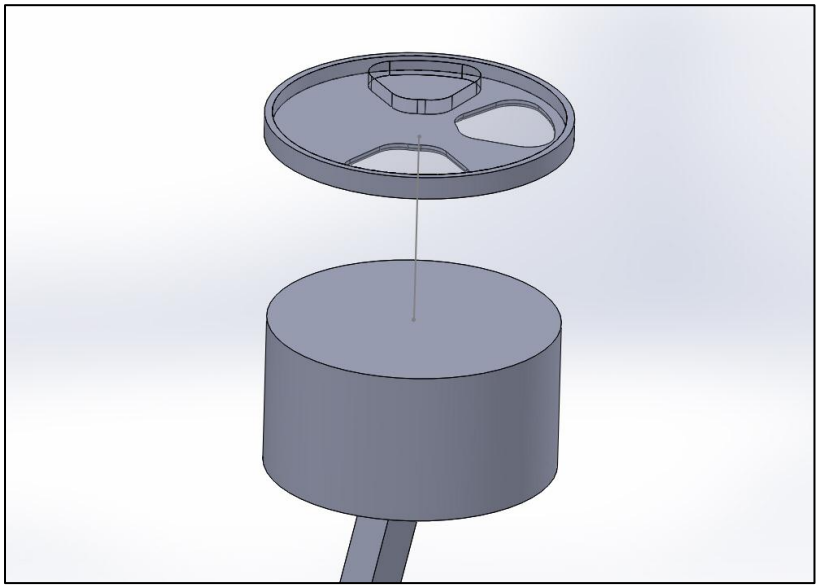

Figure 3.19 The pressure centerline used to gather data

For each 20° CAD, the simulation was analyzed, and the results were loaded into the SolidWorks Flow Simulation workspace. The pressure distribution in the cylinder was then measured along the centerline, and 100 equally spaced data points for the pressure value were collected. This allowed a high-resolution pressure sample to be collected during each CAD, for a result of 36 different pressure profiles. The results of those profiles are discussed further in Chapter CHAPTER Four:.

While the potential power availability of the engine is of most concern, the simulation data produced in a cold flow simulation will not directly provide this information. Instead, it will be necessary to utilize a full combustion cycle which includes heat generated through flame

propagation, which will be covered in Chapter 3.7. Other variables of interest (including the velocity and pressure plots) can be obtained directly in SolidWorks during this cold flow analysis and can offer insight into the functionality of the engine.

After completing the Cold Flow simulations (As covered in Chapter 4.1), the pressure centerline points can then be graphed versus rotor angle during the intake and exhaust stroke, thus providing a graph for all degrees of the intake and exhaust strokes (In 20° increments). These plots for both the traditional and RVS systems will provide helpful insight into the differences in pressure distributions throughout the cylinder and will help draw appropriate conclusions about the differences in flow and mixing capabilities. For each CAD, a cut plot of the velocity distribution in the cylinder is also taken, and this will provide ample amounts of visual data to compare the two systems subjectively. The velocity plots will also allude to any major flow interference properties influenced by geometry.

3.7 SolidWorks Combustion Simulation Background

While SolidWorks includes a simplified fluid behavior analysis routine, to analyze the performance over an entire 720° CAD of the system, it is necessary to make assumptions about the combustion process and gasses used during combustion. Firstly, a substitute for the working air fluid must be determined, as assuming pure air does not appropriately model the behavior of a fuel-air mixture. Since gasoline is the main component of fuel in internal combustion engines, a gasoline and air mixture can be composed to properly simulate this fluid. To further simplify the working fluid, the fuel/air characteristics will be modeled as a homogenous mixture, since SolidWorks does not openly support fuel droplet vaporization. This simplifying assumption will also drastically reduce the convergence time of Flow Simulations.

For this air/fuel mixture, the fuel component is assumed to be a prevalent hydrocarbon in gasoline – Heptane (C_7H_{16}). The characteristics of Heptane can then be composed with that of air, after calculating the appropriate stoichiometric air/fuel ratio. To find this ratio, the following formula is utilized:

3.4) $$C_xH_y + a(O_2 + 3.76N_2) \rightarrow xCO_2 + \left(\frac{y}{2}\right)H_2O + 3.76aN_2$$

Given that there are x = 7 carbon atoms and y = 16 Hydrogen atoms comprising Heptane, we can find a = 11, allowing us to fill in Equation *3.4* with the appropriate information. Knowing this, we can then utilize the following equation to calculate the appropriate stoichiometric A/F (Air-to-Fuel) ratio:

3.5) $$\frac{A}{F_{stoic}} = \frac{N_{air}}{N_{C_7H_{16}}}\frac{MW_{air}}{MW_{C_7H_{16}}}$$

Where N_{air} is the number of moles of air ($N_{air} = 4.76$), N_{C7H16} is the number of moles of Heptane ($N_{C7H16} = 1$), MW_{air} is the molecular weight of simplified air ($MW_{air} = 28.8514_{g/mol}$), and MW_{C7H16} is the molecular weight of Heptane ($MW_{C7H16} = 100.205_{g/mol}$). This results in a calculated $\frac{A}{F_{stoic}} = 15.0757$, or approximately 15. This value can then be used when creating the characteristics of the working fluid for the Flow Simulation software.

The important characteristics to use when modeling the behavior of the working fuel/air mixture are the fuel vapor conductivity, k, the viscosity, μ, and the specific heat, C_p. For simplification, these values can be assumed follow mathematical trends for the working temperature ranges of the combustion cycle. To calculate these values, the following formula can be used:

3.6) $$a_1 + a_2T + a_3T^2 + a_4T^3 + a_5T^4 + a_6T^5 + a_7T^6$$

Where a_n can be sourced from Appendix R. T can be used to develop the distribution of the characteristics over the entire working temperature of the fluid. After calculating these values for Heptane, the characteristics of simple air can be similarly calculated. Knowing the way that both fluids behave discretely, the combination can then be calculated using the formula found in Equation *3.5* for the stoichiometric A/F ratio. This value, along with the individual properties found for each temperature in Equation *3.6*, can be combined using:

3.7) $$C_{fluid,T} = \sum_{i=1}^{n} y_i C_{i,T}$$

Where C_{fluid} is the characteristic of the fluid at a given temperature, T. y_i is the molar mass fraction of the i^{th} component of the mixture, and $C_{i,T}$ is the characteristic of that component at a given temperature, T. Using this equation, the overall behavior of the entire fuel and air mixture can be expressed in terms of the contributions of the different components. The results of these calculations can be found tabulated in Appendix D. The resulting fluid properties were then fully defined, and the characteristics could be imported into SolidWorks Flow Simulation to more appropriately model the system.

Another important component of the full combustion simulation was the addition of intake and exhaust plenums for both systems. The intent of this addition was to produce less variance in the simulations due to the increased proximity of the inlet and outlet boundary conditions.

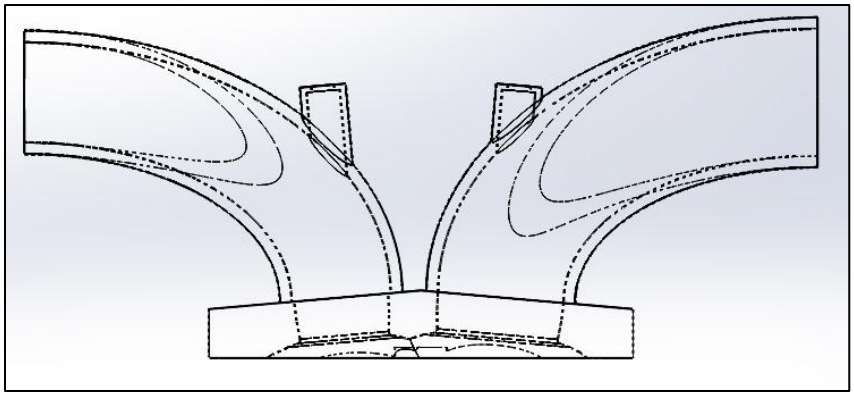

Figure 3.20 The Redesigned Traditional Head, with Plenums

As seen above in Figure 3.20, the redesigned head plenums allowed the inlet and outlet sources to be moved away from the engine head. This design was repeated for the RVS system:

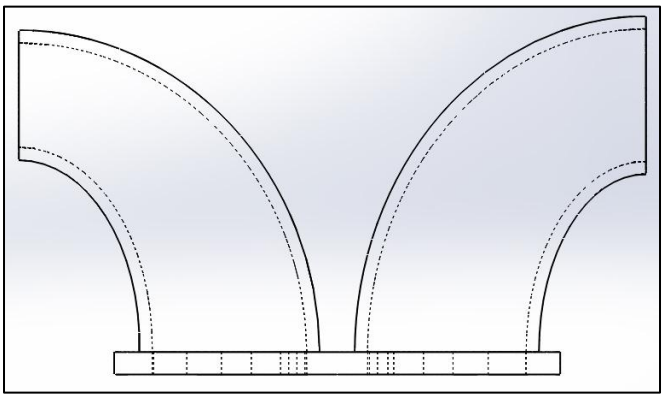

Figure 3.21 The Redesigned RVS Head, with Plenums

Before full combustion simulations could be carried out, however, several other key aspects to the system had to be addressed. Firstly, the piston motion profile was derived, to more

accurately take into consideration the effect of piston motion on the working fluid. The overarching equation for the position of a piston in a crank-slider assembly is derived as:

3.8) $$x = c + r\cos(\theta) + \sqrt{l^2 - r^2 \sin(\theta)^2}$$

Where r is the radius of the crank arm, l is the length of the connecting rod, c is the clearance at TDC, and θ is the Crank Angle Degree. These values can be found in Table 3.1. After establishing the overarching position equation, the equation for the velocity of the piston head could be implemented into the boundary conditions of the system:

3.9) $$v = -r\sin\theta - \frac{r^2 \sin\theta \cos\theta}{\sqrt{l^2 - r^2 \sin(\theta)^2}}$$

This characteristic can then be used in the simulations to express the effect of the moving piston during each CAD. In this fashion, the discrete nature of the simulations can be used more appropriately since the motion of the piston boundary is not excluded. After applying these boundaries to the systems, the Intake stroke (From CAD 0° to 220°) could be effectively run for both the RVS and the traditional system. The results of these simulations can be seen in Appendices F and I and are discussed in detail in CHAPTER Four:.

Since the conditions of the boundaries are identical for both the RVS and traditions system, the compression stroke result is not necessary to simulate, as the most important characteristics are the resulting temperature and pressure directly before the combustion stroke. To save on simulation and processing time, the compression was assumed to be adiabatic, and the resulting compression relation equations for an ideal gas could be used, given the change in specific volume:

3.10) $$\left(\frac{v_i}{v_f}\right)^k = \left(\frac{P_f}{P_i}\right)$$

Where ν_i, P_i are the initial specific volume and pressure of the mixture before compression, calculated using the final pressure and temperature of the intake fluid in the cylinder. K is the ratio of specific heats, which can be found from Appendix D. It was also possible to calculate the final temperature of the mixture after compression:

3.11) $$\left(\frac{\nu_i}{\nu_f}\right)^{1-k} = \left(\frac{T_f}{T_i}\right)$$

These characteristics could describe the nature of the gas directly prior to ignition. The properties of the gas have been assembled in the table below:

	Characteristic	Traditional System	RVS
Pre-Compression (180°)	ν_i	2.267 m^3/kg	2.4201 m^3/kg
	P_i	101328.6 Pa	101323.9 Pa
	T_i	444.45 K	472.19 K
Post-Compression (360°)	ν_f	0.090368 m^3/kg	0.096474 m^3/kg
	P_f	6.662 MPa	6.661 MPa
	T_f	1164.8 K	1237.5 K

Table 3.5: Characteristics of Pre and Post Compression Fluid

As seen above in Table 3.5, the characteristics of the fluid after compression were almost identical for both the traditional and RVS systems. These characteristics were then used to calculate a final variable to be used during the simulations; the adiabatic flame temperature.

The adiabatic flame temperature is described as the flame temperature at which reactants can burn and maintain the same standardized enthalpy as products after the process has completed. By assuming that the reactants in the simulation are burning at the adiabatic flame temperature, SolidWorks Flow Simulation can be used to approximate the heat gained through combustion, given that flame temperature. The adiabatic flame temperature is calculated using the current characteristics of the mixture before combustion:

3.12) $$H_{react} = \sum_{react} N_i \bar{h}_i$$

3.13) $$H_{prod} = \sum_{prod} N_i \left[\bar{h}^o_{f,i} + \bar{c}_{p,i}(T_{ad} - 298)\right]$$

3.14) $$H_{react} = H_{prod}$$

Where H is the enthalpy, N is the number of moles, $h_{f,i}$ is the enthalpy of formation, $c_{p,i}$ is the specific heat, and T_{ad} is the adiabatic flame temperature. The enthalpy of formation and specific heats for the mixture components can be found in Appendices S-W. This allowed the adiabatic flame temperature to be calculated with known parameters. This was a crucial component to the combustion simulation, as it allowed the change in pressure to be quantifiably linked to the change in temperature from the adiabatic flame.

After the calculations for the compression stroke had been completed, the adiabatic flame temperatures for both the traditional and RVS systems were found to be 2446.21 K and 2424.31 K, respectively. These values could then be used in the combustion and exhaust strokes to properly simulate the addition of heat through combustion. With all these characteristics defined for the simulations, it was then possible to conduct the entire 720° cycle simulation. The heat source during the combustion was modeled and implemented into the head of both systems, giving a similar comparable system for both, as seen below:

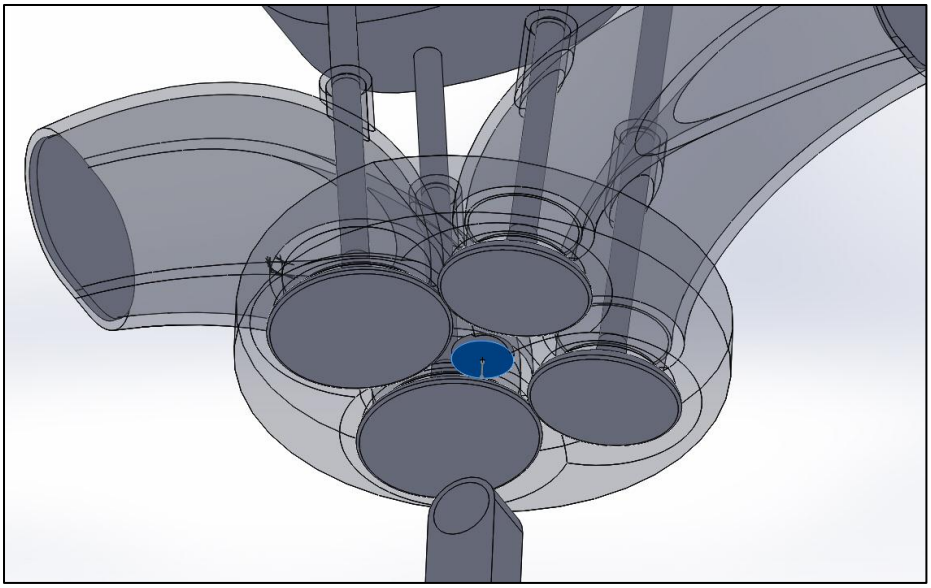

Figure 3.22 The Spark Heat Source inclusion point

3.8 Defining simulation constraints

Equally important as the actual boundary conditions was the set-up of the SolidWorks Flow Simulation parameters. The most important criteria were the convergence criteria for the numerical approximations. Firstly, SolidWorks was given an iteration limitation of 600 iterations. This was done to keep the estimation from diverging, although it should be noted that none of the simulations diverged. The convergence criteria were defined as the global average pressure in the fluid subdomain, and this was done to prioritize the accuracy of the pressure profiles. The desired accuracy of the convergence profile was left to SolidWorks to automatically calculate for every simulation.

It was also necessary to define the detail of the mesh formation. SolidWorks has a built-in meshing software, which can be used to quickly divide the fluid subdomain into comparable

elements for approximation. SolidWorks uses tetrahedrons to divide the subdomain, and the maximum side length for these tetrahedrons was limited to be 0.0083mm, which is a medium/course resolution. This prevented any large gaps in geometry from forming and allowed a high enough resolution to capture the interactions of the fluid with the valve bodies, even during minimal valve openings. The software could refine the mesh as necessary, beginning with a large basic mesh and the working fluid volume:

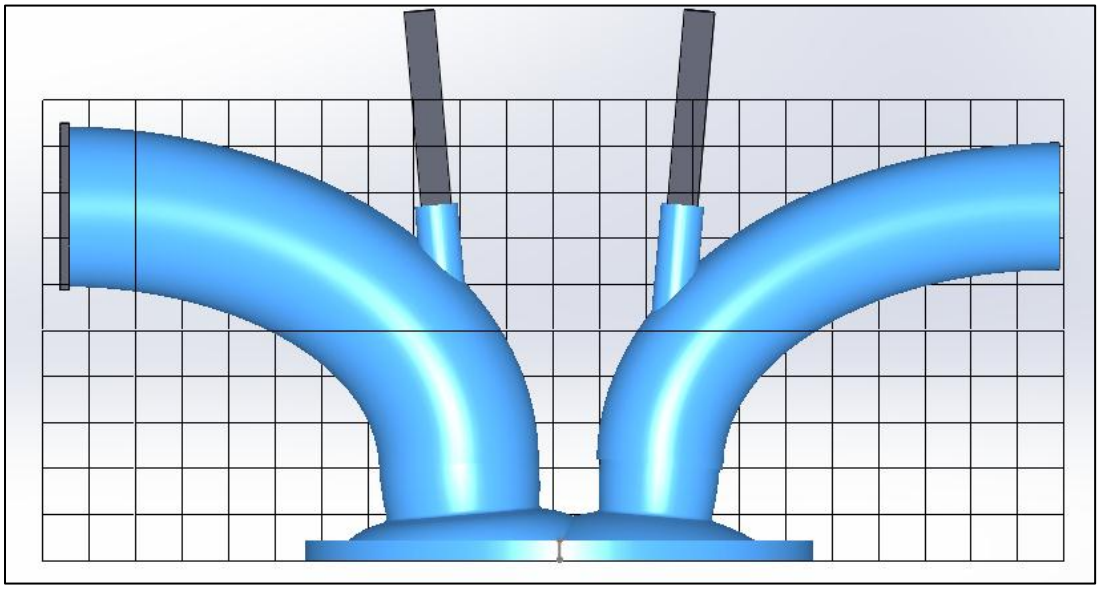

Figure 3.23 Basic mesh grid and fluid body used to refine the working mesh

This allowed a high-detail mesh to be generated for iterative solving. After the mesh had been generated, the overarching boundary conditions could be applied by the program and a solution could be generated. Post-Processing was also included in-program, so cut plots of both pressure and velocity could both be generated easily. An example of the Flow Simulation tree,

complete with all boundary conditions, mesh generation, and post-processing capabilities, can be seen below.

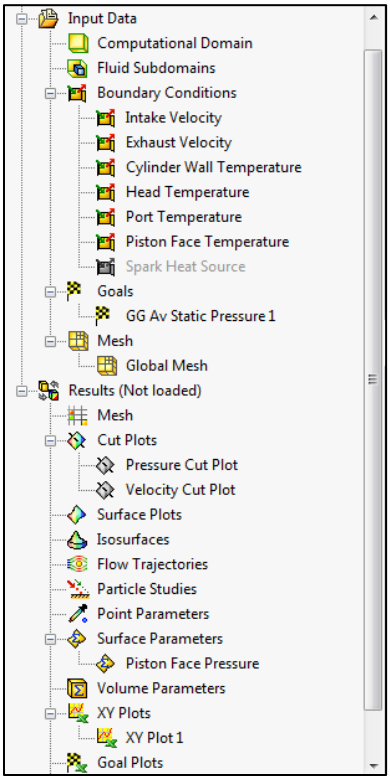

Figure 3.24 The design tree for Flow Simulation

At this point, the full 720° cycle was evaluated for both systems and the results were compiled in Chapter CHAPTER Four:. The results of the combustion simulation were also compared to the cold flow simulations, and overarching inferences could be drawn based on similarities in system function.

CHAPTER FOUR: SIMULATION RESULTS

With the RVS, a four-stroke engine is anticipated to behave similarly to a traditional poppet valve-controlled system, with some key differences. The RVS will mate similarly to the original engine block, with a comparatively lower profile than the camshaft-poppet valve system (i.e. the RVS will occupy less space while performing the same operations). The RVS is expected to change the nominal work output of the engine, which will be the result of a more efficient mixing process of fluid entering the cylinder. An intersection of the pressure profile at the center line of the cylinder is also expected to hold a more consistent average value than the traditional system, which will again suggest more efficient mixing.

4.1 Cold Flow Results from SolidWorks

Theoretically, the open rotary port will give the fluid flow a substantially larger area to flow through, as the elimination of a poppet valve head will open the port area and decrease interference with flow streamlines. By decreasing this resistance to flow, pressure variations will decrease, and the available mixing energy will be more readily accessible to the cylinder.

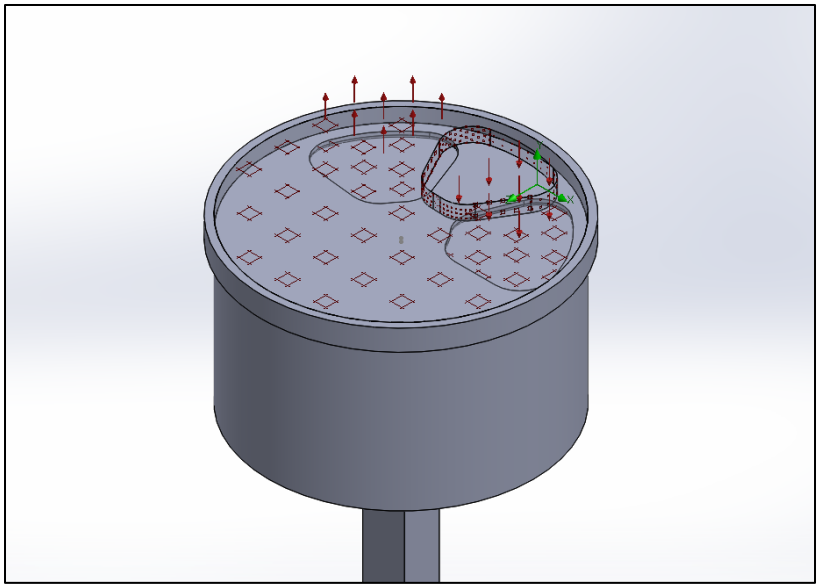

Figure 4.1 An RVS simulation set-up with imposed boundary conditions

Directly, this will translate into a more efficient mixing process and give the engine a more stable fuel-air mixture, which will translate into a more efficient burning process. Exhaust gas will contain less unburned fuels, and the output power from the combustion process will be more consistent between cycles. While the direct comparison of these inferences from a cold flow simulation does have limitations, the collected data can still be used to gain valuable insight into the basic behavior of the system.

The Cold Flow Simulation was run for every intake CAD from 0° to 220° in increments of 20°. After running each cold flow simulation, 100 pressure data points along the centerline are collected. These are then incorporated into the overarching data set for the simulation, for both the traditional and the RVS systems. After compiling the data, the following pressure plot can be assembled:

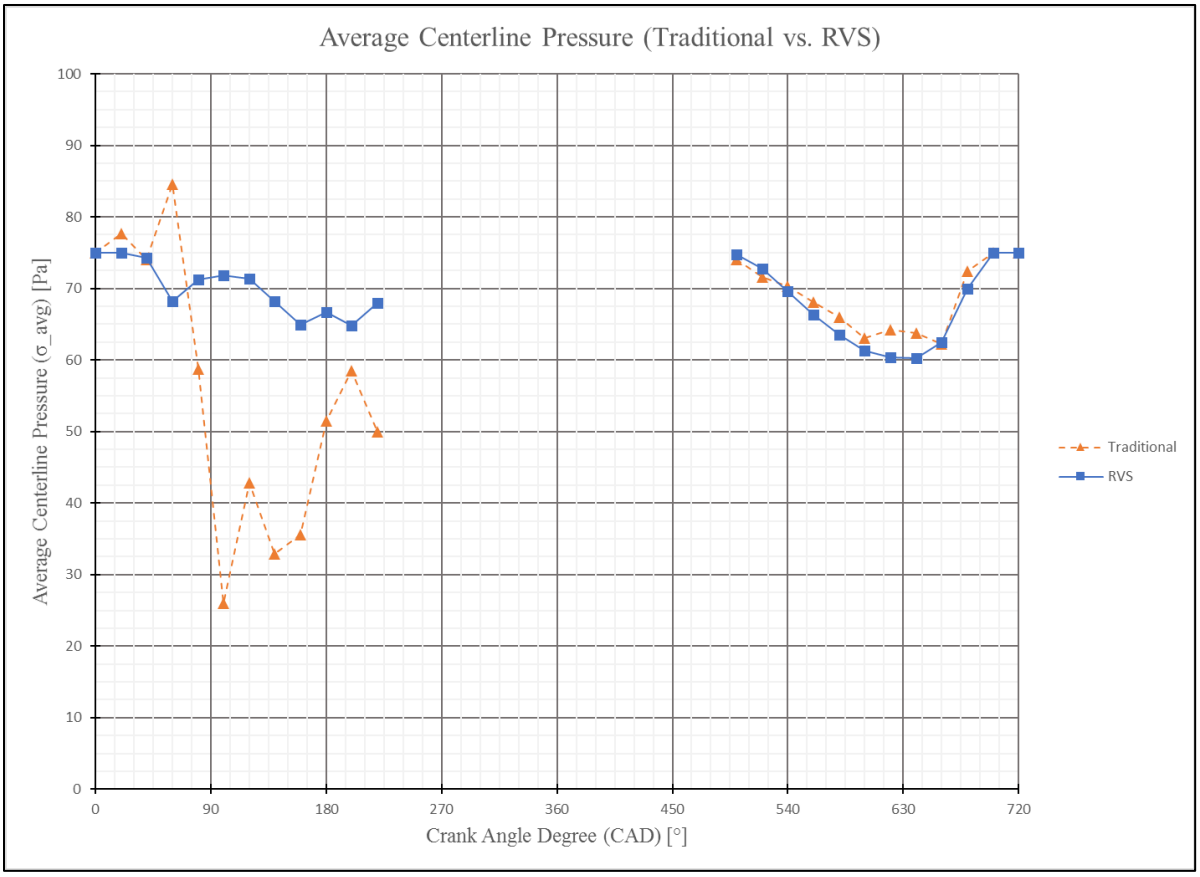

Figure 4.2 The average cylinder centerline pressure

As seen in Figure 4.2, the average pressure during the exhaust stroke for both the traditional and RVS systems align well; both systems show a minute drop in the average pressure during the peak of the exhaust stroke, on the order of ~15Pa. This suggests that, during a stroke, during periods of low flow resistance, the average pressure in the centerline of the cylinder can be less since there are fewer secondary head losses due to restrictive flow conditions at the inlet and outlet. Overall, a decrease in flow resistance means that the working fluid can move with a lower pressure gradient.

During the intake stroke, the results from the two systems deviate, albeit almost negligible in value. For the traditional system, the pressure gradient increases to promote fluid flow around the intake valve head. However, for the RVS system, the pressure drop is almost insignificant; on the order of ~5Pa. This is comparatively 10% the drop of the traditional system. This suggests that, overall, the system pressure change is minimal across the centerline, as flow can move without restriction or head loss from abrupt changes in geometry.

4.2 Velocity Cut Plot Comparisons

For every CAD simulated for both the traditional and RVS, a cut plot of the velocity was taken to be compared. The velocity plots of most interest, however, are those at 0°, 120°, and 620°. 0° is the beginning of the four-stroke cycle and represents what is known as the crossflow stage. During crossflow, both the intake and exhaust valves are opened slightly. This is done to promote complete evacuation of the remaining exhaust gasses using the momentum of rapidly flowing fresh intake fluid. In doing this, the next combustion cycle is ensured to be as clean as possible, without any residual exhaust prohibiting the combustion process.

120° is the point in the simulations at which the intake valve is at its most open position. This represents the time of greatest intake flow and can serve as an effective descriptor to the way the intake fluid is reacting to the geometry of the valve train. 620° is similarly the point at which the exhaust valve is at its most open point. This can serve as an accurate representation of how the cylinder fluid moves around the exhaust valve before exiting the cylinder.

After completing the SolidWorks cold flow simulations, the velocity cut plots for the timing positions can be analyzed for their differences and similarities. The two figures below, Figure 4.3 and Figure 4.4, are the velocity plots for the traditional and RVS, respectively.

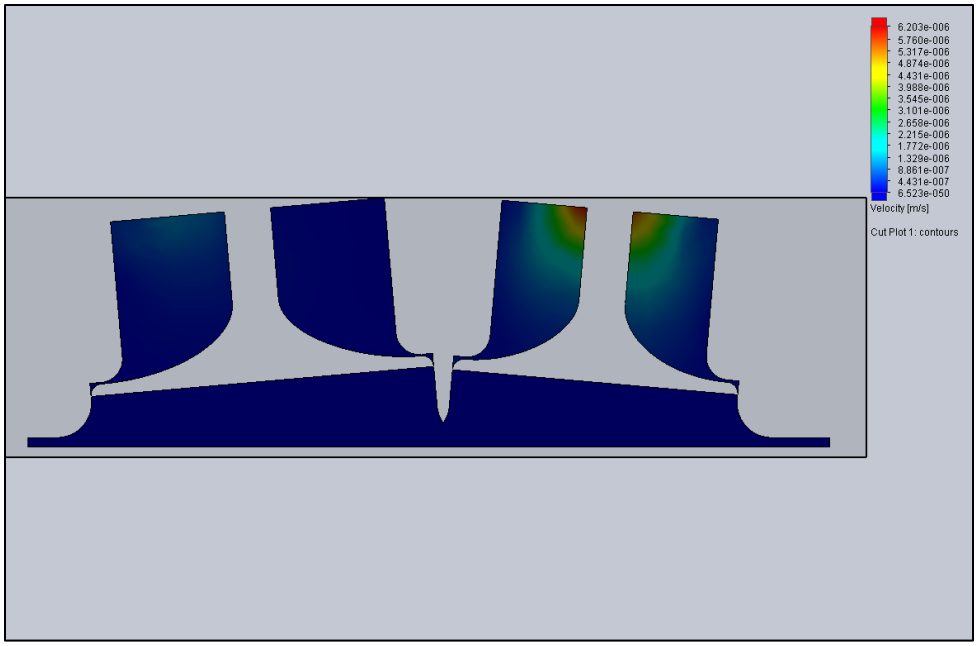

Figure 4.3 0° Crossflow velocity cut plot for the traditional system

As seen above, the velocity flow conditions for the crossflow degree in the traditional set-up can be assumed negligible. Contrarily, the cut plot for the RVS system below shows a different behavior:

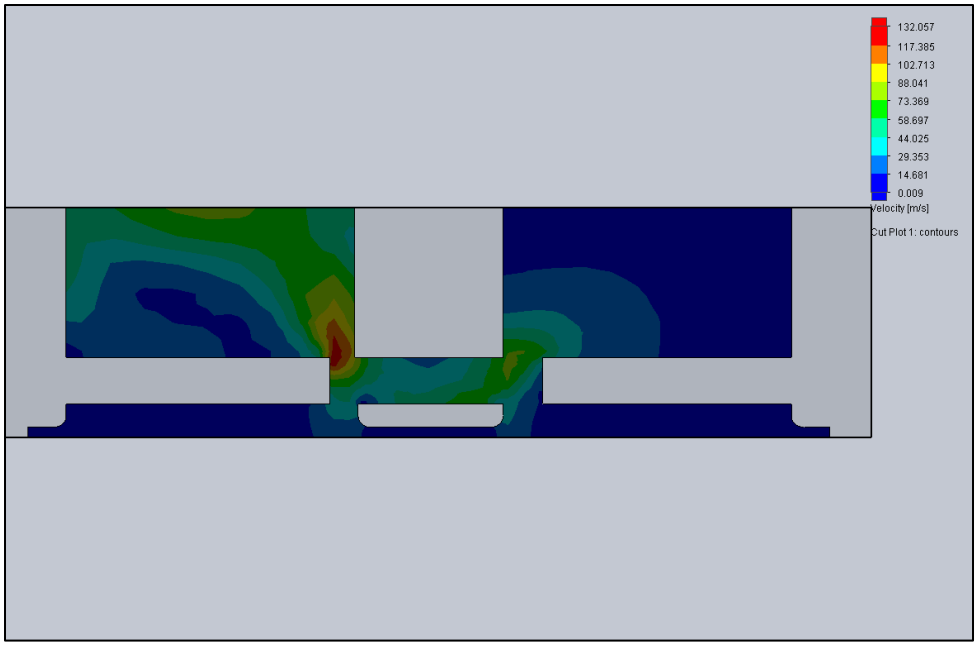

Figure 4.4 0° Crossflow velocity cut plot for the RVS

Fluid is permitted to flow freely from intake (Right port) to exhaust (Left port). This results in a high velocity value in the areas of the RVS head which may still create a bottleneck during overlap. As seen above, one such area is the interface point between the exhaust port and the rotor port, where the velocity (Highlighted in red) can reach values of 130^{+}m/s. In realistic practice, this may cause issues with high velocity flow, however for the simulation the effect on the cylinder centerline was negligible. This suggests that centerline variance remained virtually unaffected by increased crossflow conditions in the head. Since the flow condition in the traditional system left a negligible velocity profile, it was deemed inappropriate to represent the system at that point.

After comparing velocity profiles for crossflow conditions, it was then beneficial to compare them for both the intake and exhaust strokes at maximum valve lift:

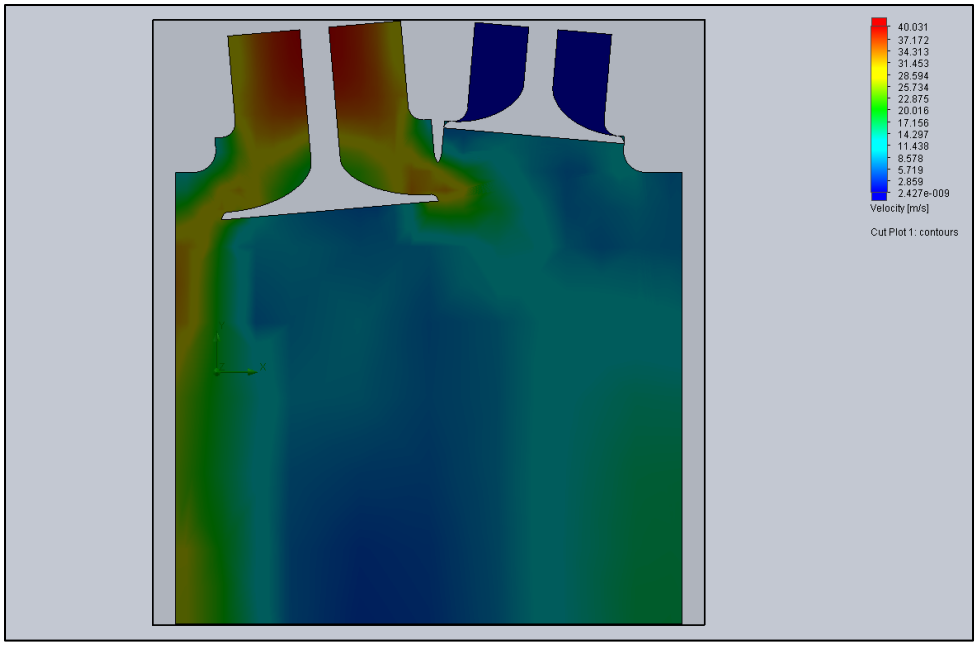

Figure 4.5 120° Intake velocity cut plot for the traditional system

As seen above in Figure 4.5, the velocity plot at the maximum intake value lift shows its highest values before striking the valve head and directly adjacent to the valve head edge. This sudden pinch in geometry suggests a rapid change in velocity into pressure potential, and the loss in momentum is characterized by areas of high velocity followed by adjacent areas of comparatively lower velocity. Above, it is apparent that the highest velocity of ~40m/s occurs right as the fluid interacts with the valve head, and then drops significantly to ~15-20m/s in the cylinder. This rapid velocity change can also produce a large pressure gradient. In contrast, the RVS shows a different velocity profile at this point:

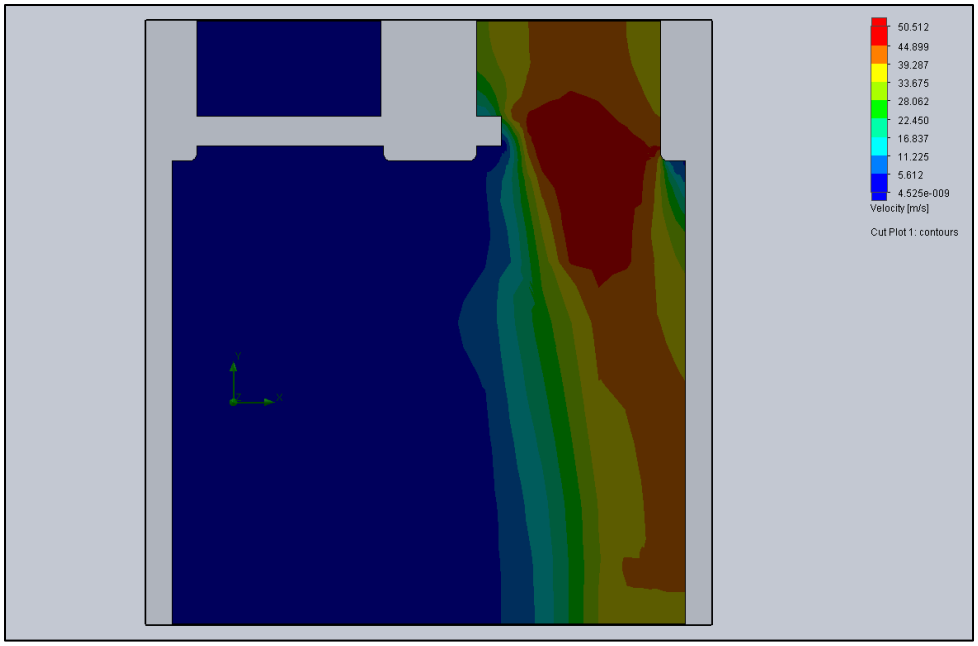

Figure 4.6 120° Intake velocity cut plot for the RVS

As seen above, the velocity plot shows a much more fully developed velocity field in the mouth of the intake port. A similar maximum velocity of ~50m/s is shown here, but the contour areas extend into the cylinder, holding a much higher magnitude even after reaching the piston face. This could suggest that, even with a higher velocity through the neck of the intake port, the cylinder is able to more readily accept the fluid without obstruction, so the pressure gradient is less pronounced.

The exhaust stroke also holds valuable information regarding the interaction of the valves with the working fluid:

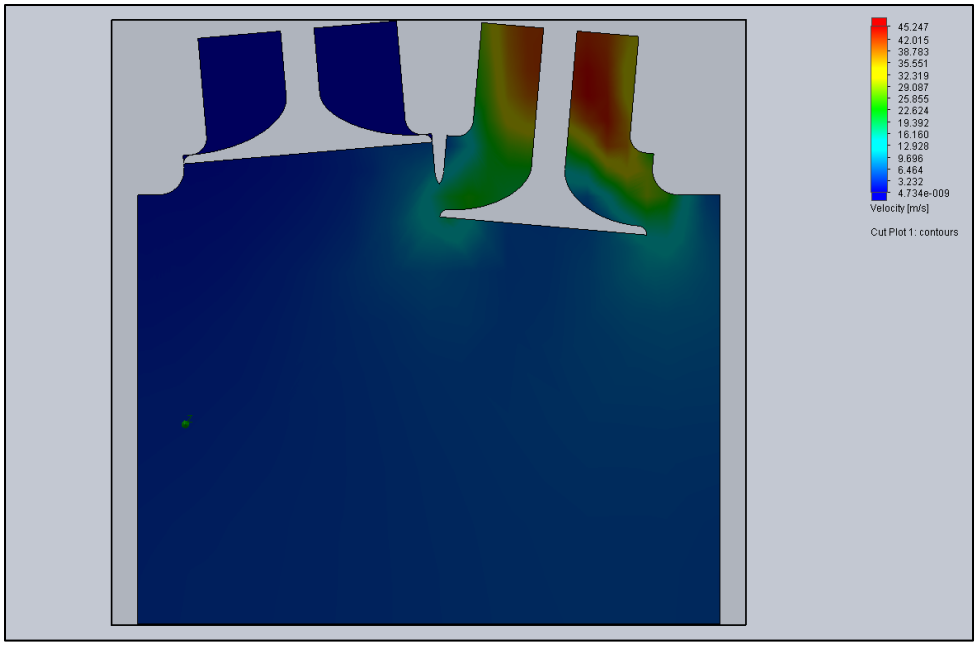

Figure 4.7 620° Exhaust velocity cut plot for the traditional system

From Figure 4.7 above, the behavior of valve obstruction also seen in Figure 4.5 is apparent again. However, in this case the overall velocity contours in the cylinder are more consistent, holding values closer to ~0m/s. Above the valve head, the velocity increases to ~45m/s, and the geometric pinch found in Figure 4.5 is not seen here; This could be contributed to the smaller diameter of the exhaust valve – 25mm versus the 30mm of the intake valve. This smaller diameter gives the valve displacement a smaller cylindrical area for the fluid to flow through but keeps this flow boundary farther away from the cylinder walls, thus reducing the tendency for flow to congest at the interface of the two faces. For the RVS system, this change in behavior is seen again:

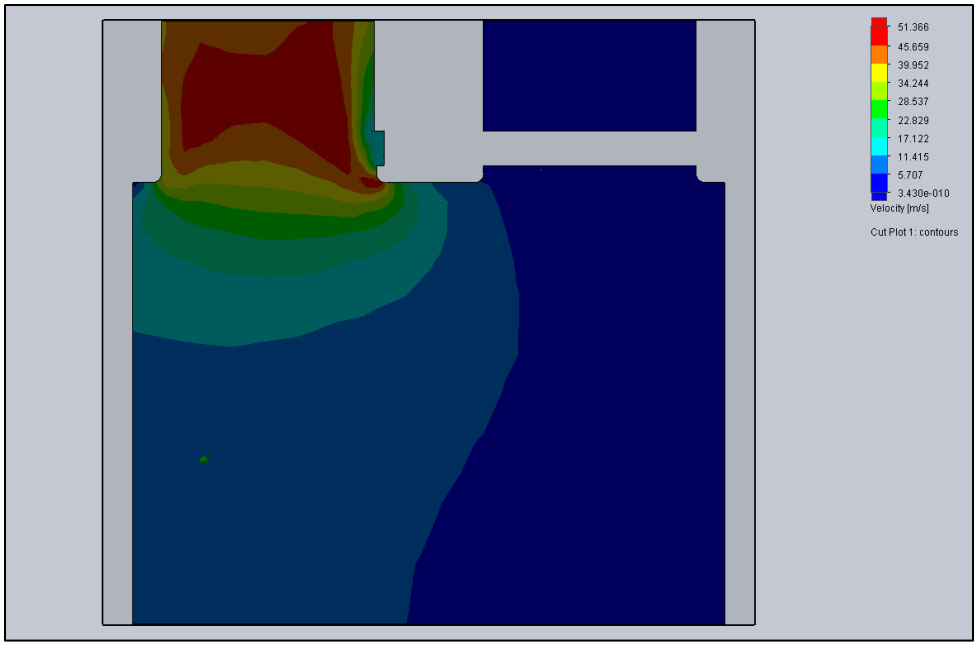

Figure 4.8 620° Exhaust velocity cut plot for the RVS system

As seen above in Figure 4.8, the RVS shows a more stratified velocity gradient within the entire cylinder. The fluid within the cylinder is not obstructed as in the traditional system by the poppet valve head, and as such can develop a more consistent streamline path into the exhaust port. The order of magnitude of flow near the exhaust port reaches ~50 m/s, which is comparable in magnitude to that of the traditional system. Overall, the system serves close to the same function as the traditional system with regards to outlet flow capabilities.

4.3 Issues with SolidWorks Cold Flow Analysis

As valuable the insight from SolidWorks is in the preliminary dissection of the RVS' efficiency, the process of modelling this system was not without its challenges. Of most concerning issues with the program was the tendency of the simulation to diverge within a

reasonable number of iterations when attempting to converge on the average pressure value goals within the constraints; However, several other issues such as boundary conditions and single flow conditions caused problems as well.

When defining the boundary conditions of the system simulation, there were several issues with vortices and their influence on iterations of the simulation. In several cases during setup of the simulation, it was found that an inlet flow boundary condition was creating significant vortex generation due to the sudden change in geometry from a short inlet source to an open cylinder; especially since the inlet was off-center with respect to the axial line of the cylinder. When such a generated vortex crosses a specified boundary, SolidWorks automatically issues a warning to the user, specifying the ratio of inlet/outlet flow caused by that vortex. In most general cases, this ratio is low enough to be ignored; that is, the vortex back-flowing into the opening boundary does not significantly affect the simulation results. However, this can still be an issue of concern during simulation, and the effective iterations can be changed by this interaction.

To help combat the issue of vortices crossing the inlet, a special 10mm plenum was added to the outer face of the cylinder head, for both the RVS and the traditional system. As seen below, the plenum served to draw the inlet further away from the valve face interaction:

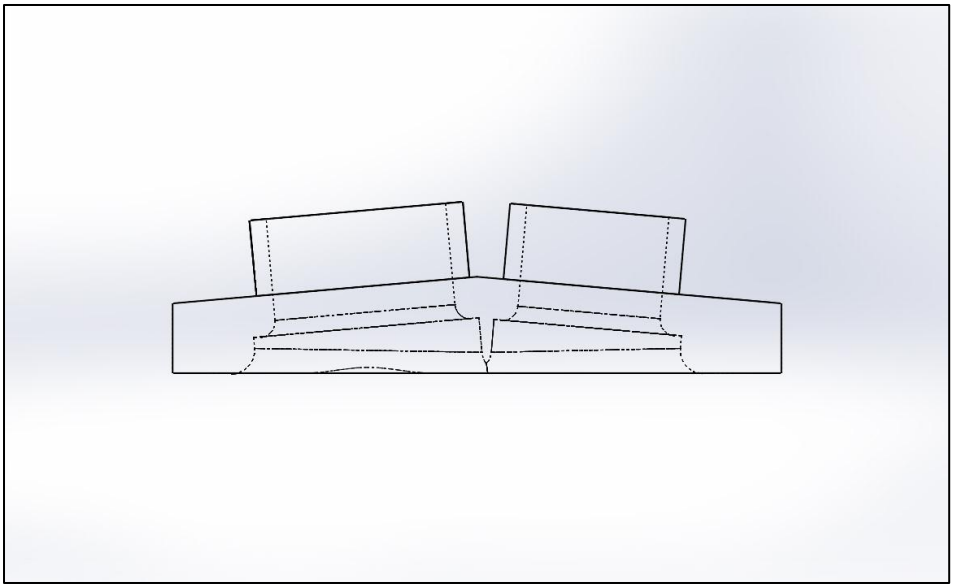

Figure 4.9 A wire-view showing the plenum drawing the inlet further away from the head ports

This 10mm plenum length was also applied to the outlet; for consistency. Likewise, this was also applied to the RVS rotor head cover:

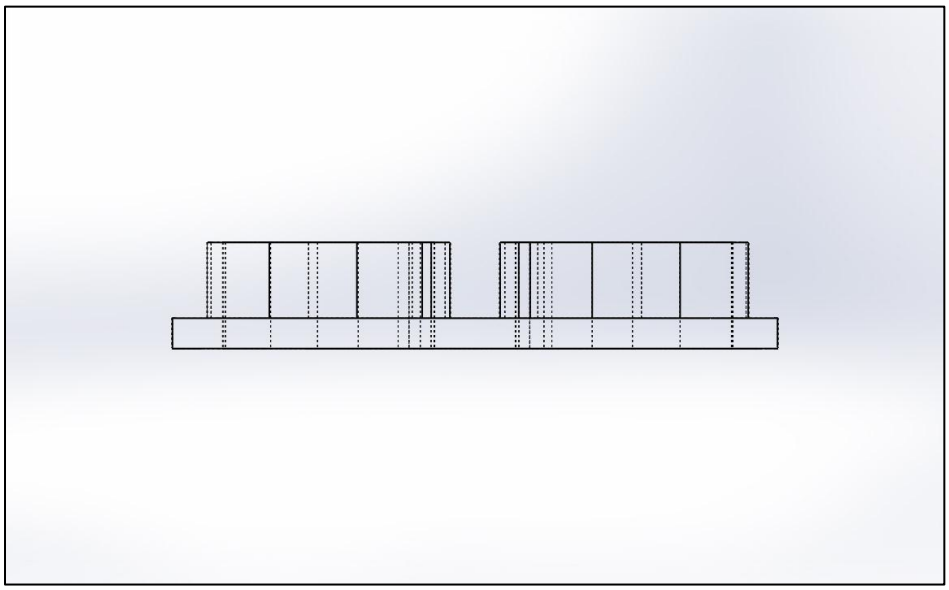

Figure 4.10 A similar plenum used on the RVS

In this way, the effect of the vortices crossing the boundary was found to be much less consistent during iterations of the simulation.

SolidWorks Flow Simulation has a built-in function that automatically creates the bounds for the computational domain based on flow conditions of a cavity. For example, the program will begin with the inlet flow face, and will then mesh any adjacent continuous cavities into a single fluid volume to use for the calculations. This is designed as a labor-saving protocol; by reducing the area to hold within the computational domain, SolidWorks can drastically cut down on RAM use during the iterations of the calculations, since drastically fewer fluid cells will need to be iterated. However, this creates an issue for the simulation during the exhaust stroke: For approximately 440° of the cycle, from 240° to 680°, the intake valve is completely closed (although in practical applications valve float can cause a valve to remain open during this time due to a necessary acceleration to the closure velocity). For the simulations, this meant that the entire inlet area was sealed off from the cylinder. This subsequently meant that SolidWorks would automatically cull the entire cylinder from the computational domain, since there were no attached inlet flow conditions to the volume This initially prevented a simulation procedure from generating any working fluid volume.

To combat this issue, two binding variables needed to be altered during the exhaust stroke. Firstly, the intake valves had to be artificially “shimmed” to connect the cylinder to the inlet boundary conditions. This was done by lengthening the valve stem by 0.05mm during these CAD (Crank Angle Degrees), from 240° to 680°. By artificially holding the intake valve open, a

simulated “valve float” could be achieved. This meant that SolidWorks would then include the entire cylinder in the computational domain.

To couple this, the inlet boundary condition for the velocity of the fluid also had to be changed. To ensure that the valve float induced from the inlet did not adversely affect the simulation, the inlet boundary condition was set to 0m/s, thus effectively rendering the inlet plenum a stagnant environment. These two conditions together made simulation of the entire system possible.

The largest issue inherent with SolidWorks Flow Simulation was the sensitive numerical simulations which often diverged during the cold flow process. Initially, the inlet and outlet boundary conditions were held constant throughout the entirety of the simulation CAD’s, but this was found to adversely affect the ability of the simulation to converge on the pressure value goals. Prior to changing the inlet and outlet velocities to be related to the valve openings, both the intake and exhaust stroke simulations suffered from divergent calculations during the end of each stroke. Most likely, this can be attributed to the geometric pinch caused when the valves close, thus increasing the required cross-sectional flow rate to keep the inlet and outlet plumes consistent with their respective boundary conditions.

After realizing this issue, the velocity profiles in Table 3.4 were developed to more accurately simulate the flow conditions. These values completely resolved the issue of divergence in the simulations.

4.4 Full Combustion Cycle Results

After running the entire 720° combustion simulation, the numerical data was compiled in Appendices F-K. Similarly, the cut plots for both systems can be found in Appendices N-Q.

While the cold flow simulations are valuable in suggesting possible influences to flow, the full combustion cycle provides much more information as to the nature of how the RVS can change the behavior of the fuel and air even after the intake stroke has ended. In order to highlight the differences between the two systems, pressure graphs are represented using a gauge pressure versus relative atmosphere (~1 Bar).

The intake stroke itself showed change from each system:

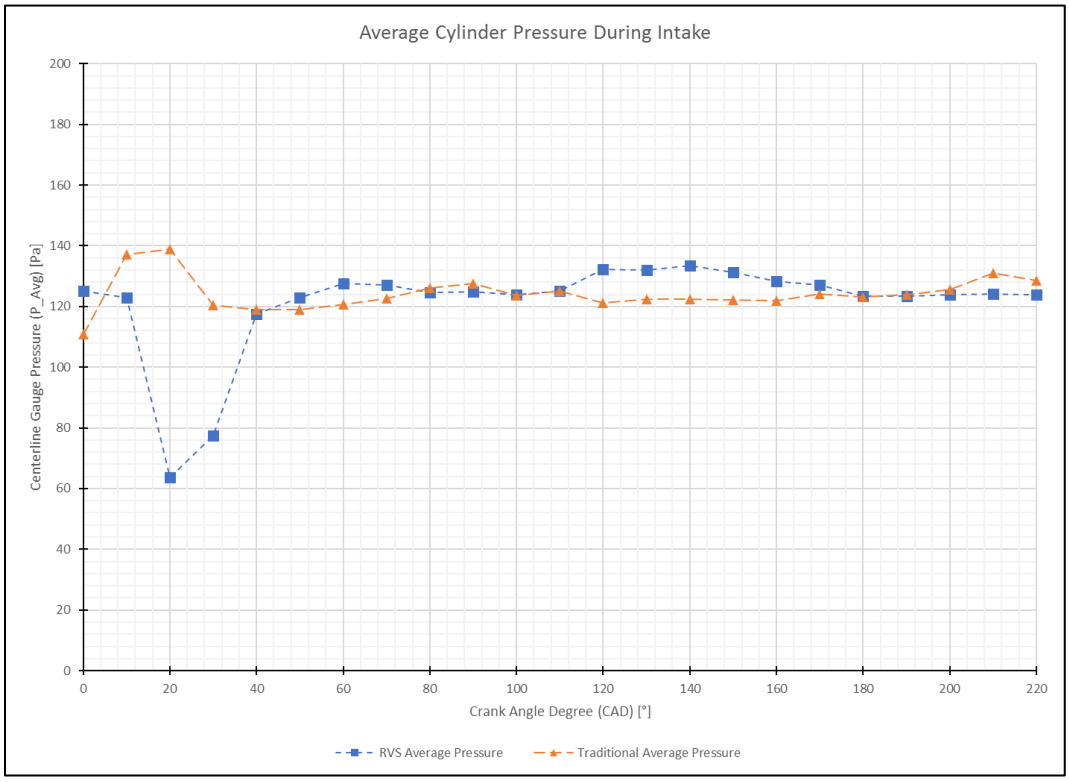

Figure 4.11 Average Cylinder Pressure during the Full Cycle Intake Stroke

As seen above in *Figure 4.11*, the average cylinder pressure during the intake stroke remains nominally consistent with the inlet boundary conditions. As the RVS intake port opens,

there is an approximately ~40 Pa drop in pressure, but this quickly normalizes as the port reaches its fullest opening. Consistently, the two systems here do not appear to differ significantly from one another.

The temperature of the fluid during the intake stroke followed a general heating trend, as expected:

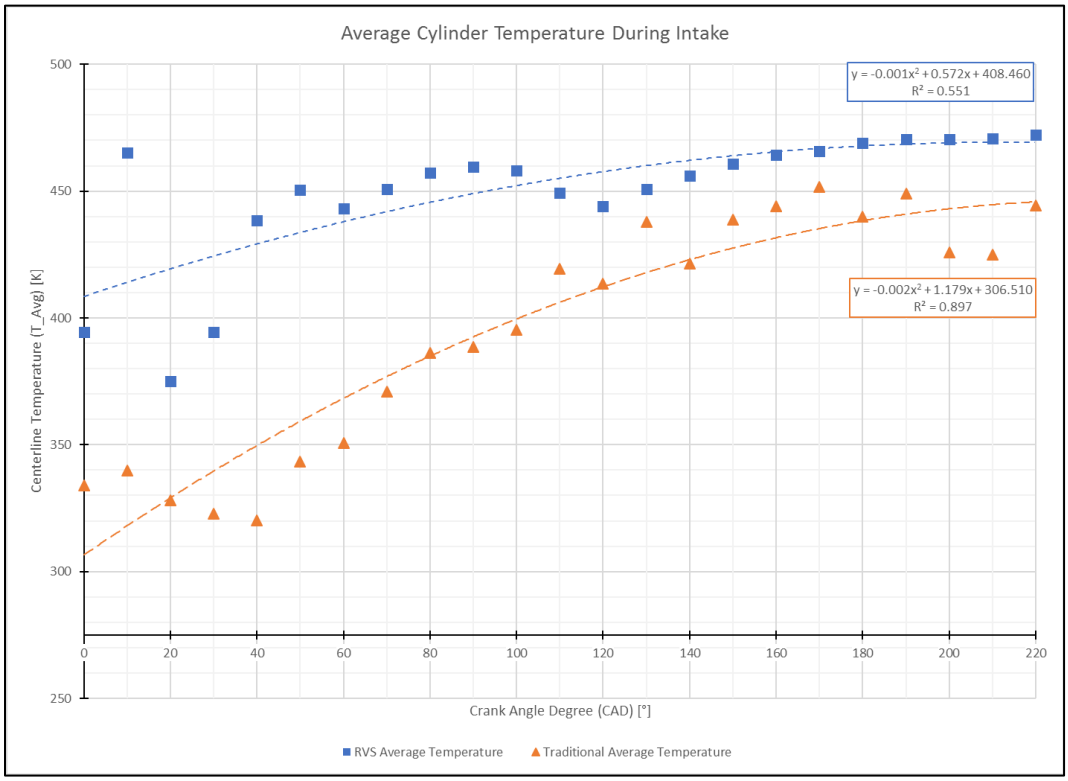

Figure 4.12 Average Centerline Temperature during Full Cycle Intake Stroke

In Figure 4.12, the average temperature of the fluid increased as the cylinder expanded, which is a logical result of the fluid coming in more contact with the walls of the cylinder. Overall, the RVS intake fluid had a higher temperature during intake than the traditional system. Most likely, this is due to the boundary conditions set for the RVS system- the rotor was given

the same face temperature as the poppet valve in the traditional system. However, the rotor is much larger than the poppet valve, and generally more surface area meets the fluid during the stroke. This would result in a longer contact time during flow into the cylinder and could result in a higher temperature.

Cut Plots of the velocity and pressure profiles also show key differences in the fluid flow:

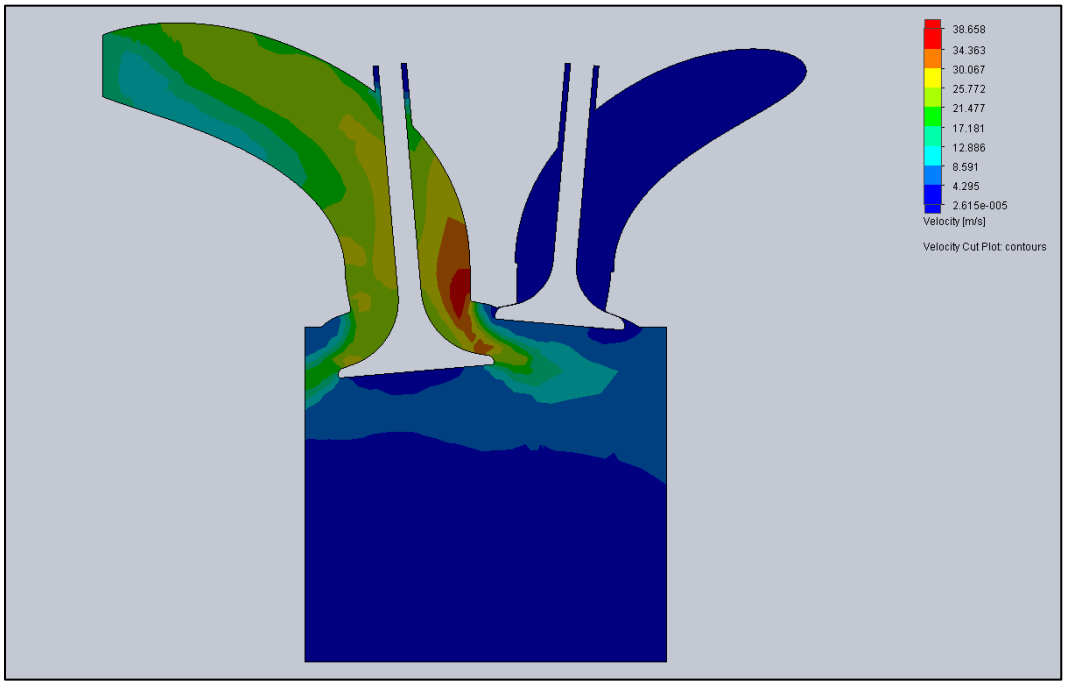

Figure 4.13 Velocity Cut Plot for Maximum Traditional Intake Valve Opening 120°

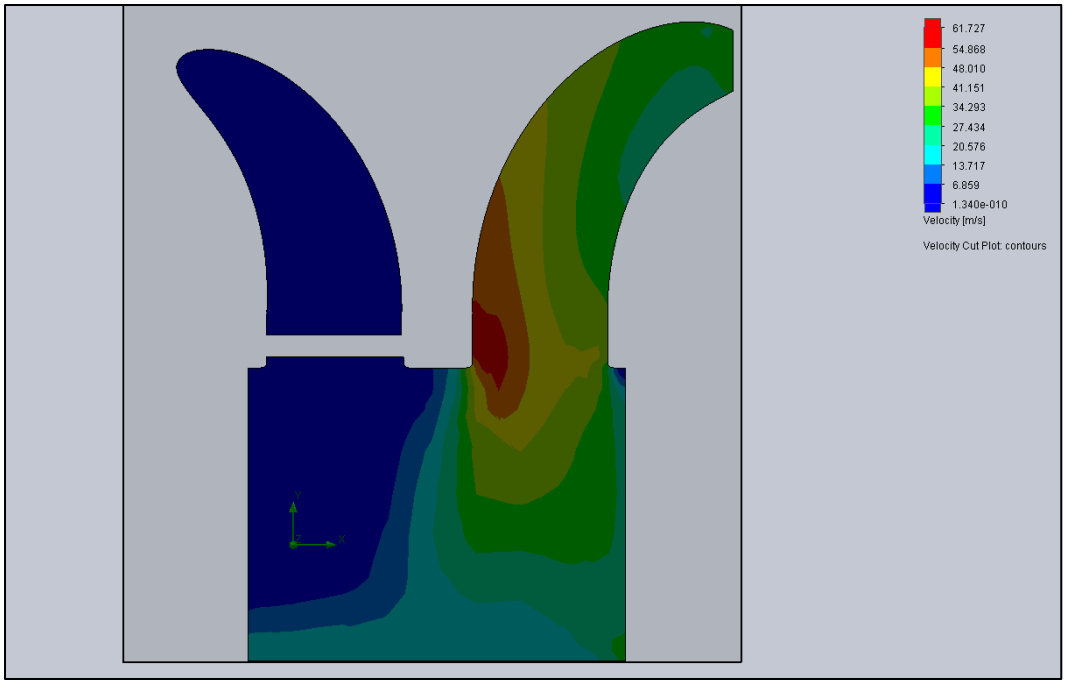

Figure 4.14 Velocity Cut Plot for Maximum RVS Intake Port Opening 120°

As seen in the above figures, the RVS and Traditional systems show the same behavior as the Cold Flow analysis. In Figure 4.13, the poppet valve head provides significant restriction to the flow of the intake fluid, limiting intake velocity to ~38 m/s. However, in Figure 4.14 the RVS allows unrestricted fluid flow, promoting flow velocities of ~60 m/s. This promotes the assumption that the RVS encourages fluid flow and is less restrictive than the traditional system.

Another valuable comparison between the two systems is the ability to generate a vortex in the cylinder during the intake stroke. By comparing velocity vectors of the two systems, the difference in vortex generation can be seen:

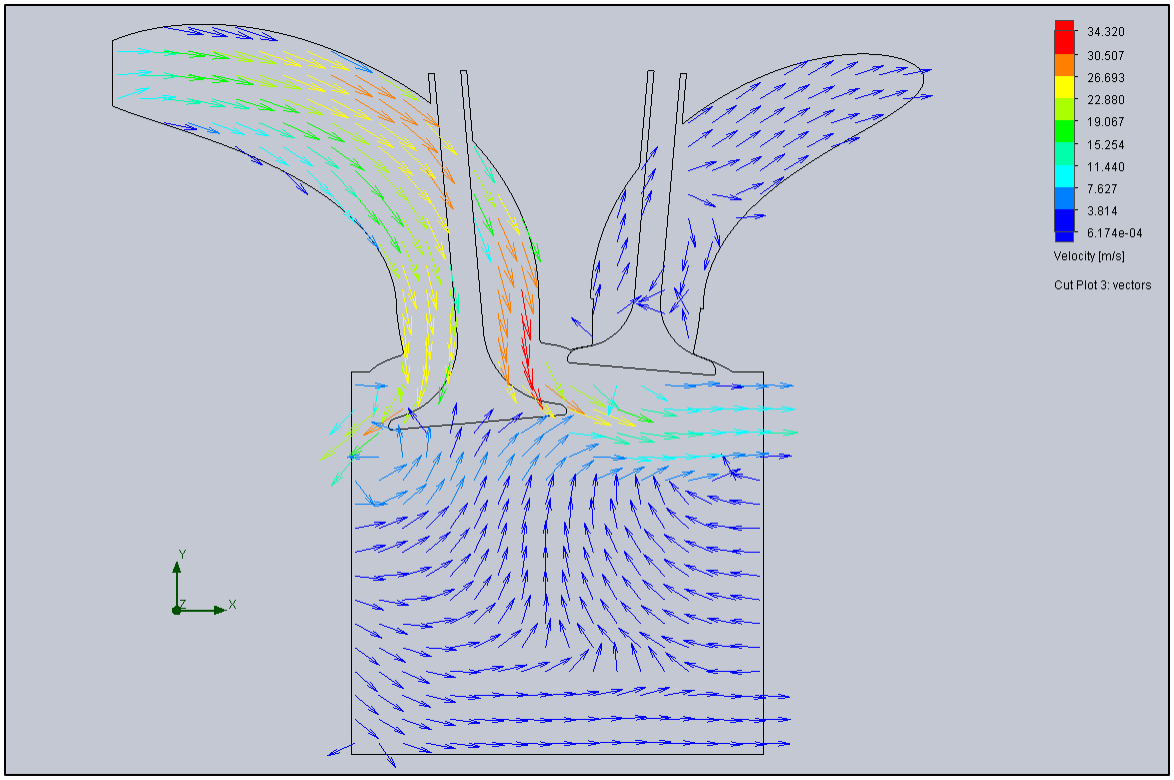

Figure 4.15 Swirl generation in the traditional system at 120° CAD

As seen above, the velocity vectors in the traditional system during the intake stroke suggest that, generally, the fluid moving into the cylinder is displaced randomly as it interacts with the poppet valve head. After moving around the obstruction, the fluid is then left to propagate throughout the cylinder, with a large portion of the fluid moving outwards perpendicular to the poppet valve before descending into the cylinder. However, this behavior is not seen in the RVS:

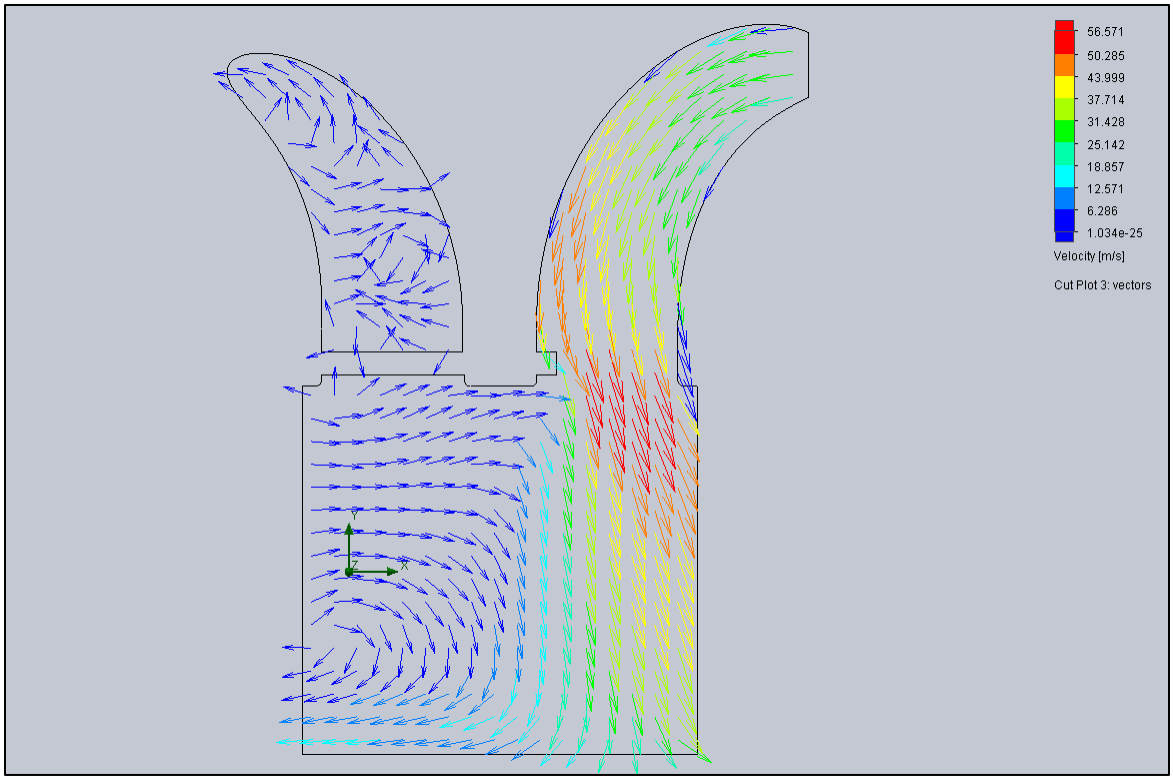

Figure 4.16 Swirl generation in the RVS at 120° CAD

As seen above, the RVS has the tendency to naturally generate a vortex in the cylinder as the fluid flows through the rotor valve. As the fluid reaches the bottom of the cylinder, the fluid tends to "curl" upwards and around the exhaust valve, resulting in a significantly well-developed vortex forming in the opposing side of the cylinder. Vortex formation is valuable during intake, as this promotes thorough mixing of the air and fuel before combustion and tends to create a more complete combustion process, with less residual unburned hydrocarbons.

The most important part of the simulation is the combustion and exhaust strokes, as these alluded to the effect of the previously mentioned intake stroke on potential work available to the

piston face. After calculating the resulting pressures from compression and simulating the full cycle, the results for the combustion stroke can be seen below:

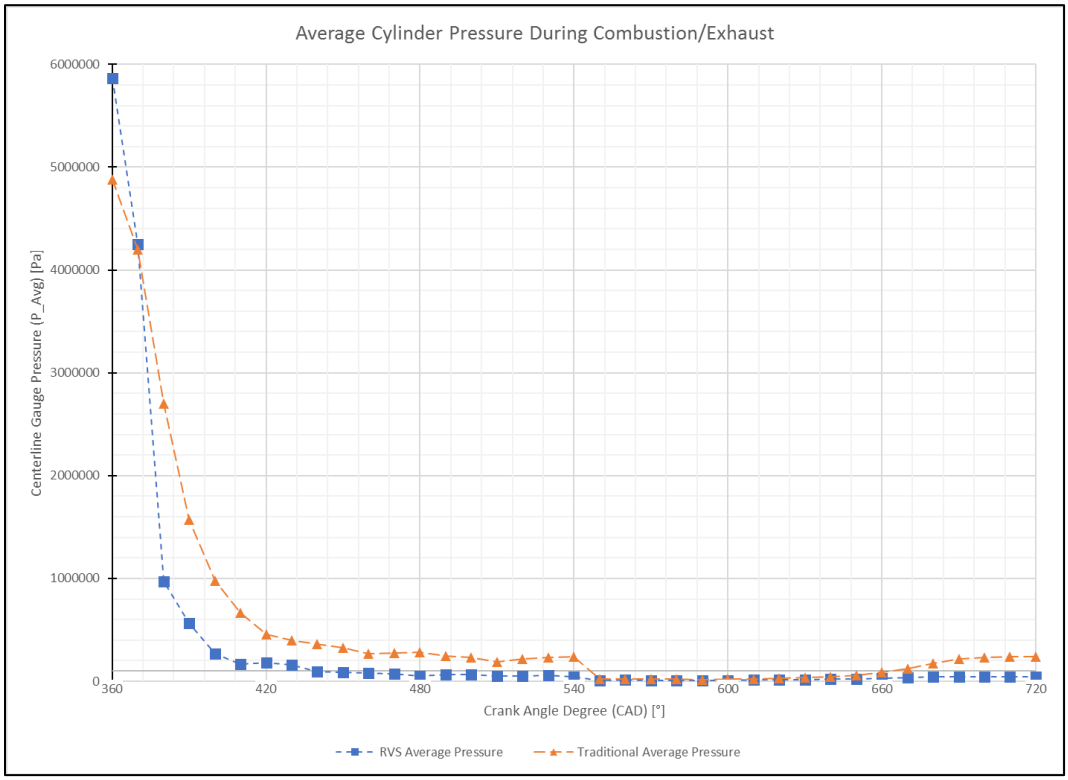

Figure 4.17 Average Cylinder Pressure During Full Cycle Combustion/Exhaust Strokes

Figure 4.17 shows valuable information regarding the combustion process for the two systems. The traditional system shows an overall higher-pressure during combustion, and it also shows the familiar pressure spike during the exhaust stroke as the fluid is forced out of the exhaust ports around the poppet valve. Of interest to note is that the RVS system shows a higher initial pressure than the traditional system. This could be due to the more uniform mixing of the fuel allowing for a faster combustion at the spark off point. While this shows information

regarding the pressure profile, of more interest is the actual pressure available to the piston face, as this is what is used during the power stroke.

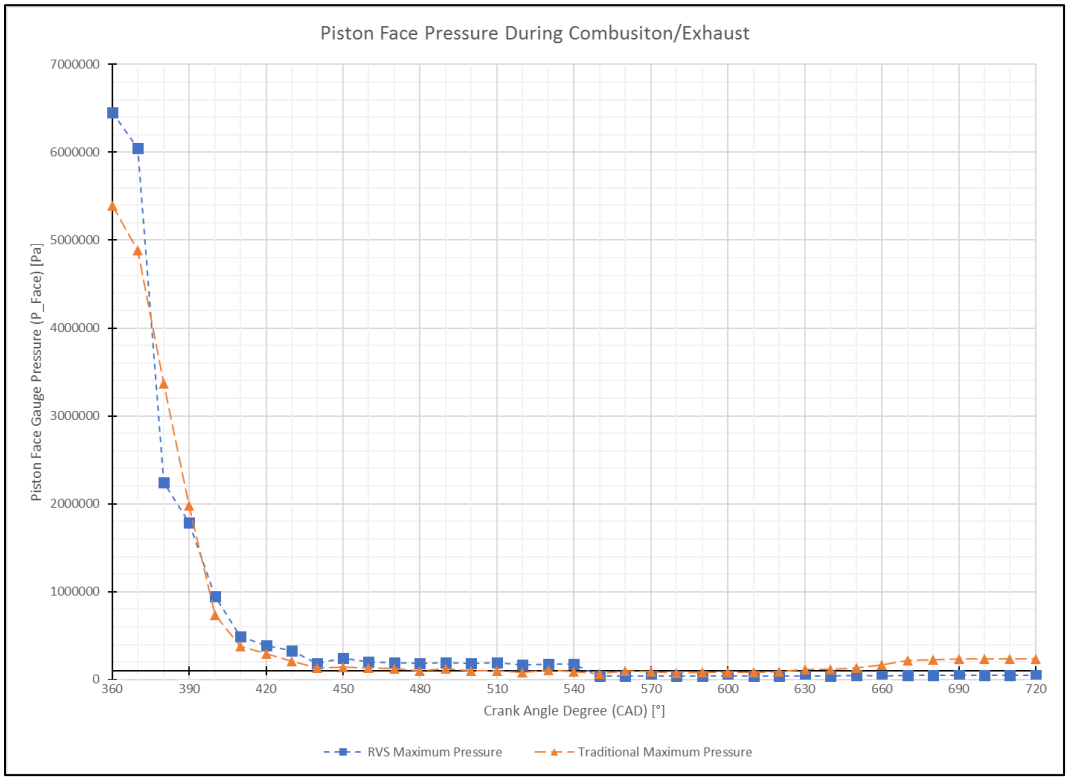

Figure 4.18 Available Piston Face Pressure during Full Cycle Combustion/Exhaust Strokes

Figure 4.18 Shows excellent comparative data for both systems. While Figure 4.17 shows that the traditional system has an overall higher-pressure during combustion in the cylinder, the RVS system appears to have much more pressure available to the piston face during combustion. The traditional system still displays the pressure spike at the end of the exhaust stroke, as expected.

The changes in the system behavior can be seen more clearly given a logarithmic scale for reference:

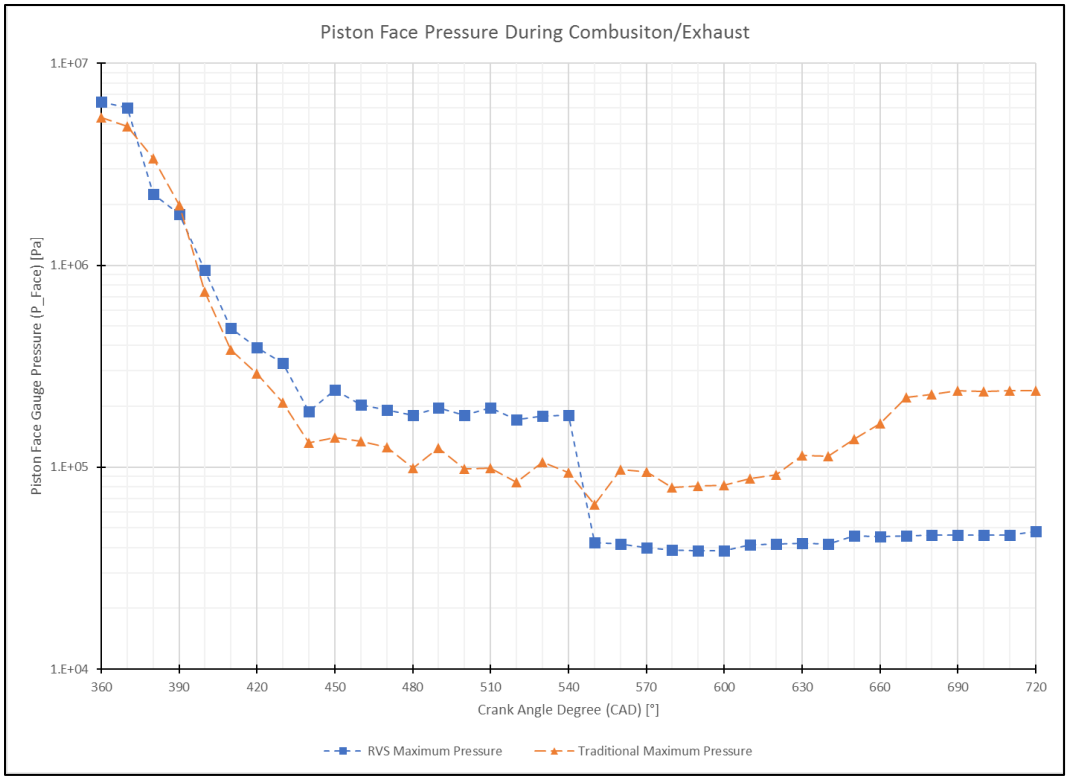

Figure 4.19 Logarithmic Scaled Piston Face Pressure for Full Cycle Combustion/Exhaust Stroke

As seen above, the RVS offers more pressure at the piston face for almost the entirety of the combustion stroke. Naturally, the high pressures at the beginning of the stroke mean that it is more beneficial to have higher pressure early on during combustion than later.

To more robustly compare the available work to the piston face, mathematical relationships can be used:

4.1) $$\delta W_b = Fds = PAds = \int_1^2 PdV$$

Where W_b is the boundary work, P is the pressure available to the piston face, and dV is the change in volume. The relationship for the piston displacement (ds) is already known from Equation *3.8*, and the area of the piston face can easily be calculated using the values from Table

3.1 as A = 0.004536 m^2. However, the relationship for the pressure available to the piston face is not constant, as discrete 10° CAD simulations were used. Instead, the integral for calculating boundary work can be approximated using the Midpoint Rule:

4.2) $$\delta W_b = \int_1^2 PdV \approx \sum_{i=1}^{n} P_i A ds_i$$

Where n is the number of CAD dividing the simulation (In the case of the combustion stroke, n=18, from 360° to 540°), ds_i is the movement of the piston face for the i^{th} CAD, and P_i is the pressure available to the piston face at that CAD. Using this formula, and the values gathered from the simulations, it is possible to calculate the total boundary work done on the piston face during the combustion process. It was found that for the traditional system 225.09 J of work was done over the stroke, while the RVS produced 247.83 J of work. This nominal increase in available work output (~20 J) is the direct result of the changes done to the system by the RVS and shows a probable effect on the associated power output that the RVS can have.

The temperature profile of the system is also useful for viewing the interactions of the systems on the exhaust gasses:

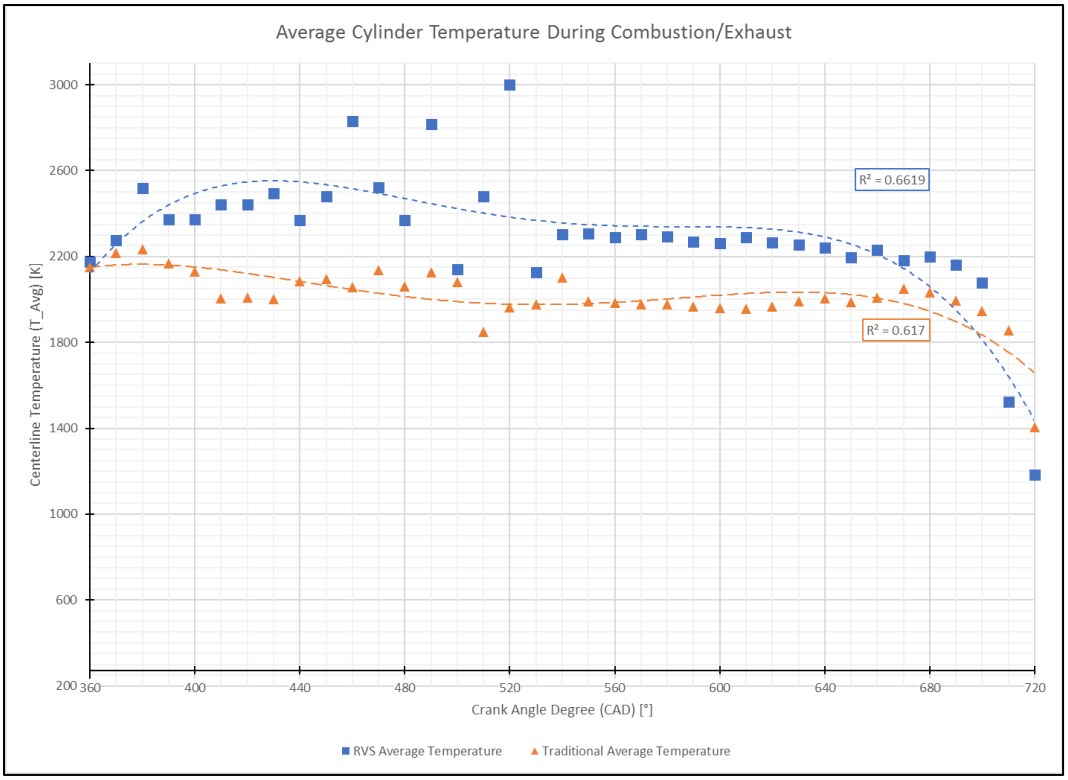

Figure 4.20 Average Cylinder Temperature during Full Cycle Combustion/Exhaust Strokes

As seen above, the RVS has an overall higher temperature than the traditional system for most of the combustion and exhaust stroke. This also suggests that the RVS system allows for the propagation of flame heat more evenly than the traditional system since the mixture is more evenly distributed.

Using Equations *3.10* and *3.11*, it becomes possible to find the mass present in each system during the compression and combustion strokes. Knowing the volume at the beginning of compression and the specific volume, it can be found that m_{trad} = 0.000128 kg and m_{RVS} = 0.00012024 kg. Knowing the mass present, as well as the values for specific heat of the Heptane and Air mixtures from Appendix R, it becomes possible to graphically compare the internal

energy of the systems. For simplification and a comparison of the pure impact of the temperature on the system, a constant average specific heat of ~280.41kJ/kg is used:

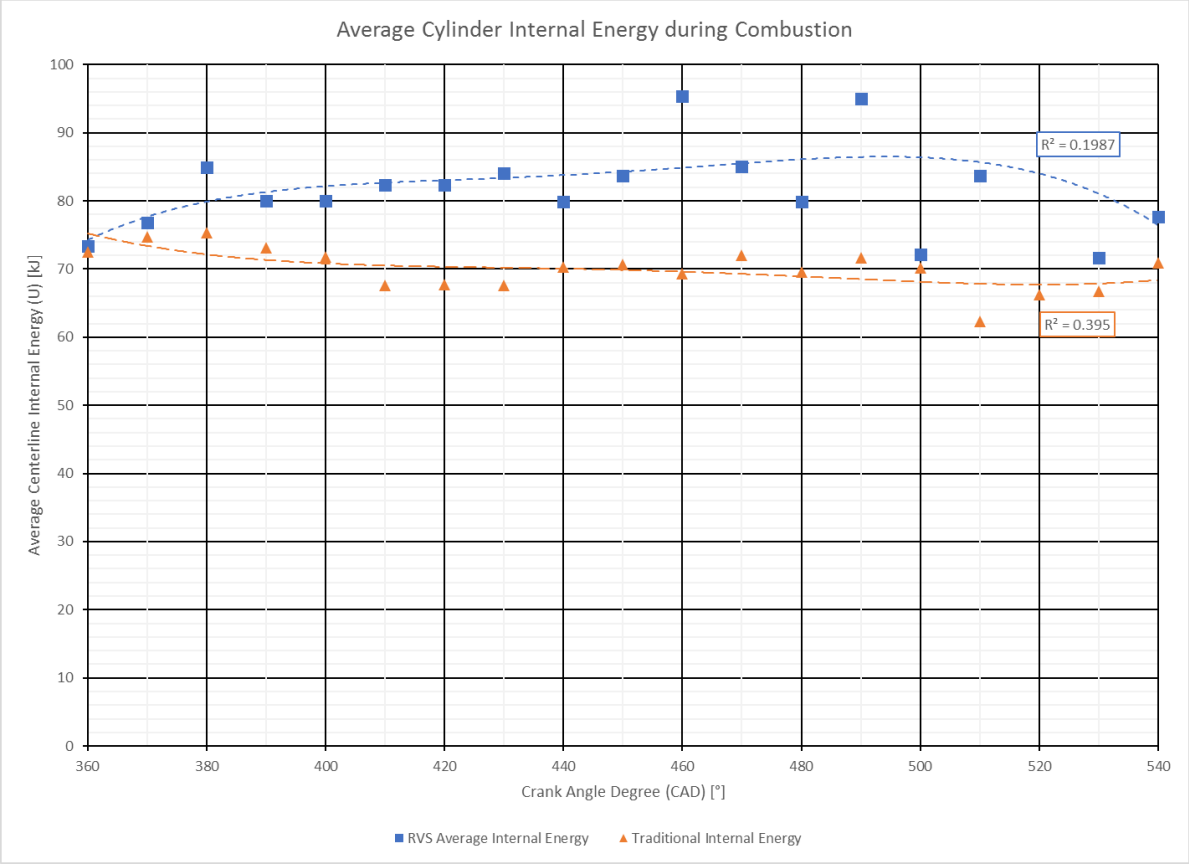

Figure 4.21 Average Centerline Internal Energy during Combustion

As seen above, the internal energy of the RVS system is consistently higher than that of the traditional. It should be noted that this is of the average internal energy during the entire combustion stroke, averaged throughout the centerline. This suggests that the distribution of pressure both encourages active energy transfer and allows propagation of the flame more readily than the traditional system. Comparing this to the pressure available from Figure 4.18, this distributed energy is not as readily available to the piston face during the combustion stroke

for the traditional system. Comparing the two systems, it can be found that, on average, the RVS system holds approximately 18% more internal energy during the combustion stroke. This change does not directly translate to gains in work output to the piston face but can be used as a comparator for changes in the systems.

CHAPTER FIVE: CONCLUSIONS AND CONTINUATION OF WORK

5.1 Changes between the Traditional System and the RVS

Overall, the Rotor Valve System shows improvement over the traditional system. The functionality of the system has been preserved, however the operating potential of the system has increased, as the overall ability to make power readily available to the piston face has increased. The restrictive flow interference of the poppet valves has been decreased, and the ability to move fluid into the cylinder has been made easier on the valve train.

The overarching goal of the thesis simulations was to determine the viability of an alternative head design, which utilized rotor valves in the place of traditional poppet valves and a camshaft. Of paramount concern was the work available to the piston face during the combustion stroke, as well as the ability to easily move fluid in and out of the combustion volume. As seen in CHAPTER Four:, the RVS provides ample evidence to an increase in potential work output at the piston face. The RVS also shows significant gain in internal energy, as evident from Figure 4.21. This roughly 18% increase in available internal energy translates to an increase in potential power that is extractable from the working fluid and confirms the initial notion that the RVS aids combustion through more efficient fluid flow.

The distribution of thermal energy in the system is also a key comparator to the differences in operation of the system. Overall, the RVS displayed an increase of approximately 238.88 kJ of thermal energy during the combustion stroke, due mostly to the increase in flame temperature. While most of this energy is not readily available to the piston face, it shows an increase in the potential work output, if the thermal energy could be more easily converted to pressure differential at the piston face. This is an approximate 18% increase in potential thermal energy production. As seen from the velocity cut plots of the traditional and RVS systems, the velocity gradient throughout the cylinder has also been normalized.

5.2 Future Work

While the simulations performed in SolidWorks were beneficial to the analysis of the potential of the RVS system, there are still many things that could be done to further verify the authenticity of the results. Performing a sensitivity analysis could help allude to which factors affect flow potential the most. Putting the system into a more in-depth CFD program such as OpenFoam or Fluent could allow a much more rigorous analysis of the performance of the system. However, experimental design and testing of the system would be the most definite way to draw conclusions about the behavior of the RVS in a real-world environment.

It is not known which parameters affect flow the most in the RVS system. It is assumed due to the nature of the RVS that the major affecting factor is the shape of the ports leading to the cylinder, but there are other characteristics which could also lead to changes in fluid behavior. The shape of the rotor itself and the timing could play a significant role in the behavior of the fluid.

The major limiting factor in the simulation is that SolidWorks Flow Simulation uses simplified CFD iteration techniques. It does not support species mixing, reactions, moving boundary conditions, or dynamic meshing. This meant that the simulations had to be divided into discrete simplified systems, and the results had to be interpolated between those points. SolidWorks lacks in the ability to include propagating flame fronts in a system, and as such the results gathered through simulation are not entirely accurate to the real-world model.

The most accurate way to analyze the behavior of a system like the RVS is to manufacture one and evaluate it experimentally. By choosing a real engine, measuring the power output at the flywheel and the species present in exhaust fumes, and reevaluating the system with an imposed RVS, very accurate and definitive results can be found. This comparison of real efficiencies and power output will help shed light to the understanding of possible gains on the RVS.

While the RVS system has been analyzed in a limited fashion through this thesis research, it would be increasingly beneficial to look more intently on the system function using more detailed and comprehensive evaluation techniques.

WORKS CITED

Albatlan, S. A., & Mohamed, E. S. (2014). Dynamic Analysis and Experimental Evaluation of Variable Valve Lift System for Internal Combustion Engine with Double Overhead Camshaft. . *International Journal of Vehicle Structures & Systems (IJVSS), 6*(1/2), 24-31.

Bachelier, L. D. (2004). *United States Patent No. 0187831.*

Bachelier, L. D. (2006). *United States Patent No. 0102130.*

Ceviz, M., & Akın, M. (2010). Design of a new SI engine intake manifold with variable length plenum. *Energy Conversion and Management*, 2239–2244.

Charlton, S. J., Price, C. E., Rogers, J., Turner, J. W., Wijetunge, R. S., & Anderson, W. (2017, June). Digitalair™ Camless FVVA System – Part 1, Valve Train Design, Capability and Performance. *SAE International Journal of Engines, 10*(3), 81-95.

Charlton, S. J., Price, C. E., Rogers, J., Turner, J. W., Wijetunge, R. S., & Anderson, W. (2017, June). DigitalAir™ Camless FVVA System - Part 2, Gasoline Engine Performance Opportunities. . *SAE International Journal of Engines, 10*(3), 111-124.

Christopher J. Greenshields. (2015). *OpenFoam Programmer's Guide V3.0.1.* OpenFoam Foundation Ltd.

Chung, T. J. (1993). *Numerical Modeling in Combustion.* Washington, D.C.: Taylor & Francis.

Conklin, R. J. (1993). *United States Patent No. 5205251.*

Davies, P. O. (1995). PISTON ENGINE INTAKE AND EXHAUST SYSTEM DESIGN. *Journal of Sound and Vibration*, 677-712.

Denny, M. J. (2014). *Potential Future Engine Cycles for Improved Thermal Effciency.* Gothenburg: Chalmers University of Technology.

Dirker, M. W. (2008). *United States Patent No. 0210190.*

Duve, D. (1998). *United States Patent No. 5711265.*

Greenshields, C. J. (2017). *OpenFoam User Guide, V5.0.* OpenFoam Foundation Ltd.

Gundmalm, S. (2009). CFD modeling of a four stroke S.I. engine for motorcycle application. *Masters of Science Thesis*. Stockholm, Sweden: KTH Industrial Engineering and Management.

He, X., Yang, S., Yuan, S., Zhu, J., & Zhang, X. (2014). Design of a Novel Bidirectional Valveless Piezoelectric Micropump With Three Chambers Using Coanda Effect Based on Numerical Simulation. *ASME 2014 4th Joint US-European Fluids Engineering Division Summer Meeting collocated with the ASME 2014 12th International Conference on Nanochannels, Microchannels, and Minichannels* (p. 7). Chicago: ASME.

Kang, K. Y., & Reitz, R. D. (1999). The effect of intake valve alignment on swirl generation in a DI diesel engine. *Experimental Thermal and Fluid Science*, 94-103.

Kannana, B., & Srivathsan, P. (2016). Numerical simulation of spark ignition engine using OpenFOAM. *Perspectives in Science*, 13-15.

Lanzanova, T., Dalla Nora, M., & Zhao, H. (2017, June). Investigation of Early and Late Intake Valve Closure Strategies for Load Control in a Spark Ignition Ethanol Engine. . *SAE International Journal of Engines, 10*(3), 137-151.

Lawes, K. (2011). *United States Patent No. 0308491.*

Lee, K., Bae, C., & Kang, K. (2007). The effects of tumble and swirl flows on flame propagation. *Applied Thermal Engineering*, 2122-2130.

Lucchini, T. (2006). *Internal Combustion Engines Simulation in OpenFoam.* Milan: Dipartimento di Energetica, POLITECNICO DI MILANO.

Lucchini, T. (2018). *Running OpemFoam Tutorials.* Department of Energy, Politecnico di Milano.

Lucchini, T. (n.d.). *Engine Simulation with Piston and Valve Action in OpenFoam.* Milan: Department of Energetics, Politecnico di Milano.

Matsson, J. (2014). *An Introduction to SolidWorks Flow Simulation 2014.* SDC Publications.

Meeks, E. (2014). ANSYS Strategy for Internal Combustion Engine Simulations. *Automotive Simulation World Congress* (p. 14). Tokyo: ANSYS, Inc.

Meeks, E. (2014). Applying FORTÉ to Design Simulations: Importance of teh Fuel Model. *Automotive Simulation World Congress* (p. 12). Tokyo: ANSYS, Inc.

Mohamed, E. (2012, March). Modeling and Performance Evaluation of an Electromechanical Valve Actuator for a Camless IC Engine. *International Journal of Energy & Environment, 3*(2), 275-294.

Muth, B. (2002). *United States Patent No. 0152983.*

MV Agusta. (2017, July 11). F4 Technical Specifications. Cascina Costa, Italy: MV Agusta.

Ohiwa, N., & Yamaguchi, S. (1989, September). A Valveless Pulse Combustor With Wide Operation Range and Low Noise Level. *J. Energy Resour. Technol , 111*(3), 187-193.

Sharke, P. (2003, May). Controlled Breathing. *Mechanical Engineering, 125*(5), 46-49.

Soder, M. (2015, March). *Creation and destruction of in-cylinder flows; Large eddy simulations of the intake and the compression strokes.* Stockholm: Royal Institute of Technology.

Thomas, A. D., Wallis, A. B., & Horrocks, G. D. (2007). *United States Patent No. 0266983.*

Thomas, G. (2009). *CFD modelling and analysis of an opposed piston.* Wollongong: University of Wollongong.

Weller, H. G., Tabora, G., Jasak, H., & Fureby, C. (1998). A tensorial approach to computational continuum mechanics using object-oriented techniques. *Computers in Physics*, 12.

Xu, C. C., & Choa, H. M. (2016). The Analysis of the CFD about the Swirl Generation in Four-Stroke Engine. *International Journal of Applied Engineering Research*, 8940-8945.

Appendix A: SolidWorks Inlet/Outlet Cold Flow Conditions

Crank Angle (CAD) [°]	Relative Angle (A) [°]	Inlet Velocity (U_i) [m/s]	Poppet Valve Displacement (y) [mm]
0	0	7.97	2.41
20	20	16.44	4.98
40	40	23.24	7.04
60	60	28.39	8.60
80	80	31.88	9.66
100	100	33.70	10.21
120	120	33.87	10.26
140	140	32.37	9.81
160	160	29.22	8.85
180	180	24.40	7.39
200	200	17.93	5.43
220	220	9.79	2.97
240	240	0.00	0.00
260	N/A	0.00	0.00
280	N/A	0.00	0.00
300	N/A	0.00	0.00
320	N/A	0.00	0.00
340	N/A	0.00	0.00
360	N/A	0.00	0.00
380	N/A	0.00	0.00
400	N/A	0.00	0.00
420	N/A	0.00	0.00
440	N/A	0.00	0.00
460	N/A	0.00	0.00
480	N/A	0.00	0.00
500	N/A	0.00	0.00
520	N/A	0.00	0.00
540	N/A	0.00	0.00
560	N/A	0.00	0.00
580	N/A	0.00	0.00
600	N/A	0.00	0.00
620	N/A	0.00	0.00
640	N/A	0.00	0.00
660	N/A	0.00	0.00
680	N/A	0.00	0.00
700	-20	0.00	0.00
720	0	7.97	2.41

Crank Angle (CAD) [°]	Relative Angle (A) [°]	Outlet Velocity (U_i) [m/s]	Poppet Valve Displacement (y) [mm]
0	720	10.31	2.44
20	740	0.00	0.00
40	40	0.00	0.00
60	60	0.00	0.00
80	80	0.00	0.00
100	100	0.00	0.00
120	120	0.00	0.00
140	140	0.00	0.00
160	160	0.00	0.00
180	180	0.00	0.00
200	200	0.00	0.00
220	220	0.00	0.00
240	240	0.00	0.00
260	260	0.00	0.00
280	280	0.00	0.00
300	300	0.00	0.00
320	320	0.00	0.00
340	340	0.00	0.00
360	360	0.00	0.00
380	380	0.00	0.00
400	400	0.00	0.00
420	420	0.00	0.00
440	440	0.00	0.00
460	460	0.00	0.00
480	480	0.00	0.00
500	500	4.78	1.13
520	520	15.33	3.63
540	540	23.87	5.65
560	560	30.40	7.20
580	580	34.92	8.27
600	600	37.43	8.87
620	620	37.94	8.99
640	640	36.43	8.63
660	660	32.91	7.80
680	680	27.39	6.49
700	700	19.85	4.70
720	720	10.31	2.44

Appendix B: Solidworks Cold Flow Simulation Results – Traditional Model

Intake	Crank Angle Degree (CAD) [°]	0	20	40	60	80	100	120	140	160	180	200	220
	Average Centerline Pressure (P_{avg}) [Pa]	101325	101327.7	101324.1	101334.5	101308.7	101276	101292.8	101282.9	101285.6	101301.4692	101308.5	101300
	Standard Deviation of Pressure Centerline (σ_P) [Pa]	0.00000	1.068478	1.23326	12.32577	26.29572	32.17597	31.20299	35.60612	33.28839	25.58193612	8.726478	4.006222
Exhaust	Crank Angle Degree (CAD) [°]	500	520	540	560	580	600	620	640	660	680	700	720
	Average Centerline Pressure (P_{avg}) [Pa]	101324	101321.6	101320.3	101318.1	101316	101313.1	101314.2	101313.8	101312.2377	101322.3964	101325	101325
	Standard Deviation of Pressure Centerline (σ_P) [Pa]	0.690097	2.198251	2.077578	3.274336	4.348807	7.33938	4.407676	4.592127	5.207826604	0.115247622	0.018777	0

Appendix C: SolidWorks Cold Flow Simulation Results – RVS Model

Intake	Crank Angle Degree (CAD) [°]	0	20	40	60	80	100	120	140	160	180	200	220
	Average Centerline Pressure (P_{avg}) [Pa]	101325	101325	101324.3	101318.2	101321.2	101321.9	101321.4	101318.1	101314.9	101316.6517	101314.9	101318
	Standard Deviation of Pressure Centerline (σ_P) [Pa]	0.000753	0.001846	0.02181	0.432196	0.446189	0.566809	0.321415	1.47546	0.954029	0.877987458	1.075323	0.873574
Exhaust	Crank Angle Degree (CAD) [°]	500	520	540	560	580	600	620	640	660	680	700	720
	Average Centerline Pressure (P_{avg}) [Pa]	101324.7	101322.8	101319.6	101316.4	101313.5	101311.3	101310.3	101310.2	101312.5	101320	101325	101325
	Standard Deviation of Pressure Centerline (σ_P) [Pa]	0.146799	1.216204	2.995244	4.701808	6.090214	7.309727	7.237432	6.661915	4.325424	0.79778	0.010969	0.000656

Appendix D: Combustion Simulation Working Fluid Properties

Temperature [C]	Temperature [K]	Heptane Cp [J/kg K]	Air Cp [J/kg K]	Combined Cp [J/kg K]	Heptane Vapor Thermal Conductivity [W/m K]	Air Vapor Thermal Conductivity [W/m K]	Combined Vapor Thermal Conductivity [W/m K]	Heptane Dynamic Viscosity [Pa s]	Air Dynamic Viscosity [Pa s]	Combined Dynamic Viscosity [Pa s]
-173	100	660.8143185	0.001032	41.10737801						
-73	200	1186.67184	0.001007	73.81868419	0.004139808	1.81E+04	16974.07728	43408800	1.33E+09	1.25E+09
27	300	1671.087682	0.001007	103.9521056	0.01211732	2.63E+04	24663.99112	60767200	1.85E+09	1.73E+09
127	400	2112.485854	0.001014	131.4095897	0.021421664	3.38E+04	31697.44903	79270400	2.30E+09	2.16E+09
227	500	2508.825255	0.00103	156.0641703	0.03273375	4.07E+04	38168.23048	98100000	2.70E+09	2.54E+09
327	600	2857.599677	0.001051	177.7599434	0.045040928	4.69E+04	43982.55597	116437600	3.06E+09	2.88E+09
427	700	3155.837804	0.001075	196.3120742	0.057934268	5.24E+04	49140.42548			
527	800	484.9774437	0.001099	30.16938683	0.07201296	5.73E+04	53735.61848			
627	900	2016.534214	0.001121	125.4409521	0.087395834	6.20E+04	58143.2527			
727	1000	3899.042252	0.001141	242.543681	0.10034	6.67E+04	62550.88676			
827	1100	6168.693987	0.001159	383.7289487	0.097966608	7.15E+04	67052.29931			
927	1200	8854.137978	0.001175	550.7788583	0.051093728	7.63E+04	71553.70908			
1027	1300	11977.42255	0.001189	745.0649412						
1127	1400	15554.93944	0.001207	967.6068623						

Appendix E: Combustion Simulation Flow COnditions

Crank Angle Dependent Variables						
Crank Angle Degrees (CAD) [°]	Crank Angle Degrees (CAD) [rad]	Piston Face Displacement (X_Cyl) [m]	Cylinder Displacement (V_Cyl) [m^3]	Piston Face Velocity (U_p) [m/s]	Intake Port Fluid Velocity (U_i) [m/s]	Exhaust Port Fluid Velocity (U_e) [m/s]
0	0.00E+00	2.55E-03	1.16E-05	0.00E+00	7.96875	10.30814991
10	1.75E-01	3.12E-03	1.42E-05	8.75E-03	12.40966797	4.782338555
20	3.49E-01	4.82E-03	2.18E-05	1.70E-02	16.43554688	0
30	5.24E-01	7.58E-03	3.44E-05	2.44E-02	20.04638672	0
40	6.98E-01	1.13E-02	5.14E-05	3.06E-02	23.2421875	0
50	8.73E-01	1.59E-02	7.24E-05	3.52E-02	26.02294922	0
60	1.05E+00	2.13E-02	9.66E-05	3.82E-02	28.38867188	0
70	1.22E+00	2.72E-02	1.24E-04	3.95E-02	30.33935547	0
80	1.40E+00	3.35E-02	1.52E-04	3.92E-02	31.875	0
90	1.57E+00	4.01E-02	1.82E-04	3.75E-02	32.99560547	0
100	1.75E+00	4.66E-02	2.11E-04	3.47E-02	33.70117188	0
110	1.92E+00	5.29E-02	2.40E-04	3.10E-02	33.99169922	0
120	2.09E+00	5.88E-02	2.67E-04	2.68E-02	33.8671875	0
130	2.27E+00	6.42E-02	2.91E-04	2.23E-02	33.32763672	0
140	2.44E+00	6.88E-02	3.12E-04	1.77E-02	32.37304688	0
150	2.62E+00	7.25E-02	3.29E-04	1.31E-02	31.00341797	0
160	2.79E+00	7.53E-02	3.42E-04	8.61E-03	29.21875	0
170	2.97E+00	7.70E-02	3.49E-04	4.27E-03	27.01904297	0
180	3.14E+00	7.76E-02	3.52E-04	2.99E-18	24.40429688	0
190	3.32E+00	7.70E-02	3.49E-04	-4.27E-03	21.37451172	0
200	3.49E+00	7.53E-02	3.42E-04	-8.61E-03	17.9296875	0
210	3.67E+00	7.25E-02	3.29E-04	-1.31E-02	14.06982422	0
220	3.84E+00	6.88E-02	3.12E-04	-1.77E-02	9.794921875	0
230	4.01E+00	6.42E-02	2.91E-04	-2.23E-02	0	0

240	4.19E+00	5.88E-02	2.67E-04	-2.68E-02	0	0
250	4.36E+00	5.29E-02	2.40E-04	-3.10E-02	0	0
260	4.54E+00	4.66E-02	2.11E-04	-3.47E-02	0	0
270	4.71E+00	4.01E-02	1.82E-04	-3.75E-02	0	0
280	4.89E+00	3.35E-02	1.52E-04	-3.92E-02	0	0
290	5.06E+00	2.72E-02	1.24E-04	-3.95E-02	0	0
300	5.24E+00	2.13E-02	9.66E-05	-3.82E-02	0	0
310	5.41E+00	1.59E-02	7.24E-05	-3.52E-02	0	0
320	5.59E+00	1.13E-02	5.14E-05	-3.06E-02	0	0
330	5.76E+00	7.58E-03	3.44E-05	-2.44E-02	0	0
340	5.93E+00	4.82E-03	2.18E-05	-1.70E-02	0	0
350	6.11E+00	3.12E-03	1.42E-05	-8.75E-03	0	0
360	6.28E+00	2.55E-03	1.16E-05	-1.24E-17	0	0
370	6.46E+00	3.12E-03	1.42E-05	8.75E-03	0	0
380	6.63E+00	4.82E-03	2.18E-05	1.70E-02	0	0
390	6.81E+00	7.58E-03	3.44E-05	2.44E-02	0	0
400	6.98E+00	1.13E-02	5.14E-05	3.06E-02	0	0
410	7.16E+00	1.59E-02	7.24E-05	3.52E-02	0	0
420	7.33E+00	2.13E-02	9.66E-05	3.82E-02	0	0
430	7.50E+00	2.72E-02	1.24E-04	3.95E-02	0	0
440	7.68E+00	3.35E-02	1.52E-04	3.92E-02	0	0
450	7.85E+00	4.01E-02	1.82E-04	3.75E-02	0	0
460	8.03E+00	4.66E-02	2.11E-04	3.47E-02	0	0
470	8.20E+00	5.29E-02	2.40E-04	3.10E-02	0	0
480	8.38E+00	5.88E-02	2.67E-04	2.68E-02	0	0
490	8.55E+00	6.42E-02	2.91E-04	2.23E-02	0	0
500	8.73E+00	6.88E-02	3.12E-04	1.77E-02	0	4.782338555
510	8.90E+00	7.25E-02	3.29E-04	1.31E-02	0	10.30814991
520	9.08E+00	7.53E-02	3.42E-04	8.61E-03	0	15.33161478

530	9.25E+00	7.70E-02	3.49E-04	4.27E-03	0	19.85273316
540	9.42E+00	7.76E-02	3.52E-04	8.97E-18	0	23.87150506
550	9.60E+00	7.70E-02	3.49E-04	-4.27E-03	0	27.38793046
560	9.77E+00	7.53E-02	3.42E-04	-8.61E-03	0	30.40200939
570	9.95E+00	7.25E-02	3.29E-04	-1.31E-02	0	32.91374182
580	1.01E+01	6.88E-02	3.12E-04	-1.77E-02	0	34.92312777
590	1.03E+01	6.42E-02	2.91E-04	-2.23E-02	0	36.43016723
600	1.05E+01	5.88E-02	2.67E-04	-2.68E-02	0	37.4348602
610	1.06E+01	5.29E-02	2.40E-04	-3.10E-02	0	37.93720669
620	1.08E+01	4.66E-02	2.11E-04	-3.47E-02	0	37.93720669
630	1.10E+01	4.01E-02	1.82E-04	-3.75E-02	0	37.4348602
640	1.12E+01	3.35E-02	1.52E-04	-3.92E-02	0	36.43016723
650	1.13E+01	2.72E-02	1.24E-04	-3.95E-02	0	34.92312777
660	1.15E+01	2.13E-02	9.66E-05	-3.82E-02	0	32.91374182
670	1.17E+01	1.59E-02	7.24E-05	-3.52E-02	0	30.40200939
680	1.19E+01	1.13E-02	5.14E-05	-3.06E-02	0	27.38793046
690	1.20E+01	7.58E-03	3.44E-05	-2.44E-02	0	23.87150506
700	1.22E+01	4.82E-03	2.18E-05	-1.70E-02	0	19.85273316
710	1.24E+01	3.12E-03	1.42E-05	-8.75E-03	3.112792969	15.33161478
720	1.26E+01	2.55E-03	1.16E-05	-2.48E-17	7.96875	10.30814991

Appendix F: Traditional Combustion Simulation Results (Intake)

Crank Angle Degree (CAD)	0	10	20	30	40	50	60	70	80	90	100	110	120	130	140	150	160	170	180	190	200	210	220
Average Cylinder Temperature [K]	333.8082	339.9542	328.1657	322.7991	320.1761	343.2062	350.7356	371.0506	386.2926	388.4301	395.4165	419.412	413.3733	437.8775	421.3994	438.8498	444.084	451.7199	439.9725	449.09	425.6867	424.9838	444.4509
Temperature Points [K]	380	380	380	380	380	380	380	380	380	380	380	380	380	380	380	380	380	380	380	380	380	380	380
	355.9381	332.7318	307.8915	301.2478	302.04	301.0639	300.3112	299.3129	298.9309	298.8702	298.7629	297.9742	297.6483	297.7871	297.4246	301.7273	301.9666	305.6234	324.9249	320.9342	327.9293	338.795	353.466
	331.8761	303.394	301.9274	300.7987	300.8842	300.3833	299.9349	298.6531	298.5873	298.2048	299.1652	300.2803	298.8472	303.9408	309.1209	324.8079	326.8191	345.6609	363.1561	360.4846	365.0858	361.5206	374.1215
	314.8051	303.3647	301.6	300.3496	299.7283	300.9775	300.5918	299.7491	301.0356	304.7868	306.805	312.3377	315.7804	327.7579	345.0529	360.9661	365.8984	381.8737	389.8427	394.67	389.7803	380.8499	388.9234
	310.9092	303.3355	301.4431	299.9005	299.1916	302.3291	303.0521	303.8507	309.0076	318.6481	327.7196	339.9718	345.8461	353.4533	376.8652	387.8949	396.593	409.9541	402.7569	418.5351	401.6799	396.9906	406.6874
	307.0133	303.3063	301.2861	299.9946	298.8827	305.3838	308.5149	312.7329	324.9383	340.8671	349.4274	368.5689	375.6324	377.6037	393.8993	409.5409	418.1147	435.9204	411.9648	435.9671	409.9829	411.7384	423.499
	305.9051	303.2771	301.1292	300.265	298.6359	309.5591	315.808	325.3923	345.1984	364.8692	367.871	392.3832	396.0525	406.1797	404.9456	427.9408	436.912	458.834	420.7935	451.7636	417.1574	421.6852	435.1322
	306.03	303.2479	300.9723	300.5354	299.0003	315.1842	323.8832	338.0462	362.9037	377.2178	383.9091	416.1975	412.6232	434.008	414.501	441.8099	448.5409	467.7877	427.1382	458.7439	420.9312	424.9321	444.0011
	306.1549	303.2187	300.847	300.8075	299.3648	320.8076	331.9559	349.8279	377.41	389.1928	397.2829	433.6928	428.5776	453.0465	422.5802	454.7927	459.98	476.7414	433.4829	465.7242	424.7058	428.211	451.7529
	306.2798	303.1895	300.8724	301.1335	299.8645	326.405	338.5085	361.2041	391.7671	401.0378	410.333	443.2469	436.0156	467.0636	428.6735	463.2468	466.1788	478.2214	444.1864	469.2039	428.5042	431.6538	457.4928
	306.4047	303.1603	300.8978	301.4596	300.5274	330.9992	344.9216	372.0552	405.8604	406.136	422.4991	452.8011	443.2256	478.2556	434.9293	471.7008	472.3777	479.4003	455.1816	472.5427	432.3026	435.0966	463.0147
	306.5295	303.1671	300.9233	301.7857	301.1903	335.5933	350.9138	381.8635	416.6534	408.6074	423.3939	458.1955	448.8849	482.7545	443.0942	475.0276	475.792	479.7405	463.7174	473.3696	436.2702	438.5179	465.9771
	306.6544	303.2081	300.9487	302.1511	301.9395	340.1875	354.8643	391.6718	418.9373	411.0787	424.2887	460.484	449.0787	487.2534	451.2592	477.9323	478.5994	479.8189	471.4022	473.4125	440.2747	441.9376	468.9394
	306.7793	303.2492	300.9741	302.6071	302.7083	343.0578	358.8149	398.0051	421.2334	412.6605	425.1396	462.7725	449.2724	489.1284	457.9673	478.216	480.5327	480.1949	475.1934	473.1296	443.8436	444.0922	470.2351
	306.9042	303.2905	301.0302	303.0631	303.5847	345.0273	361.6511	404.2943	423.5787	413.2186	424.0335	462.7794	448.4233	490.9039	464.311	477.2896	481.9002	480.8019	475.7809	472.5937	447.1306	445.6629	471.1139
	307.0291	317.5795	301.1205	303.5191	304.9714	346.9968	362.985	408.481	425.7451	413.7768	422.9273	461.8174	446.3893	492.9354	466.5747	476.1841	483.6518	482.48	476.6808	473.602	449.4403	445.5148	471.61
	307.1539	373.1833	301.2106	303.9038	306.3581	348.5053	364.319	411.4848	426.5389	414.242	421.8212	460.8554	444.3553	495.1173	465.0924	474.8545	485.9963	486.0312	478.1502	477.3105	450.2413	443.2177	471.7547
	329.1981	428.7874	365.4928	304.2384	307.5354	348.9217	364.8883	413.9955	427.3412	414.356	422.0384	460.2052	443.0086	497.0005	463.1347	473.7019	488.188	489.4856	479.6511	481.0384	450.8406	440.9605	471.9131
	434.5991	484.3937	452.746	408.2224	357.1138	422.7412	408.7939	430.3906	430.185	460.8305	460.9114	483.6761	467.8039	503.3607	468.562	479.3626	493.6379	495.8278	485.4457	488.7749	457.6326	448.2995	479.384
	540	540	540	540	540	540	540	540	540	540	540	540	540	540	540	540	540	540	540	540	540	540	540
Average Cylinder Pressure [Pa]	101310.9	101337.1	101338.9	101320.5	101319.1	101318.9	101320.7	101322.7	101326.1	101327.5	101323.6	101325.1	101321.3	101322.5	101322.4	101322.1	101321.9	101324.1	101323.1	101323.8	101325.6	101331.1	101328.6
Cylinder Pressure [Pa]	101296.1	101307.4	101307.2	101292.3	101268.2	101299.6	101276.3	101296.5	101298.3	101294.4	101294.8	101285.4	101256	101266.1	101272.6	101268.2	101266.8	101298.2	101304	101297.8	101340.8	101415.5	101360.8
	101297.2	101312.7	101308.3	101300.5	101282.2	101285.8	101290.3	101298.1	101303.4	101300.6	101296	101312	101302.6	101317.5	101330.9	101336.6	101329.5	101332.6	101322.5	101328.4	101332.7	101349	101353.9
	101298.3	101317.1	101310.2	101303.8	101294	101299.1	101309	101325.7	101337.8	101363.2	101351.2	101357	101363.1	101349.7	101340.3	101323.6	101324.6	101327.6	101320.1	101327.1	101322.4	101329.7	101328.2
	101299.5	101320	101314.3	101307.2	101305.8	101320.1	101328.4	101344.6	101351.6	101380.6	101348.6	101342.7	101333	101329.6	101320.6	101321.3	101322.3	101324	101320.5	101325.3	101320.4	101323.8	101326.5
	101300.8	101322.9	101318.8	101310.5	101314	101339.3	101342.6	101343.7	101348.3	101350.8	101329.1	101332.7	101317.9	101322	101319.3	101322	101322.6	101324.9	101322.6	101324.7	101322	101323.1	101325.8
	101302.1	101325.8	101323.2	101313.2	101321	101338.7	101345.4	101340.5	101341.8	101333.5	101324	101326.8	101317.9	101321.2	101320.3	101323	101323.5	101324.8	101323.7	101324.6	101323.4	101323.5	101325.1
	101303.7	101328.7	101327.7	101315.6	101327.1	101335	101341.2	101333.7	101333.9	101323.4	101321.9	101325.7	101319.4	101322.6	101321.8	101323.7	101324.2	101324.6	101324.7	101324.5	101324.6	101323.9	101325.1
	101305.4	101331.6	101332.2	101318.1	101325.3	101329.8	101334.1	101326.8	101328.6	101322.5	101321.9	101324.6	101321.4	101323.7	101323.4	101324.2	101324.5	101324.7	101324.8	101324.7	101324.7	101324.6	101325.4
	101307.2	101334.5	101336.5	101320.5	101323.5	101324.7	101327	101323.1	101326.6	101321.9	101322.3	101324.1	101323.4	101324.2	101324.4	101324.6	101324.8	101324.8	101324.8	101324.9	101324.8	101325.2	101325.6
	101308.9	101337.4	101340.2	101321.5	101321.7	101319.7	101323.2	101320.8	101324.7	101321.5	101322.7	101324.2	101323.8	101324.4	101324.6	101324.7	101324.8	101324.9	101324.9	101324.9	101324.9	101325.1	101325.4
	101310.6	101340.3	101344	101322.5	101319.8	101318.7	101319.8	101319.1	101323	101321.9	101323	101324.4	101324.1	101324.6	101324.8	101324.9	101324.9	101324.9	101325	101325	101324.9	101325.1	101325.2
	101312.3	101342.9	101347.7	101323.5	101317.9	101317.7	101316.9	101318.3	101321.8	101322.5	101323.3	101324.5	101324.4	101324.7	101324.9	101324.9	101324.9	101324.9	101325	101325	101325	101325.1	101325.2
	101314	101345	101351.4	101325	101319	101316.6	101316.7	101317.6	101322.1	101323	101323.6	101324.6	101324.6	101324.8	101324.9	101325	101325	101325	101325	101325	101325	101325.1	101325.1
	101315.8	101347.1	101355.1	101327.5	101320.7	101316.7	101316.5	101318.1	101322.3	101323.5	101323.9	101324.6	101324.7	101324.9	101325	101325	101325	101325	101325	101325	101325	101325.3	101325.1
	101317.5	101349.2	101357.6	101329.9	101323.2	101317.3	101317.1	101318.7	101322.5	101323.8	101324.1	101324.7	101324.8	101324.9	101325	101325	101325	101325	101325	101325	101325	101325.5	101325
	101319.2	101351.4	101358.7	101332.4	101329.3	101317.9	101318.9	101319.7	101322.7	101324	101324.3	101324.7	101324.8	101325	101325	101325	101325	101325	101325	101325	101325.1	101325.8	101325
	101320.9	101353.7	101359.7	101334.3	101335.3	101318.7	101320.6	101321	101322.9	101324.3	101324.4	101324.8	101324.9	101325	101325	101325	101325	101325	101325	101325	101325.2	101326.2	101325
	101323.5	101356	101360.9	101335.7	101340.3	101319.7	101322.1	101322.1	101323.1	101324.5	101324.5	101324.8	101324.9	101325	101325	101325	101325	101325	101325	101325	101325.2	101326.5	101325.1
	101329.2	101358.3	101362	101337.3	101344.5	101320.9	101323.1	101322.8	101323.3	101324.7	101324.5	101324.8	101324.9	101325	101325	101325	101325	101325	101325	101325	101325.3	101326.7	101325.1
	101334.9	101360.6	101363.2	101338.8	101348.9	101322	101324.4	101323.5	101323.5	101325	101324.6	101324.8	101324.9	101325	101325	101325	101325	101325	101325	101325	101325.3	101327	101325.1

Appendix G: Traditional Combustion Simulation Results (Combustion)

Crank Angle Degree (CAD)	360	370	380	390	400	410	420	430	440	450	460	470	480	490	500	510	520	530	540
Average Cylinder Temperature [K]	2149.956	2215.843	2235.145	2167.485	2130.069	2003.657	2010.187	2003.103	2085.697	2094.891	2055.911	2136.904	2061.568	2125.524	2080.298	1848.702	1964.071	1978.28	2101.727
Temperature Points [K]	2466.679	2452.579	2401.717	2396.809	2384.823	2390.821	2327.27	2363.236	2351.906	2396.388	2372.678	2387.919	2411.996	2397.653	2395.825	2329.783	2372.475	2394.931	2400.071
	2468.099	2454.966	2391.007	2381.175	2360.107	2348.432	2275.735	2292.585	2282.803	2283.615	2240.31	2261.251	2269.403	2241.798	2219.742	2207.545	2220.409	2236.423	2243.714
	2469.519	2457.502	2385.849	2357.551	2323.146	2292.926	2224.622	2216.751	2204.74	2153.002	2089.326	2159.563	2107.314	2095.53	2029.9	2111.749	2112.682	2124.096	2133.415
	2470.94	2460.281	2386.556	2333.926	2286.186	2230.075	2170.341	2144.624	2151.541	2045.121	1975.043	2091.042	2011.444	1979.941	1897.771	2019.948	2020.126	2033.515	2047.156
	2472.36	2463.06	2388.056	2310.301	2242.782	2165.876	2111.219	2076.865	2114	1984.118	1888.45	2022.52	1978.62	1925.84	1859.794	1969.06	1985.386	1989.862	2006.322
	2473.78	2465.839	2389.556	2278.965	2197.008	2106.329	2052.097	2011.348	2076.459	1924.616	1873.406	1990.107	1949.137	1874.739	1833.024	1940.867	2017.741	2029.785	2059.413
	2475.2	2468.618	2391.056	2245.125	2151.649	2048.667	1992.975	2018.691	2038.918	1866.107	1860.149	2036.68	1983.567	1977.052	1908.69	1918.459	2058.608	2065.721	2112.907
	2476.621	2471.397	2392.556	2211.286	2110.38	1993.144	1933.853	2026.084	2037.248	1941.838	1856.531	2083.253	2042.017	2085.168	2042.7	1904.602	2125.158	2080.8	2169.055
	2478.041	2474.176	2395.376	2178.715	2069.112	1937.621	1874.731	2034.42	2080.578	2021.076	1943.392	2141.413	2100.466	2183.833	2160.405	1887.283	2187.551	2095.878	2225.204
	2479.25	2476.955	2404.492	2188.606	2061.128	1884.012	1881.279	2043.292	2123.907	2100.315	2030.254	2214.132	2143.124	2276.95	2248.742	1852.271	2135.251	2031.576	2217.051
	2480.319	2479.734	2413.607	2198.498	2093.295	1906.321	1893.85	2060.327	2167.236	2186.144	2117.131	2286.852	2185.36	2341.758	2329.056	1817.258	2082.951	1964.077	2204.595
	2481.388	2481.288	2422.722	2208.389	2125.207	1928.631	1922.092	2093.572	2211.326	2274.541	2204.286	2329.501	2221.07	2339.497	2315.131	1792.438	2023.935	1944.191	2206.58
	2482.457	2481.678	2431.837	2228.098	2154.735	1950.941	2026.348	2126.816	2257.377	2362.937	2291.441	2349.696	2233.784	2337.236	2301.206	1768.459	1963.455	1939.167	2213.562
	2400.942	2482.069	2440.952	2270.381	2183.347	2010.27	2130.604	2160.061	2303.427	2411.839	2377.041	2369.891	2246.497	2344.08	2295.923	1779.271	1936.125	1952.666	2215.426
	2154.257	2482.46	2447.095	2312.664	2219.583	2088.945	2207.105	2193.305	2349.477	2415.295	2393.374	2384.951	2252.579	2351.27	2292.802	1806.146	1930.251	1980.546	2213.08
	1907.573	2365.71	2449.924	2354.947	2292.028	2167.62	2246.188	2207.214	2390.518	2418.751	2409.706	2397.831	2251.126	2356.431	2287.435	1832.875	1925.231	2013.585	2216.727
	1640.844	1909.275	2452.757	2380.853	2364.474	2231.308	2285.27	2205.657	2392.717	2422.176	2426.039	2410.71	2249.673	2360.399	2280.007	1859.423	1921.53	2055.646	2231.303
	1273.896	1452.842	1938.523	2394.763	2411.434	2259.181	2280.597	1979.776	2190.349	2425.848	2423.847	2411.752	2249.873	2365.378	2276.047	1880.206	1918.354	2094.335	2245.693
	906.948	996.4211	1239.261	1578.65	2030.96	1592.012	1827.568	1267.431	1449.421	1724.087	1805.805	1869.016	1804.311	2135.929	2091.763	1756.395	1804.212	1998.79	2133.269
	540	540	540	540	540	540	540	540	540	540	540	540	540	540	540	540	540	540	540
Average Cylinder Pressure [Pa]	4984387	4299689	2800601	1669181	1080176	768969.8	555441.9	502981.7	463392.4	430350.9	371294.6	376819.5	381963	349767	329981.2	288517.3	320297.6	334909.3	339325.3
Cylinder Pressure [Pa]	4643850	3968435	3245308	3195562	3039332	3148714	2469290	2777277	2644079	3113143	2886364	3083647	3280102	3202071	3088363	2474645	2900007	3135887	3187797
	4680316	3971517	3066225	2998588	2765836	2638715	1918390	2020125	1901783	1860548	1639164	1565876	1586488	1407230	1370021	1006776	1171313	1238834	1265158
	4716782	3989154	2990860	2726311	2390742	2052115	1416460	1316059	1165452	1049647	781629.4	714407.7	749791.8	564230	432866.7	568092.9	562630.2	550533.4	551649.9
	4753248	4030581	2899698	2454035	2015648	1594571	1056355	818666.4	781186.8	517326.6	376090.4	490676.4	345867	267232.3	204902.1	240533.6	271928.1	280409.3	286453.4
	4789714	4072008	2805244	2181758	1715980	1187945	879662.5	586423.8	599689.1	372345.1	202415.4	266945.1	224656.2	165100.7	129420.4	104417.1	101615.5	97360.79	99224.47
	4826180	4113435	2710790	1939431	1444052	830249.4	702970.1	359340.7	418191.4	234137.2	152204.5	106915.6	111009.4	71359.93	71809.06	74494.59	71012.46	69385.12	73215.44
	4862646	4154862	2616336	1706828	1175883	573704.7	526277.7	299868.8	236693.7	100408.7	104920.8	86228.99	77117.18	59194.59	50331.45	57882.51	49739.75	47169.43	51625.72
	4899112	4196289	2521882	1474225	944729.9	465598.2	349585.3	240612.9	130164.7	86448.05	63514.77	65542.39	73196.97	50109.6	48982.76	60952.04	56620.48	55095.71	59191.92
	4935578	4237717	2452287	1245548	713577.1	357491.6	172892.9	185396.1	117678.5	75616.93	64246.74	57002.72	69276.76	53590.34	52721.75	64847.07	63686.64	63021.99	66758.12
	4970403	4279144	2501237	1148294	562254.8	251227.8	135060	132476.2	105192.3	64785.81	64978.72	63728.34	75531.01	64445.45	65623.97	72960.05	75869.52	74523.86	75812.22
	5004124	4320571	2550187	1051040	507232.5	218082.3	109964	99270.33	92706.06	69010.81	66202.25	70453.97	82057.54	74640.8	78101.1	81073.04	88052.41	86169.77	84965.88
	5037850	4360415	2599137	953785.4	452645.2	184936.7	90531.85	105211.4	86345.66	79098.13	76088.62	77872.43	88159.89	83273.07	85584.95	87669.63	94253.02	93146.22	90874.11
	5071576	4398755	2648087	917076.6	402131.6	151791.2	98573.14	111152.5	95778.97	89185.45	85974.99	85808.23	92767.23	91905.35	93068.8	94141.34	99149.58	98665.19	95659.38
	5105949	4437097	2697037	1019571	353185.6	158696.8	106614.4	117093.6	105212.3	99667.05	95865.49	93744.04	97374.56	98731.05	99264.41	99324.93	103570.6	103729.7	100361.4
	5141615	4475443	2758323	1122065	325699.6	186532.7	122322	123034.6	114645.6	110602.3	105940	101409	102458.4	105488.2	105137.8	103913.8	107683.8	108441.3	104995
	5177281	4514606	2833356	1224560	400122.1	214368.5	148365.1	132121.9	123685.1	121537.6	116014.6	108958.9	108083.7	113243.3	111805	108452.3	111675.7	112856.9	109847.4
	5213090	4556140	2908361	1332466	474544.5	243149	174408.2	142722.9	129428.4	131513.2	126089.1	116508.8	113708.9	121584.1	119201	112927.9	115480.4	116754.7	115098.8
	5249617	4597673	2987959	1444318	553551.1	274504.2	195224.2	153365.1	134529.9	137746.4	132657.4	121820.2	117463.1	128914.1	125932.4	116954.4	118909.9	120316.6	119938
	5286143	4639200	3069212	1563494	638266.5	307132.3	209107	164182.5	139705.1	143884.7	139405.6	126909.2	120524.4	133932.1	130781.1	119038.9	120529	122037.8	122575.7
	5322669	4680728	3150486	1684661	728113	339870.7	226785.9	175233.4	145699.6	150367	146125.9	131934.2	123625	139063	135704.7	121250.1	122224.1	123848.6	125303.4
Average Piston Face Pressure [Pa]	371095.8	403156.3	237626.1	181595.1	175743.9	180521.5	194847.2	190198.9	170135.1	160939.8	154628.7	138844.5	129710.2	137176.4	136181.5	129073.6	129095.2	128505	125879.2
Maximum Piston Face Pressure [Pa]	5491110	4990254	3474651	2083812	840886	481389.4	393309.3	310751.6	232905.5	241857	235992.1	227105.1	199785.8	225806.4	199395.5	200347.2	185304.2	207032.4	194991.2
Minimum Piston Face Pressure [Pa]	114258.4	103463.3	23675.94	13805.41	24870.02	54288.61	49435.02	99120.44	110503.4	107085.7	104239.4	101196.9	102304.5	102141.6	102711.2	98893.61	102295	102068.3	101053.5

Appendix H: Traditional Combustion Simulation results (Exhaust)

Crank Angle Degree (CAD)	550	560	570	580	590	600	610	620	630	640	650	660	670	680	690	700	710	720
Average Cylinder Temperature [K]	1992.78	1985.125	1976.206	1976.154	1968.641	1959.936	1956.871	1966.68	1989.896	2004.292	1986.996	2010.132	2048.953	2032.562	1993.08	1945.051	1856.459	1404.458
Temperature Points [K]	2135.197	2148.975	2136.849	2155.267	2152.451	2158.066	2158.7	2154.004	2161.518	2162.763	2162.839	2157.48	2148.558	2135.282	2116.427	2104.287	2088.592	1552.877
	2065.519	2081.543	2091.407	2095.182	2111.639	2120.604	2132.015	2125.677	2138.32	2152.151	2157.147	2158.675	2148.927	2135.184	2116.3	2104.157	2087.464	1556.497
	2012.093	2009.939	2015.782	2001.328	2029.756	2026.489	2061.612	2067.956	2086.077	2118.13	2136.031	2149.332	2148.904	2135.039	2116.018	2104.066	2084.999	1560.118
	1998.239	1988.05	1988.587	1978.113	1987.265	1976.066	2000.447	2026.218	2033.471	2072.315	2103.489	2134.454	2145.465	2134.893	2115.736	2103.3	2080.351	1563.738
	2013.578	1998.205	1993.334	1993.172	1978.069	1955.829	1974.416	1995.702	1989.47	2024.447	2069.775	2116.033	2141.022	2134.91	2115.454	2102.437	2075.703	1567.358
	2032.023	2015.978	2006.786	2007.908	1991.86	1973.276	1970.146	1984.581	1972.498	1998.664	2036.1	2098.793	2136.931	2134.986	2114.906	2101.574	2071.055	1570.979
	2046.929	2029.485	2016.278	2017.176	2004.686	1991.943	1986.118	1988.47	1973.4	1993.642	2024.977	2087.728	2133.201	2135.07	2114.272	2100.71	2066.407	1574.599
	2052.545	2036.498	2022.079	2023.962	2016.609	2010.298	1999.858	2002.686	1993.725	2000.865	2013.853	2079.768	2129.97	2135.227	2113.637	2099.847	2061.759	1578.219
	2058.161	2043.53	2028.049	2031.142	2025.409	2027.223	2012.763	2020.888	2013.799	2023.446	2017.179	2071.808	2126.739	2135.384	2112.979	2098.591	2057.111	1581.84
	2064.446	2051.071	2034.888	2039.033	2032.506	2038.051	2025.008	2039.316	2032.446	2045.186	2027.228	2072.66	2123.611	2135.136	2111.515	2095.46	2052.463	1585.336
	2070.759	2058.613	2041.728	2047.25	2040.556	2048.716	2037.253	2057.743	2049.897	2065.442	2038.981	2074.319	2124.577	2134.402	2110.051	2092.329	2047.815	1588.747
	2080.196	2068.817	2053.181	2059.298	2050.86	2059.914	2051.095	2073.127	2066.883	2083.222	2054.114	2077.473	2125.542	2133.667	2108.588	2089.198	2043.744	1592.159
	2090.607	2079.601	2065.015	2071.347	2061.164	2072.996	2066.129	2088.511	2083.869	2094.624	2069.247	2087.873	2126.508	2131.493	2105.896	2086.067	2040.222	1595.571
	2101.85	2091.695	2079.064	2084.61	2073.445	2086.078	2081.164	2103.683	2098.137	2106.039	2082.913	2098.274	2127.537	2128.989	2100.383	2082.937	2036.692	1553.287
	2113.74	2104.637	2094.137	2098.176	2085.8	2095.847	2090.194	2109.424	2109.276	2117.513	2096.561	2107.605	2128.752	2125.661	2094.87	2080.175	2033.15	1419.611
	2122.332	2114.759	2106.116	2107.24	2093.295	2101.853	2096.673	2115.165	2120.918	2127.785	2106.934	2115.494	2131.048	2118.424	2089.357	2077.823	1940.712	1285.935
	2125.158	2120.527	2114.227	2112.172	2097.937	2107.858	2103.152	2120.906	2130.163	2128.832	2115.464	2123.383	2129.862	2111.186	2084.489	2075.466	1590.498	1141.141
	2127.078	2125.117	2120.788	2115.459	2100.49	2109.051	2103.291	2119.412	2130.036	2129.717	2122.023	2126.791	2119.596	2104.739	2080.101	1661.75	1240.293	940.761
	2005.152	1995.456	1975.82	1945.239	1899.028	1698.572	1647.396	1600.129	2074.018	2101.064	1765.076	1724.703	2042.303	1771.571	1400.612	1100.855	890.1466	740.3805
	540	540	540	540	540	540	540	540	540	540	540	540	540	540	540	540	540	540
Average Cylinder Pressure [Pa]	122468.8	123473	124010.3	122027	118870.9	120108.9	124030.1	128492.9	134322	143979.6	161611.3	189007.4	222881	273531	317310.9	335445.8	339035.4	339082.7
Cylinder Pressure [Pa]	90100.46	104073.9	118059.6	115765.5	108380.8	111870.6	116709.8	128044.2	115964.2	123907.6	130073.2	151101.9	191954.9	261960.5	312056.5	334775.3	339016.1	339080.7
	96223.06	104893.7	120364.9	116298.4	116248.9	117899.1	121629.3	131271.6	120258.3	126529.8	132190.4	151725.4	191459.4	261620.7	311992.6	334782.1	339016.7	339080.9
	93406.54	100216.7	110869	110682.7	114494.5	116864.8	121425	131655.1	125818.7	128789.9	135004.4	154480.2	192006.4	261359.2	311993.9	334786.4	339018	339081.1
	92783.37	95594.57	100532.1	101164.5	106411.2	108739.1	115978.8	125067.9	125918.7	128054.2	137433.6	158435	195057.9	261097.7	311995.3	334852.6	339020.5	339081.3
	96599.33	95309.63	96788.74	99257.25	97338.84	100546.1	108875.7	115352.3	119267.3	124626.2	138462.5	163171.1	198812.8	261339	311996.6	334927.8	339022.9	339081.5
	101717.2	97701.42	96153.95	97378.52	95774.08	96992.3	103430	104543.4	112616	121095	137887.3	167293.6	202152.5	261765.4	312534.1	335003	339025.4	339081.7
	106149.2	100053.7	96851.11	97997.05	97848.53	97270.84	102055.5	99247.09	105964.6	118233	136041.1	169444.7	205400.4	262287.4	313245.7	335078.2	339027.9	339081.9
	108862.6	103813.9	99836.69	100161.9	99616.47	98811.3	100343.3	98084.34	107049.8	118755.2	134195	170616.9	208575.7	263752.2	313957.3	335153.4	339030.3	339082.1
	111576	107582	102920.7	102758.2	101981.1	100021.2	101009.3	102044.7	108249.9	123522.6	135918.2	171789.2	211751	265216.9	314683.2	335236.5	339032.8	339082.3
	114431.8	111564.8	106507.3	106131.3	104762.5	104113.8	104722.9	105864.4	109285.7	128113.1	139302.7	174761.5	214945.7	267182.8	315886.8	335357.1	339035.2	339082.5
	117293.3	115547.6	110094	109692.2	108230	108283.6	108436.5	109806.8	115259.5	132391.2	144271.4	177899	218912.4	269753.2	317090.4	335477.8	339037.7	339082.7
	122093.5	120890.1	116036.9	115458.9	113323.4	113029.4	114262.4	117787.2	123156	137828.7	152385.8	181872.1	222879.1	272323.7	318293.9	335598.4	339039.8	339083
	127499	126529.1	122174	121225.5	118416.9	119805.8	121665.7	125767.6	131052.4	146255.8	160500.1	189898.4	226845.8	275532.9	319456.3	335719	339041.5	339083.2
	134140.5	133706.5	130401.5	128780.7	124996.7	126582.2	129069	133748.5	140167.4	154648.8	171132.7	197924.6	232947.1	278888.5	320523.8	335839.6	339043.3	339083.4
	141741.8	141879.7	139594.3	136783.4	131633	133347.5	136646.8	141752.3	150684.6	162903.5	181797.3	207667	240228.2	282355.8	321591.3	335926.5	339045.1	339083.6
	148917.5	149865.7	148632.7	144490.1	137927.9	140100.4	144298.8	149756.2	161490.6	170988.7	193465.4	219722.9	247967.8	286353.6	322658.8	335976	339047	339083.9
	155348.9	157562.6	157478.1	151925.1	144022.3	146853.3	151950.7	157760	171533.5	177773.9	205697.9	231778.8	255663.4	290351.4	323370.5	336026.2	339049.1	339084.1
	161120.3	164419.4	165244.7	158289.6	149118.4	150749.6	155931.6	160874.1	178498.3	184361.6	216153.8	240216.2	263049.9	293440.8	323818	336079.5	339051.1	339084.3
	163466.5	167537.4	168946.5	161522.7	151996	153705	159400.2	164138	181784.4	185026.8	222049.1	246701.1	267352.4	295777.7	324293	336133.5	339052.9	339084.6
	165905.3	170718.3	172718.3	164776.2	154896.1	156591.2	162761.6	167292.7	182419.3	185787.3	228263.6	253647.7	269657.2	298261.2	324780.9	336187	339054.8	339084.8
Average Piston Face Pressure [Pa]	147495.7	152294.8	153741.8	152035.4	148740.7	150494.5	154282.9	156843.3	161713.1	165927.4	174575.2	188173.3	214932	258388.8	296444.1	317707.7	326981	329177.3
Maximum Piston Face Pressure [Pa]	166656	198153.2	196379.5	180352.4	181723.4	182395.4	188796	192653.5	215740	214788.1	238596.4	265436.4	322149.5	331201	339525.8	339369.2	339732.1	339773.3
Minimum Piston Face Pressure [Pa]	104351.3	103376.5	103098.6	100397	99618.86	99869.68	100203.9	99623.38	98825.34	98377.38	96078.39	93388.58	105753.5	139000.6	160052.6	186618.4	201280.1	209525.6

Appendix I: RVS Combustion Simulation Results (Intake)

Crank Angle Degree (CAD)	0	10	20	30	40	50	60	70	80	90	100	110	120	130	140	150	160	170	180	190	200	210	220
Average Cylinder Temperature [K]	394.5311	465.2312	375.1453	394.2732	438.5341	450.4356	443.1344	450.8141	457.095	459.682	458.0035	449.4279	443.973	450.6603	456.1496	460.7211	464.311	465.7149	469.0741	470.5261	470.5098	470.657	472.1972
Temperature Points [K]	380	380	380	380	380	380	380	380	380	380	380	380	380	380	380	380	380	380	380	380	380	380	380
	386.2245	405.1545	378.5062	389.0879	447.3785	441.4833	455.0396	439.5852	443.0195	456.6606	464.9902	458.6056	460.3914	465.095	464.4248	465.7207	465.0006	467.3689	467.4186	469.0718	464.2036	460.7339	459.6359
	386.9218	429.4052	376.5104	393.537	450.2922	452.7279	458.5194	454.4485	460.865	465.0594	466.936	471.7081	467.1139	468.0439	476.1752	478.7767	478.2851	478.9297	478.6472	479.1747	479.3448	478.7304	475.9923
	387.6191	432.3469	374.0289	393.3245	453.2112	456.3569	462.3479	465.3203	471.0139	474.1553	469.2776	472.3169	464.2626	467.0597	474.5407	477.7402	478.3653	479.6498	479.5934	479.8214	479.753	479.5094	478.148
	388.3166	435.513	370.8714	392.8939	456.163	459.9858	466.2249	472.9697	473.1527	474.8585	471.2038	467.5535	461.4113	465.1332	471.9716	473.5318	475.0619	476.9753	478.3625	479.3683	479.7788	479.7518	479.2532
	389.014	441.2129	367.3838	392.4633	459.1253	463.6147	468.283	477.1297	474.7341	475.5192	472.9939	462.913	458.8386	463.9759	470.6363	472.3811	474.5021	475.4517	477.6405	479.1683	479.8808	479.9577	479.786
	389.7114	446.9128	363.7123	392.0327	459.5676	465.6751	468.7552	477.4645	476.013	476.1592	474.4562	458.8775	456.3509	462.3349	468.7557	470.9784	473.9404	474.787	477.6576	479.2719	479.9121	479.9672	479.6727
	390.4088	452.6126	360.0407	391.4085	458.3885	467.5326	469.23	477.2487	477.1882	476.8391	475.6909	457.4218	454.0006	460.6939	466.8952	469.6503	473.3817	474.1593	477.7321	479.3894	479.9421	479.9717	479.57
	391.1063	458.3125	356.3692	390.7317	457.2094	469.3902	469.7284	476.2093	478.3319	477.2352	476.9256	456.4648	451.9726	459.2228	465.0654	468.6643	472.9078	473.9312	477.9451	479.4826	479.9367	479.9528	479.4834
	391.8037	464.0124	352.6976	390.0549	456.0303	469.9946	470.2269	475.1414	476.9268	477.4875	477.0491	455.8485	449.9446	457.7696	463.3884	467.7228	472.4367	473.7229	478.1691	479.5746	479.9315	479.9341	479.4313
	392.5018	469.7122	351.1166	388.7305	454.6332	468.669	463.8161	474.0139	475.4604	477.7399	476.9766	456.1945	447.6672	456.2299	462.0313	467.0476	472.0805	473.6744	478.3896	479.6165	479.932	479.9157	479.4513
	393.2034	475.4121	350.5081	386.8787	447.5061	467.3433	453.9598	469.3704	473.9941	475.5871	476.155	456.5406	445.3391	454.609	460.6286	466.3589	471.7227	473.6334	478.6098	479.6559	479.9323	479.8966	479.4864
	393.905	480.0647	349.8996	385.0268	440.3791	466.0177	444.0545	454.0775	468.3759	472.5779	470.1813	454.5214	442.3152	452.7321	459.09	465.558	471.2294	473.4775	478.7275	479.5659	479.9252	479.8722	479.5665
	394.5994	482.8202	349.291	382.0153	433.2924	451.0548	434.048	438.664	453.1125	469.5688	464.2076	451.4193	438.0745	449.1078	457.0261	464.53	470.736	473.3164	478.8385	479.47	479.918	479.7961	479.5446
	395.2928	485.5785	348.6825	376.4906	426.2191	434.608	424.0302	423.0099	437.849	452.7063	451.9853	446.5689	433.8338	445.4835	452.5575	460.5548	466.8995	469.6711	477.0953	477.7303	479.0025	479.0486	479.0559
	398.5483	488.3393	348.4557	370.966	412.8403	418.1612	404.6015	406.5325	422.5856	432.5863	430.5341	427.6423	420.2475	432.9131	446.7194	456.1108	463.0622	465.8757	475.2448	475.9198	478.0867	477.6427	477.266
	403.6564	498.5948	348.3705	365.5548	392.1653	402.1598	382.8244	382.4583	408.1534	412.4664	409.0829	408.7157	405.5797	417.1892	429.49	439.001	445.4872	447.5983	454.7004	457.0745	457.4677	458.4429	464.6519
	408.4774	512.4121	377.6402	361.4343	372.5289	387.0559	364.648	382.4209	394.3108	394.9415	391.3452	391.805	392.2773	402.5139	412.3968	421.8912	427.7452	428.7281	433.2091	437.532	436.6092	439.2431	452.0564
	412.5963	526.2081	458.8222	422.8331	373.7525	446.8808	382.351	450.2181	456.8129	431.4928	420.0777	413.4409	409.8398	413.0978	401.1984	408.2027	413.3761	413.3474	413.5008	419.6342	416.6386	420.7736	441.8926
	416.7151	540	540	540	540	540	540	540	540	540	540	540	540	540	540	540	540	540	540	540	540	540	540
Average Cylinder Pressure [Pa]	101325	101323	101263.6	101277.5	101317.5	101322.9	101327.4	101327.1	101324.5	101324.8	101323.9	101325	101332.1	101332.1	101333.5	101331.3	101328.4	101327.1	101323.5	101323.5	101324	101324.1	101323.9
Cylinder Pressure [Pa]	101325	101323	101262.9	101278	101316.5	101322.6	101322.9	101322.8	101323.1	101323.5	101322.2	101322.9	101322	101323.4	101323.2	101322.9	101323.5	101323.3	101322.8	101322.7	101323.2	101323.5	101322.9
	101325	101323	101262.1	101278.1	101316.6	101322.6	101322.9	101323	101323.1	101323.6	101322.3	101323.1	101322.3	101323.3	101323.3	101323	101323.5	101323.4	101323.1	101322.9	101323.2	101323.5	101323
	101325	101323	101261.4	101278.1	101316.7	101322.6	101323	101323.2	101323.2	101323.7	101322.6	101323.2	101322.7	101323.4	101323.7	101323.3	101323.9	101323.3	101323.1	101323.1	101323.4	101323.6	101323.1
	101325	101323	101260.7	101278.1	101316.7	101322.6	101323.1	101323.5	101323.3	101323.7	101322.9	101323.2	101323.2	101323.6	101323.9	101323.5	101324	101323.1	101322.9	101323.3	101323.7	101323.7	101323.3
	101325	101323	101260.1	101277.9	101316.8	101322.6	101323.2	101323.7	101323.3	101323.7	101323.3	101323.3	101323.7	101323.8	101324	101323.8	101324.1	101323.3	101323.1	101323.5	101323.8	101323.9	101323.4
	101325	101323	101259.5	101277.7	101316.9	101322.7	101323.4	101323.8	101323.4	101323.7	101323.7	101323.6	101324	101324.1	101324.1	101324.1	101324.2	101323.7	101323.5	101323.8	101324	101324	101323.7
	101325	101323	101258.9	101277.5	101316.9	101322.6	101323.6	101323.8	101323.5	101323.9	101324	101324	101324.2	101324.3	101324.3	101324.5	101324.4	101324.1	101323.8	101324	101324.1	101324.1	101323.9
	101325	101323	101258.4	101277.2	101316.8	101322.6	101323.9	101323.8	101323.5	101324	101324.2	101324.3	101324.4	101324.4	101324.4	101324.8	101324.7	101324.5	101324.1	101324.3	101324.2	101324.2	101324.2
	101325	101323	101257.8	101276.8	101316.8	101322.6	101324.1	101323.9	101323.6	101324.1	101324.4	101324.5	101324.3	101324.4	101324.3	101324.7	101324.6	101324.5	101324.1	101324.2	101324.3	101324.3	101324.3
	101325	101323	101257.2	101276.3	101316.7	101322.5	101324.4	101324	101323.7	101324.3	101324.4	101324.8	101324.3	101324.5	101324.3	101324.6	101324.5	101324.4	101324.1	101324.2	101324.3	101324.3	101324.5
	101325	101323	101258.4	101276.1	101316.7	101322.5	101325	101324.1	101323.9	101324.5	101324.3	101324.8	101324.6	101324.5	101324.2	101324.5	101324.4	101324.2	101323.9	101324.1	101324.3	101324.4	101324.5
	101325	101323	101260.3	101275.9	101316.8	101322.5	101325.8	101324.4	101324	101324.5	101324.2	101324.9	101324.9	101324.7	101324.3	101324.4	101324.2	101324	101323.8	101324	101324.3	101324.4	101324.5
	101325	101323	101262.3	101275.8	101316.9	101322.4	101326.7	101325.6	101324.2	101324.5	101324.1	101324.7	101326	101325.2	101324.9	101324.5	101324.1	101323.8	101323.5	101323.8	101324.2	101324.4	101324.3
	101325	101323	101264.3	101275.9	101317	101322.7	101327.4	101326.8	101324.8	101324.5	101324	101324.3	101328.6	101327.6	101326.1	101324.8	101324.1	101323.6	101323.1	101323.6	101324.1	101324.4	101324.2
	101325	101323	101266.2	101276.6	101317.2	101323	101328.2	101327.9	101325.3	101325	101324	101324.1	101331.1	101330.1	101330.3	101327.8	101325.6	101324.4	101322.7	101323.3	101324	101324.4	101323.9
	101325	101323	101268.1	101277.3	101317.7	101323.2	101330.8	101329.3	101325.9	101325.6	101324.2	101325.3	101339	101337.5	101335.6	101331	101327.1	101325.3	101322.3	101323	101324	101324.3	101323.7
	101325	101323	101270	101278	101318.7	101323.5	101333.8	101333.4	101326.5	101326.3	101324.4	101326.5	101347.6	101346.6	101349	101342.3	101334.4	101331.2	101322.9	101322.9	101324	101324.1	101323.9
	101325	101323	101272.1	101278.7	101319.7	101323.8	101336.7	101336.3	101327	101327	101324.7	101328	101355.6	101355.3	101362.3	101353.6	101341.7	101337.3	101323.6	101322.8	101324.1	101324	101324
	101325	101323	101274.2	101279.3	101320.5	101324.1	101338.8	101338	101327.4	101327.6	101325.1	101329.4	101361.6	101361.6	101371.9	101362.1	101347.7	101342.5	101324.4	101322.9	101324.1	101323.9	101324.2
	101325	101323	101276.3	101280	101321.4	101324.3	101341.4	101340.8	101328.1	101328.3	101325.4	101331.1	101368.4	101368.9	101382	101370.9	101353.7	101347.8	101325.2	101322.9	101324.2	101323.7	101324.5

Appendix J: RVS Combustion Simulation Results (Combustion)

Crank Angle Degree (CAD)	360	370	380	390	400	410	420	430	440	450	460	470	480	490	500	510	520	530	540
Average Cylinder Temperature [K]	2176.581	2276.556	2519.933	2374.345	2372.082	2443.296	2443.155	2492.769	2370.282	2481.31	2829.572	2520.447	2368.631	2816.726	2138.76	2480.623	3001.925	2125.116	2302.06
Temperature Points [K]	2424.295	2424.169	2423.649	2423.734	2423.674	2423.769	2423.787	2423.643	2423.797	2423.786	2423.759	2423.7	2423.783	2423.782	2423.763	2423.76	2423.646	2423.77	2423.679
	2447.505	2445.337	2399.28	2403.01	2378.199	2632.679	2509.863	2569.132	2483.536	2741.459	2998.729	2830.91	2673.051	2910.432	2425.048	2702.995	3698.35	2365.276	2556.422
	2447.32	2465.869	2387.842	2393.982	2353.452	2627.707	2515.258	2543.173	2435.193	2652.994	2922.702	2725.004	2553.129	2859.498	2322.919	2638.248	3598.265	2248.724	2516.007
	2447.135	2471.428	2389.335	2396.107	2328.938	2594.741	2475.046	2501.359	2388.734	2540.707	2890.302	2629.531	2460.122	2860.261	2209.233	2571.506	3465.215	2217.524	2513.64
	2446.95	2477.258	2412.206	2388.508	2305.844	2561.787	2433.848	2446.745	2344.238	2472.502	2846.909	2560.637	2367.115	2908.728	2120.922	2519.048	3282.151	2189.36	2481.986
	2446.765	2486.159	2464.189	2380.91	2283.205	2528.833	2392.426	2412.043	2314.911	2411.107	2882.989	2522.658	2353.523	2966.514	2094.134	2504.292	3235.673	2181.274	2488.405
	2446.579	2495.059	2532.368	2373.312	2262.649	2482.185	2350.809	2399.169	2293.821	2359.289	2882.483	2482.719	2364.151	2961.981	2123.225	2517.455	3222.442	2184.603	2465.304
	2446.394	2503.96	2600.547	2353.646	2243.432	2433.766	2311.503	2399.979	2275.554	2330.402	2850.652	2489.622	2374.244	2957.448	2148.504	2532.293	3208.231	2188.405	2439.138
	2446.209	2512.86	2668.726	2330.703	2224.215	2385.347	2292.843	2421.251	2258.144	2333.402	2818.82	2505.673	2383.085	2966.045	2167.952	2554.81	3167.101	2188.87	2408.577
	2446.024	2521.76	2736.905	2307.761	2204.997	2372.212	2274.182	2448.752	2320.491	2351.867	2824.686	2522.576	2391.925	2976.025	2177.232	2572.499	3125.253	2189.169	2377.665
	2445.839	2530.661	2795.166	2336.289	2191.169	2413.424	2333.883	2489.221	2384.752	2370.331	2837.196	2541.887	2394.358	2977.796	2165.229	2561.303	3053.439	2164.676	2335.099
	2445.653	2539.561	2848.814	2406.743	2318.954	2454.636	2432.662	2549.554	2449.013	2467.622	2859.254	2561.199	2395.49	2971.874	2153.575	2548.978	2981.755	2139.008	2291.688
	2445.466	2546.483	2902.462	2477.196	2446.738	2495.848	2536.494	2670.054	2526.392	2592.982	2946.976	2604.459	2409.743	2968.359	2142.961	2527.261	2921.14	2103.495	2245.81
	2445.282	2549.822	2956.111	2561.956	2568.83	2598.113	2650.766	2797.268	2634.243	2718.342	3034.697	2658.685	2446.944	2981.274	2139.145	2509.106	2860.524	2067.536	2199.773
	2445.098	2553.163	3009.759	2677.715	2689.026	2707.02	2766.198	2937.855	2742.094	2838.438	3138.556	2716.295	2484.145	2994.188	2166.438	2537.191	2887.736	2081.564	2213.687
	2203.644	2556.508	3030.655	2793.475	2815.027	2815.928	2877.536	3081.495	2849.946	2957.297	3266.248	2801.155	2570.892	3042.938	2200.115	2567.948	2914.968	2097.744	2231.069
	1787.732	2185.653	3038.962	2902.523	2947.746	2895.299	2987.853	3229.259	2917.214	3076.155	3393.94	2886.016	2663.372	3104.321	2286.889	2670.909	3040.256	2207.761	2338.062
	1371.821	1636.958	2661.134	2934.813	3057.905	2937.895	3066.48	3046.691	2955.899	3115.128	3476.984	2948.597	2740.025	3162.076	2372.848	2773.871	3166.737	2321.618	2449.593
	955.9103	1088.46	1600.558	2104.517	2857.639	1964.738	2691.653	1948.735	1867.674	2332.396	2755.564	2457.625	2383.518	2800.987	2395.07	2838.981	3245.62	2401.934	2525.598
	540	540	540	540	540	540	540	540	540	540	540	540	540	540	540	540	540	540	540
Average Cylinder Pressure [Pa]	5964630	4353614	1073284	665547	367975.3	267580.8	282670.5	260452.9	192521.7	185393.9	181418.2	175575.6	155385.1	163238.1	163352.8	149262.9	153220.1	160056.3	147203.5
Cylinder Pressure [Pa]	5542760	3197792	471032.1	526087.8	408302.3	341281.2	873960.2	1780399	698231.2	376067.1	650967.5	703679.6	375497	474765.3	677118.9	382167.7	480009.7	717404.6	539438.1
	5586916	3353505	445401.6	479160.4	351447.1	375121.8	402632.3	293464.5	342723.3	381783.4	326004.5	318035.7	293003.3	351944.4	268899.4	306971	273835.3	283063.4	220362.7
	5631017	3504987	430236.7	455660.9	325800.7	353793.8	385889.4	263798.1	287531.6	327524.5	265959.3	244409	217507.1	254684.8	189202.4	192335	177403	165890.9	139302.1
	5675117	3556693	425473.8	454790	300421.4	325180.7	338460.6	228508.8	233974.9	256166.5	200247.6	180783.7	163274.3	181859.1	133359.9	130893.5	125995.5	118802	108565.6
	5719218	3615802	437404	447122.1	276669.7	296566.6	290160.5	188680.4	182119.9	195749.9	154537.7	134048.6	109041.5	124847.7	97681.57	97278.31	105077.5	96512.19	95018.65
	5763319	3758482	489755.7	439454.2	253440.1	267952.5	250152.2	156430.4	147937.4	152770.7	109410.7	105561.3	88546.78	82575.71	76428.89	72092.62	83129.94	78463.05	84731.42
	5807419	3901163	564593.9	431786.3	234726	239802.4	217373.6	132488	123261.8	121923	85130.98	79386.26	78341.51	72757.51	69787.91	69132.95	83526.6	75721.27	83229.55
	5851520	4043843	639432.2	417799	218917	211712.2	184982.2	116081	100168.2	91837.47	76330.21	70928.4	71357.28	62939.31	67784.86	68071.11	84143.01	73753.97	82472.92
	5895621	4186523	714270.6	402095.7	203108	183622.1	156047	110940.9	77555.2	77615.21	67529.43	65908.67	71932.28	65517.91	72877.34	75709.05	90790.37	79902.43	87647.35
	5939721	4329203	789108.9	386392.4	187299	163554.9	127111.7	105675.4	79726.25	71357.58	68603.68	63819.61	72507.29	69402.79	79558.74	83685.29	97389.76	86453.39	93296.37
	5983831	4471883	928016.2	399322.8	173231.7	155844.9	125959.7	100149	82492.19	65099.95	71418.06	70012.16	79672.04	78114.04	89566.12	93685.13	101983.9	94304.77	98583.26
	6027990	4614563	1096726	435576	204930.3	148134.9	138662.6	100542.4	85258.13	74442.78	76377.25	76204.7	88174.21	91348	99390.08	103271.4	106535.1	102217.8	103843.9
	6072149	4738821	1265436	471829.2	236628.9	140424.8	151095.6	118865.6	94795.84	89340.82	96086.3	92569.76	100211	105037.9	108667.6	109419.6	107424.7	106500.5	105893.8
	6116206	4829709	1434145	555707.5	269024.3	179155.7	162970.7	136687.6	120065.3	104238.9	115795.4	113592.6	118429.3	121839.4	118303	115764.5	108314.4	110619	107734.7
	6160249	4920686	1602855	742789	301651.8	222939.9	174783.7	153511.5	145334.7	138150.5	140862.1	135589.7	136647.6	138640.8	129576.6	124663.2	116044.9	118824.1	115262.3
	6206863	5011746	1726087	929870.5	391840.2	266724.1	225631.2	173063.1	170604.1	176533.2	173842	165431.4	163496.6	159575.5	142824.9	134347.2	123776.9	127205.3	123118.8
	6255336	5109016	1831871	1113331	548634.5	308415.2	286219.7	218801.4	191351.1	214915.8	206821.9	195273	191344.5	181967.1	172499	165256.6	156193.6	154588.5	150910.5
	6303847	5209237	1941519	1255392	699028.9	348450.5	341660.5	254990.7	210005	240119.5	229341.6	216886.4	213783.8	201435.3	201900.3	196165.9	188910.3	182749.4	179712.1
	6352448	5309299	2057958	1405212	820793.6	390995.8	385971.7	276228.5	229331.5	264012.2	247414.5	232099.4	229508.1	215513.2	224251.5	219882.6	214034.9	203483.4	201398.6
	6401049	5409331	2174361	1561560	953610.8	431942.6	433685.4	299752	247965.7	288228.4	265684	247292.2	245425.7	229996.8	247377.7	244465.1	239882.8	224666.5	223546.5
Average Piston Face Pressure [Pa]	392327	259051.5	103699.3	124258.4	128768.8	129768.4	142387	123471.2	127194.5	139322.3	127813.6	128113.3	125000.5	129667.1	125481.9	125389.2	124120.9	128139.3	124025.6
Maximum Piston Face Pressure [Pa]	6554400	6143824	2345168	1885578	1047413	589763.5	491374.4	428566.4	290232.4	342622.2	305691.9	292829	282811.4	298221.5	282722.6	298025.1	273345.7	280846.4	282112.9
Minimum Piston Face Pressure [Pa]	66026.42	23427.27	10313.25	12120.8	22763.19	57646.73	71412.24	93841.99	95681.53	78484.92	94034.13	98052.99	94877.64	95774.68	95514.97	95708.03	94680.22	92500.27	95654.35

Appendix K: RVS Combustion Simulation Results (Exhaust)

Crank Angle Degree (CAD)	550	560	570	580	590	600	610	620	630	640	650	660	670	680	690	700	710	720
Average Cylinder Temperature [K]	2308.282	2290.28	2301.965	2294.644	2269.137	2260.709	2289.812	2265.241	2255.23	2240.976	2197.192	2230.187	2183.578	2199.932	2162.905	2077.5	1521.756	1183.209
Temperature Points [K]	2433.133	2409.111	2417.531	2411.214	2376.847	2371.813	2423.795	2381.474	2398.272	2386.382	2351.501	2342.865	2320.479	2307.543	2302.822	2302.084	2007.216	1322.021
	2413.578	2392.61	2406.558	2407.03	2380.47	2379.813	2413.259	2381.404	2378.712	2381.395	2353.999	2345.465	2321.522	2307.243	2302.76	2302.013	1968.422	1349.787
	2407.216	2385.161	2398.16	2394.508	2373.857	2373.067	2406.041	2379.691	2378.614	2378.587	2352.541	2345.901	2321.578	2307.136	2302.717	2301.947	1930.618	1341.265
	2399.468	2377.304	2392.632	2386.404	2367.76	2365.733	2401.991	2376.469	2378.284	2376.608	2350.652	2344.884	2321.121	2307.031	2302.689	2301.886	1916.167	1332.743
	2392.137	2371.84	2387.081	2381.048	2362.784	2358.399	2398.825	2373.799	2374.863	2375.492	2348.415	2343.831	2320.664	2306.932	2302.573	2301.836	1898.343	1324.221
	2387.677	2367.72	2383.197	2378.811	2360.259	2357.99	2395.288	2372.177	2372.408	2374.619	2347.452	2342.656	2320.207	2306.835	2302.456	2300.316	1842.444	1315.698
	2388.055	2368.689	2383.708	2379.788	2362.558	2359.692	2393.405	2373.621	2370.736	2373.915	2347.887	2341.372	2319.408	2306.546	2302.339	2297.978	1786.546	1307.176
	2388.667	2369.683	2384.495	2381.159	2364.858	2361.585	2395.638	2377.245	2369.618	2373.981	2348.09	2340.136	2318.564	2306.134	2302.206	2295.64	1730.649	1298.654
	2390.721	2371.352	2386.544	2383.135	2368.205	2363.924	2398.663	2380.869	2371.241	2374.282	2347.948	2339.324	2317.721	2305.723	2302.069	2293.301	1674.752	1290.131
	2392.846	2373.065	2388.883	2385.571	2371.664	2366.263	2401.882	2384.555	2374.228	2376.131	2347.872	2338.513	2316.676	2305.311	2301.932	2290.963	1618.854	1281.609
	2397.089	2376.618	2392.959	2388.971	2375.807	2369.415	2405.655	2388.252	2377.215	2378.017	2347.932	2337.862	2315.323	2304.879	2301.683	2264.42	1562.957	1273.003
	2401.431	2380.195	2397.145	2392.44	2380.591	2372.733	2409.428	2391.614	2379.455	2379.903	2347.117	2337.291	2313.969	2303.913	2301.344	2226.617	1507.06	1263.961
	2407.099	2385.796	2402.244	2396.114	2385.209	2375.707	2411.346	2392.679	2381.43	2379.734	2343.653	2336.707	2312.615	2302.946	2301.006	2188.815	1456.199	1254.918
	2412.826	2391.397	2407.137	2399.211	2388.689	2378.082	2412.415	2393.743	2383.404	2374.789	2340.312	2336.098	2304.612	2302.007	2292.208	2151.012	1414.458	1246.781
	2415.948	2395.962	2409.352	2399.664	2392.168	2380.457	2412.345	2390.993	2378.307	2369.844	2337.214	2335.487	2295.886	2301.076	2265.081	2113.21	1373.023	1238.779
	2418.958	2400.527	2410.997	2398.689	2387.169	2374.489	2403.098	2382.61	2371.547	2364.899	2333.377	2325.039	2287.159	2289.284	2237.953	2077.102	1331.874	1147.889
	2406.265	2391.994	2397.222	2385.84	2379.182	2367.554	2393.852	2374.226	2364.787	2359.662	2322.218	2312.137	2278.812	2264.925	2210.85	2041.583	1172.145	997.0634
	2392.929	2383.302	2383.447	2373.031	2370.886	2360.423	2385.047	2366.313	2357.744	2354.214	2123.816	2299.446	2270.887	2240.674	2184.017	1792.709	956.0603	845.6568
	2379.602	2373.265	2370.008	2330.244	2093.773	2037.042	1994.263	1903.086	1803.736	1547.062	1411.852	2018.718	1554.355	2082.497	1599.4	1166.575	747.3246	692.8284
	540	540	540	540	540	540	540	540	540	540	540	540	540	540	540	540	540	540
Average Cylinder Pressure [Pa]	110919.5	112846.6	111471.5	110609.7	112305.7	111860.2	115095.6	116420.4	118843.2	120298.6	125531.8	131202.5	138875.4	144470.6	146537.4	147135	147201.3	147203
Cylinder Pressure [Pa]	78800.51	86017.13	85949.5	85963.91	93582.47	89669.02	85018.07	91400.54	87730.09	96373.05	113241.7	120187.7	135165.2	143320.9	146410.4	147132.6	147201.3	147202.9
	91641.87	90836.82	92010.67	93582.37	95635	94713.04	89953.92	93261.65	92126.28	101579	114655.8	120940.4	135525.8	143288.7	146408.7	147132.4	147201.3	147202.9
	97422.8	97672.7	97865.02	98232.88	99025.53	98928.98	95443.07	96753.67	97826.7	105095.5	115517.8	121531.4	135776.7	143375.8	146407.2	147132.3	147201.3	147202.9
	101583.7	101602.4	101921.4	101316.7	101578.3	102010.9	100253	100757.9	104512.3	108113	116514.3	122996.9	136098.4	143468.4	146405.9	147132.1	147201.3	147203
	103805.8	104150.7	104423	103889.7	103634	105092.8	104242.6	103984.8	107957.3	110611.3	117619.5	124491.9	136420	143594.5	146414.1	147132	147201.3	147203
	105883.8	106577	106489.1	105615.3	105463.5	106710.7	107480.3	107195	110926.8	113036.9	118926.7	126007.9	136741.7	143731.4	146422.4	147132.2	147201.3	147203
	106697.5	107392.1	107102.9	106393.7	106771.6	107882	110708.8	110000.8	113587	115424.8	120455.4	127542.3	137142.6	143895.1	146430.6	147132.6	147201.3	147203
	107446.1	108212.1	107736.6	107176.8	108079.6	108982.1	112723.4	112507.5	116327.1	117832.8	122041.2	129079.3	137553.7	144076	146453.5	147133	147201.3	147203
	108295.9	109167.2	108461.2	107966.9	109388.7	109914.8	114501.4	115014.1	118648.1	120247.1	123712.4	130639.4	137964.9	144256.9	146480.5	147133.5	147201.3	147203
	109150.8	110144.2	109304.1	108970.7	110697.8	110847.6	116340.7	117412.4	120756.3	121989.9	125380.4	132199.5	138426.3	144437.7	146507.4	147133.9	147201.3	147203
	110659.9	112033.3	110854.7	110421.8	112389.3	112393.6	118353.3	119791.7	122864.5	123716.6	127041.9	133316.9	138965.2	144617.1	146536.4	147134.6	147201.3	147203
	112200	113933.7	112495.3	112050.5	114439.1	114064.1	120365.9	122144.3	124997.2	125443.3	128601	134213.5	139504.1	144757.5	146567.1	147135.3	147201.3	147203
	114466.3	116787.9	114883.9	114208.5	116525.6	115868.1	122422.2	124313.9	127138.6	127042.5	129850.2	135108.2	140043	144897.9	146597.7	147136.1	147201.3	147203
	116765.4	119642.2	117300.8	116408.4	118862.7	117905.7	124498.6	126483.6	129280	128345.6	131098.2	135999	140553	145042.4	146624.9	147136.9	147201.3	147203
	119564.9	122840.9	120084.9	118800.4	121199.8	119943.3	126528.9	128366.4	130898.5	129648.6	132343.5	136889.5	141059.9	145188.3	146644.7	147137.7	147201.3	147203
	122385.8	126039.6	122849.8	121139.9	123122.7	121756.9	128188.5	129825.7	132394.1	130951.7	133551	137562.4	141566.8	145321.6	146664.4	147138.1	147201.3	147203
	125028.9	128477.9	125097.5	123043.4	124899.6	123544.6	129848	131284.9	133889.7	131793.1	134412.2	138181.1	141948	145440.3	146683.1	147138.4	147201.3	147203
	127664.6	130906.8	127345.2	124906.3	126284.7	124894.9	130988.3	132113.6	134502.9	132344	135102.2	138700.2	142145.8	145542.2	146689.4	147138.6	147201.3	147203
	128867.9	131803.5	128189.5	125661.8	126930.9	125648.9	131673.3	132627.1	134995.5	132901.9	135275.5	139048.4	142349.3	145566.4	146696.1	147138.9	147201.3	147203
	130056.6	132693.9	129064.5	126444.7	127603.1	126432.2	132380.6	133169	135505.5	133480.9	135294.9	139413.9	142558.1	145592.7	146703.1	147139.1	147201.3	147203
Average Piston Face Pressure [Pa]	125455	126479.5	124846.4	123235.8	124170.7	122727.3	127357	127982.2	127001.7	127478.3	129118.8	130605.9	132227.7	135848.3	138792.6	142133.3	144458.2	145496
Maximum Piston Face Pressure [Pa]	143694.6	142987.7	141165	140119.4	139667.8	139896	142488	143014.9	143226.6	142849.6	146755.3	146588	146821	147268.2	147195.8	147203.5	147218	149489.2
Minimum Piston Face Pressure [Pa]	100263.6	99428.76	100831.5	99050.98	100128.9	99742.47	100699.5	100606.1	98885.62	99343.94	98771.94	99412.72	100261.8	100519	100596.9	103470	106462	107466.3

Appendix L: Traditional COld Flow Velocity Cut Plots

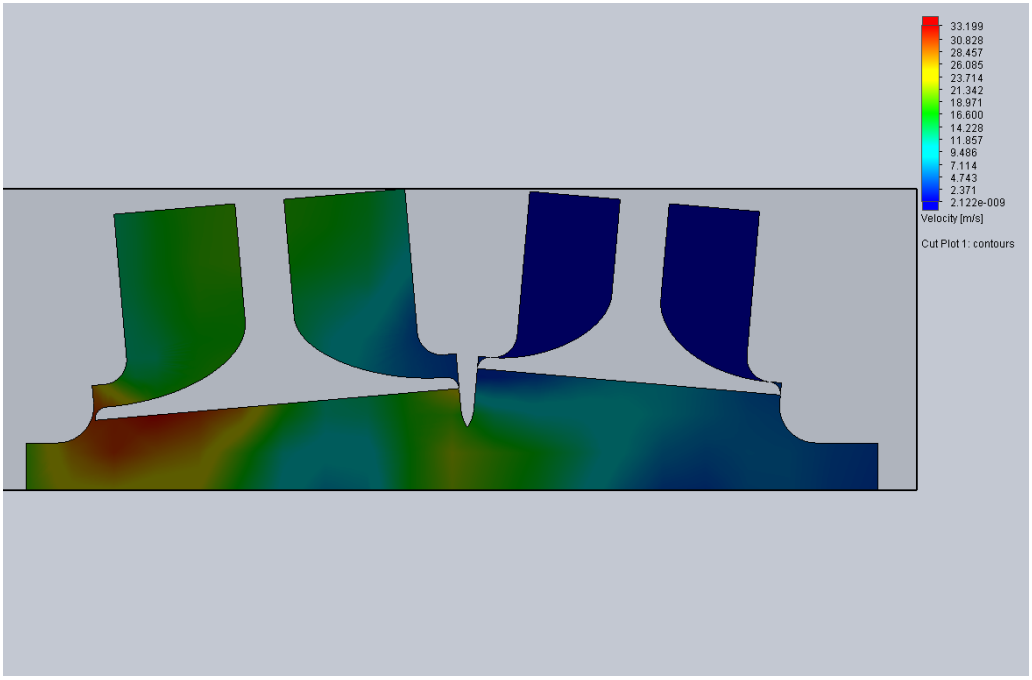

Intake Valve Opens - 20°

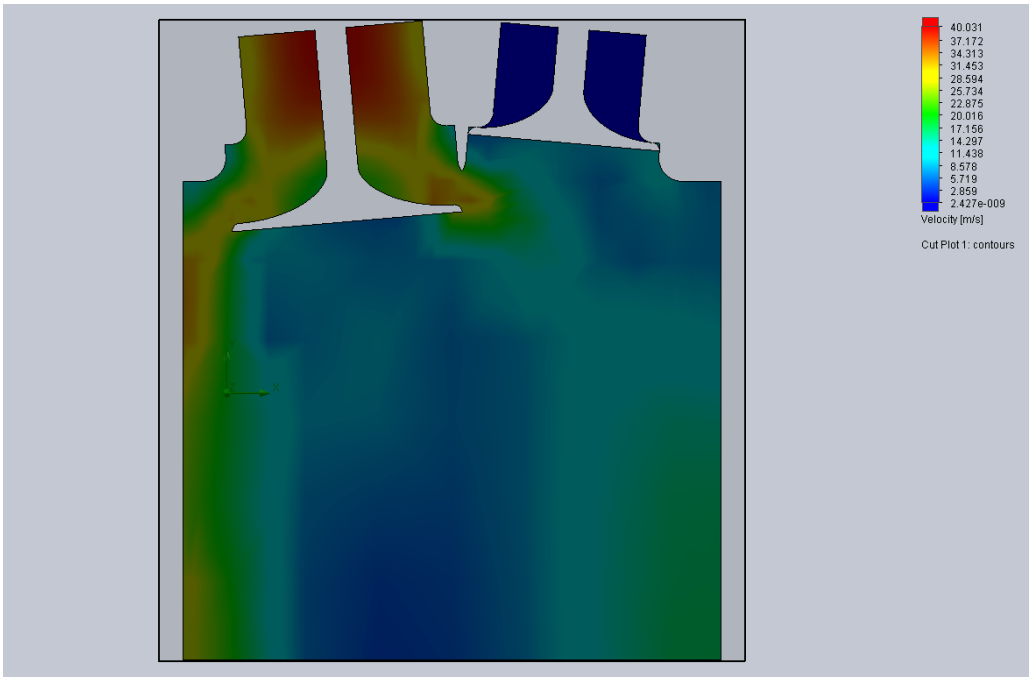

Maximum Intake Valve Opening - 120°

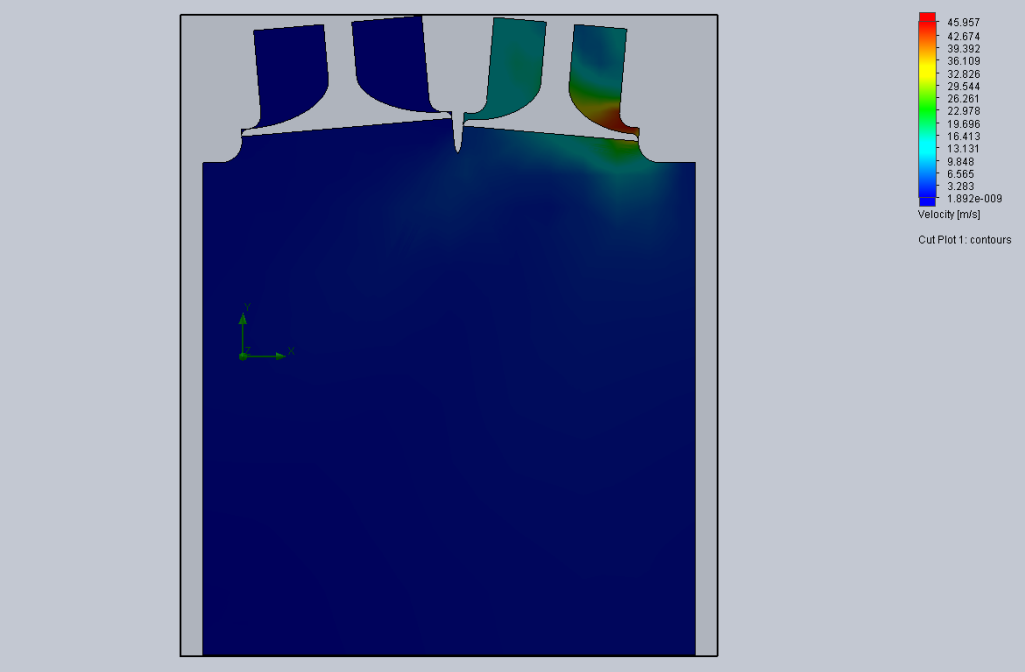

Exhaust Valve Opens - 500°

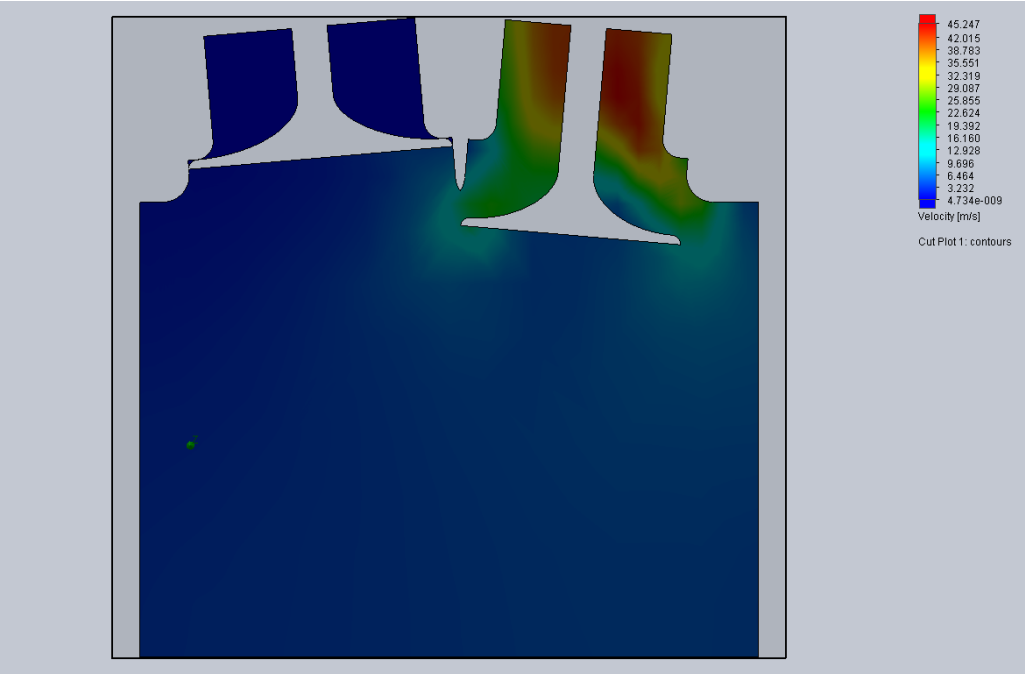

Maximum Exhaust Valve Opening - 620°

Appendix M: RVS Cold Flow Velocity Cut Plots

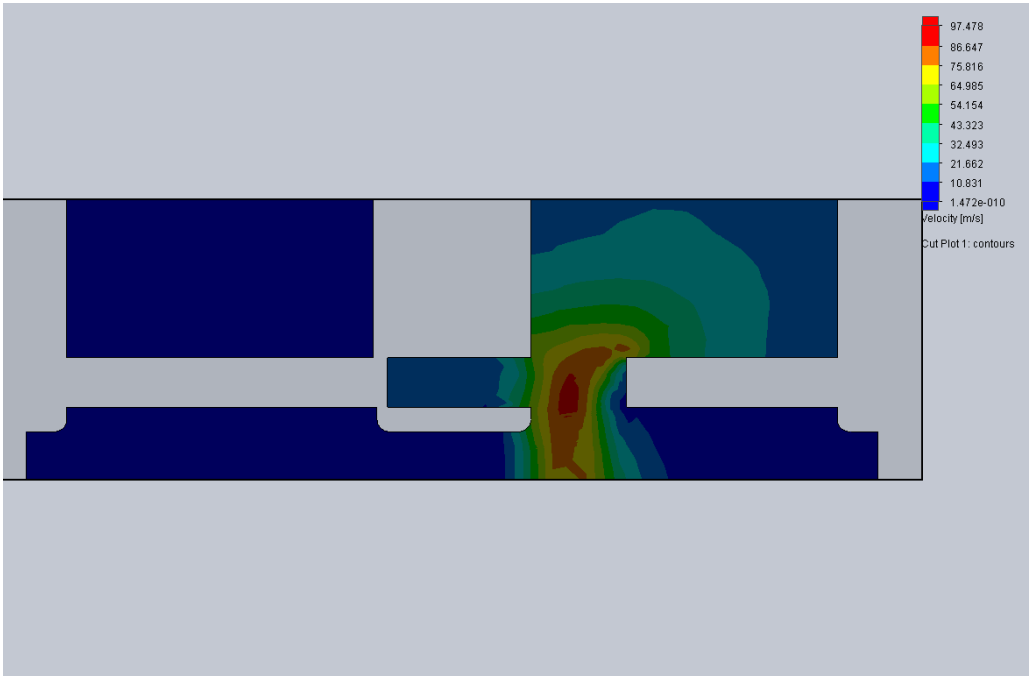

Intake Port Opens - 20°

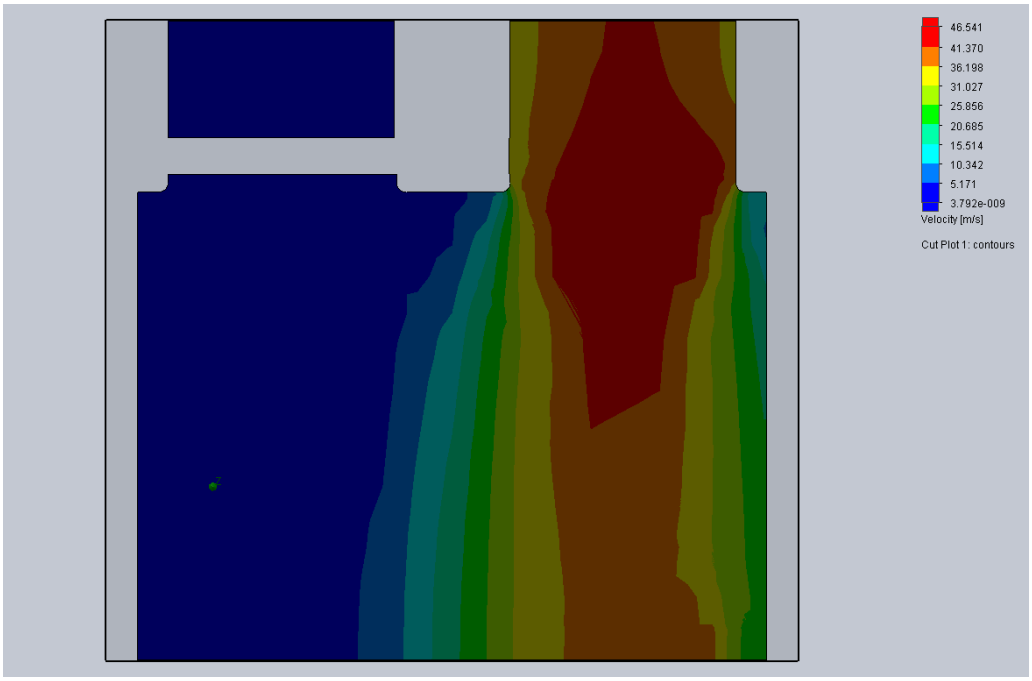

Maximum Intake Port Opening - 100°

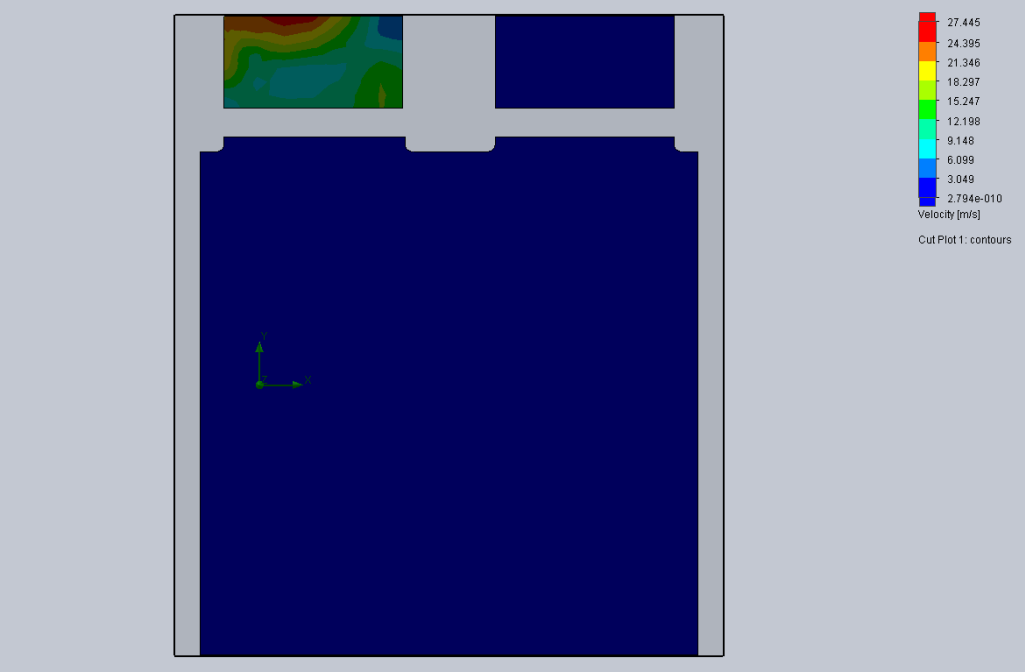

Exhaust Port Opens - 500°

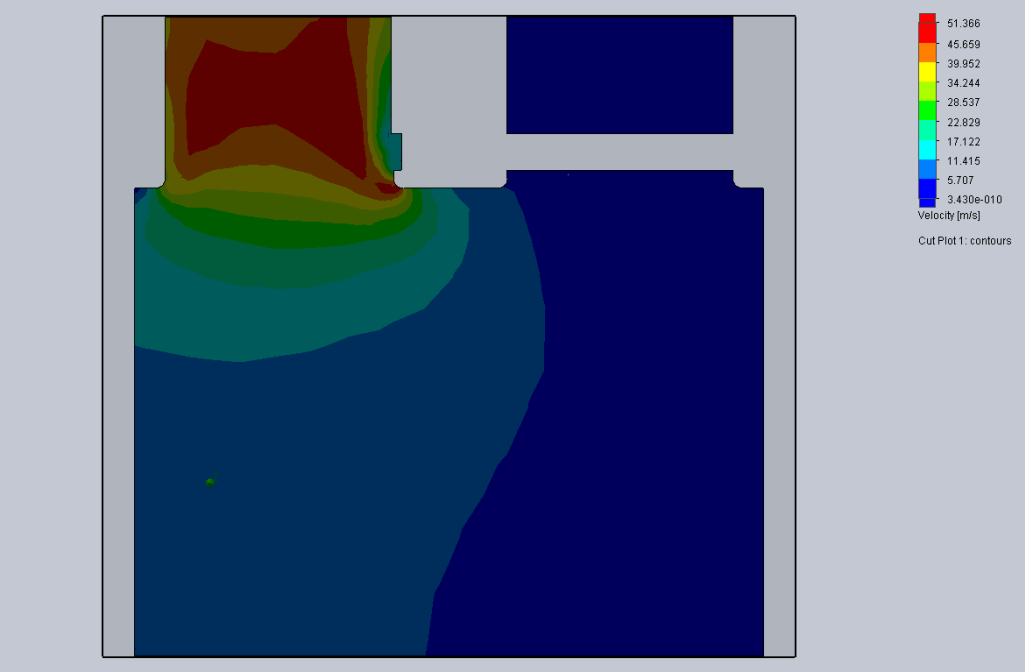

Maximum Exhaust Port Opening - 620°

Appendix N: Traditional Combustion Velocity Cut Plots

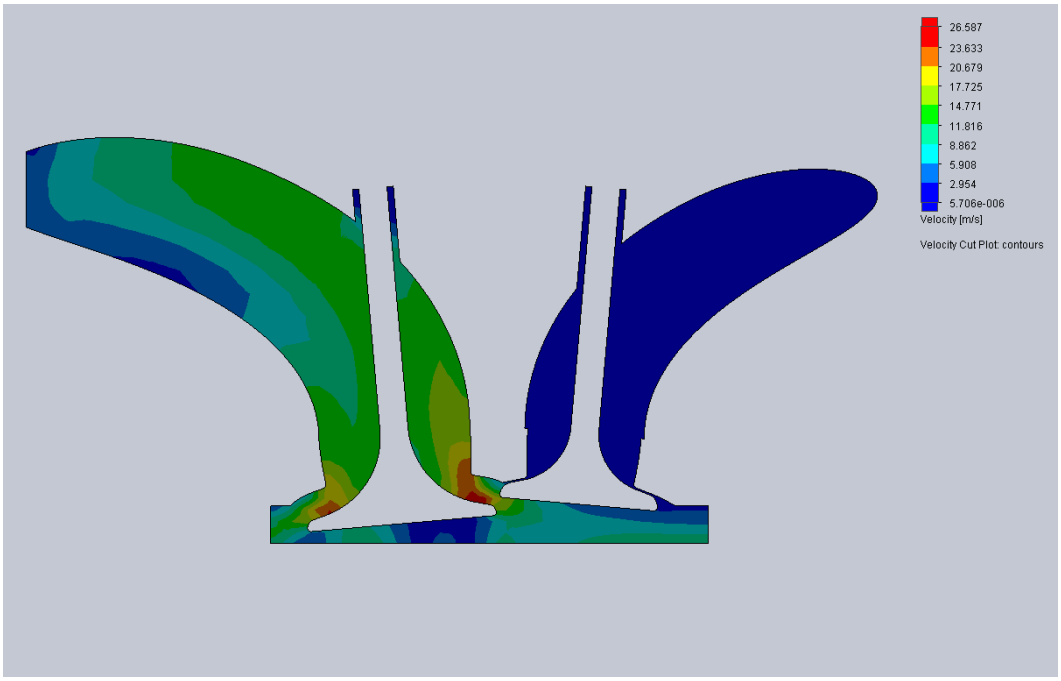

Intake Valve Opens - 20°

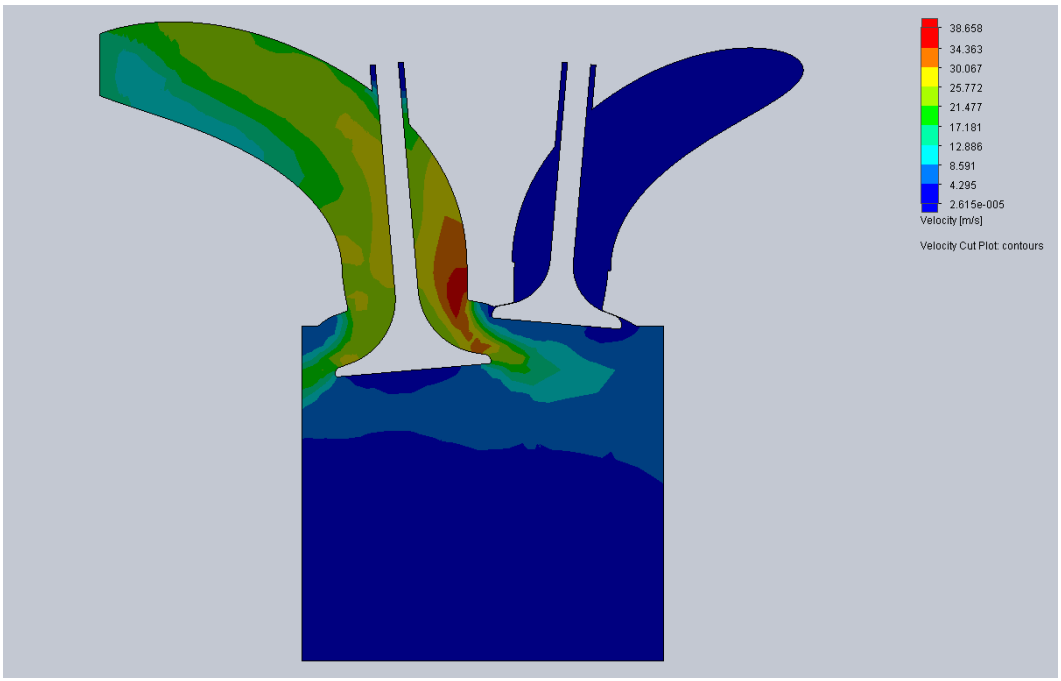

Maximum Intake Valve Opening – 120°

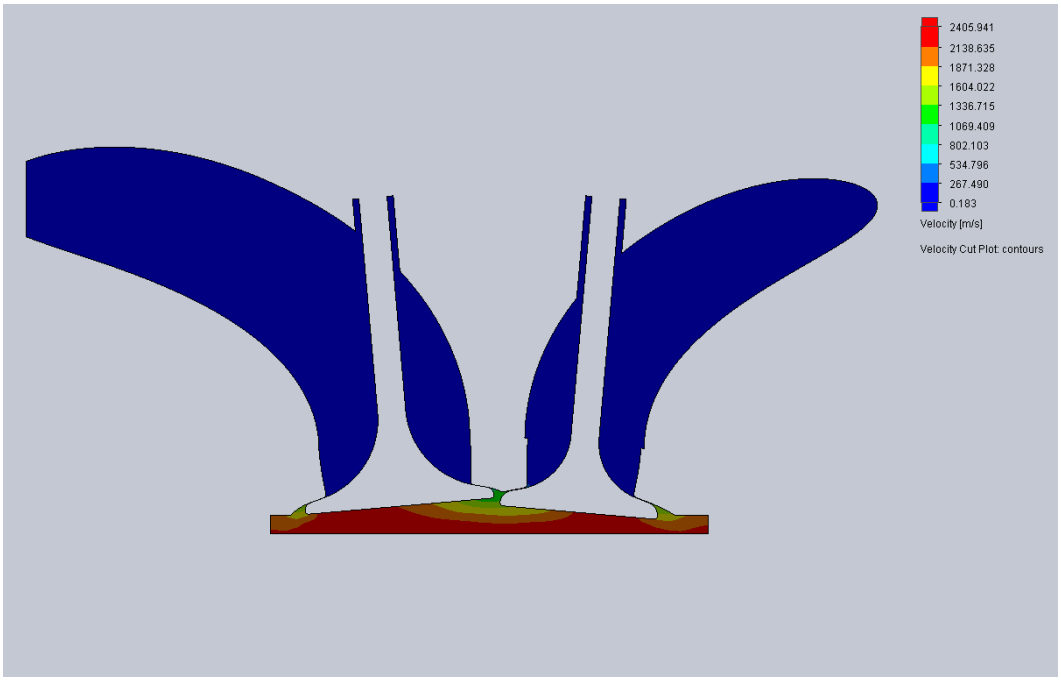

Combustion Begins – 360°

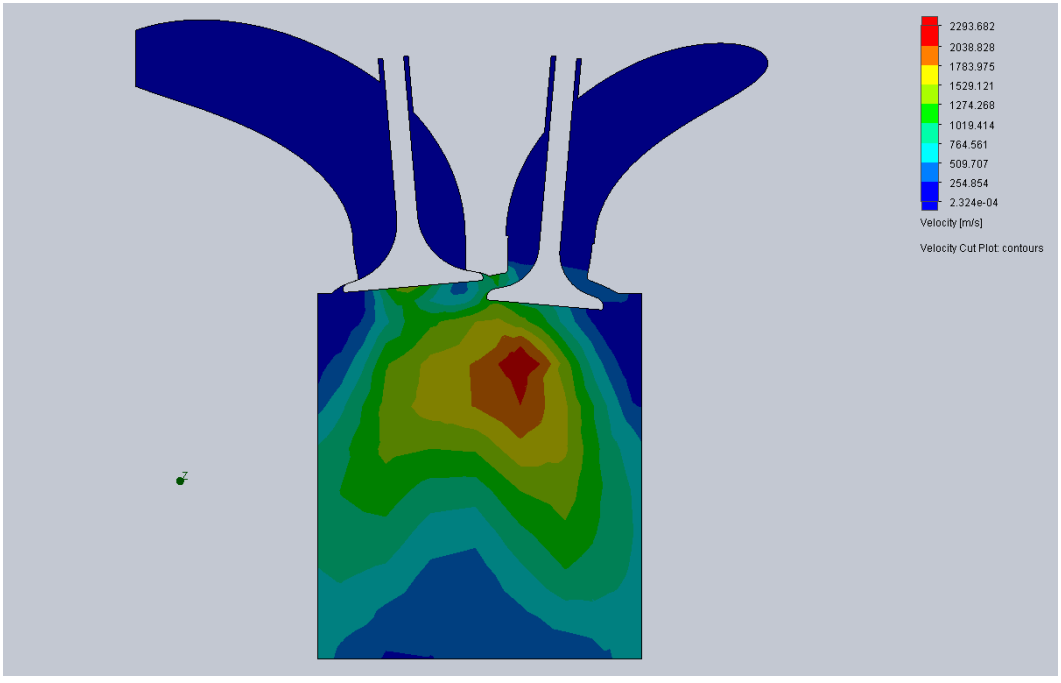

Combustion Concludes – 540°

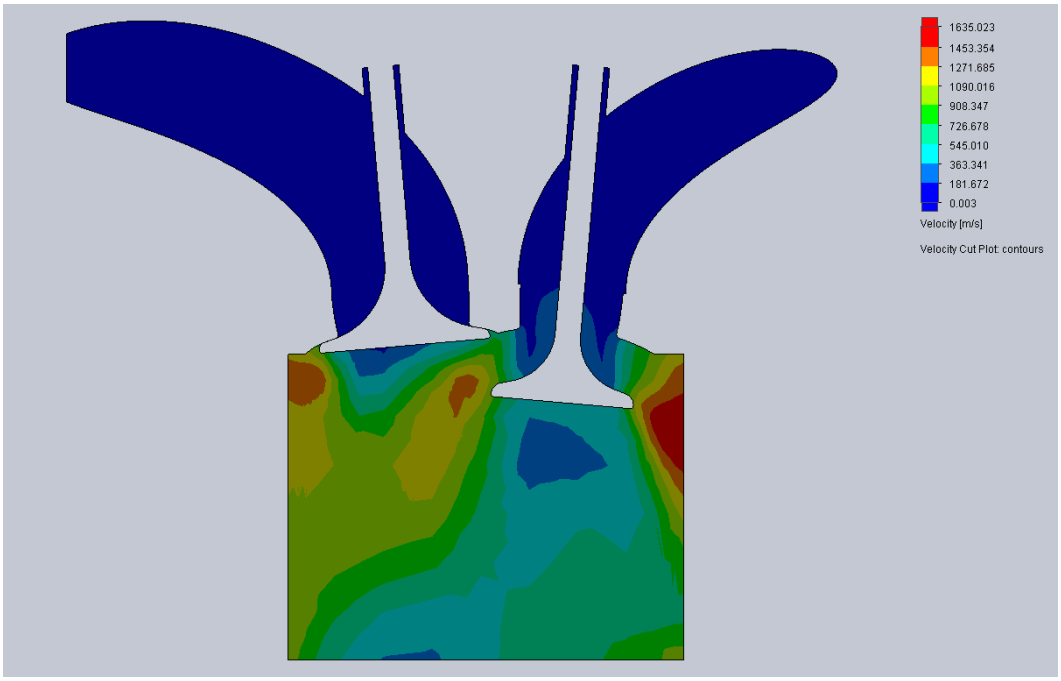

Maximum Exhaust Valve Opening – 620°

Appendix O: RVS Combustion Velocity Cut Plots

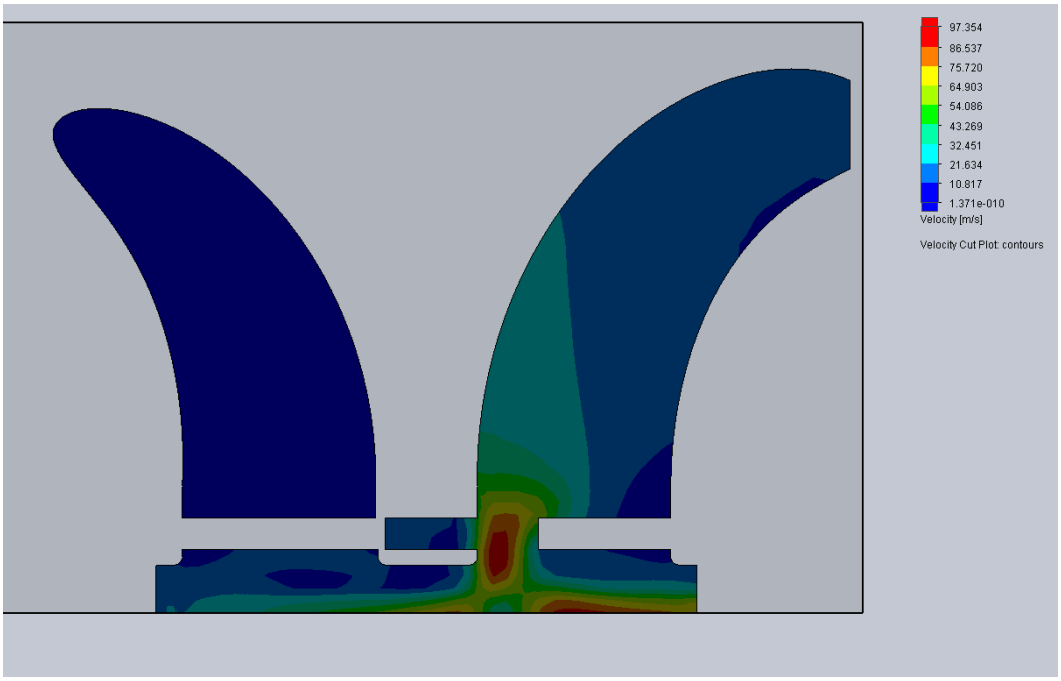

Intake Port Opens – 20°

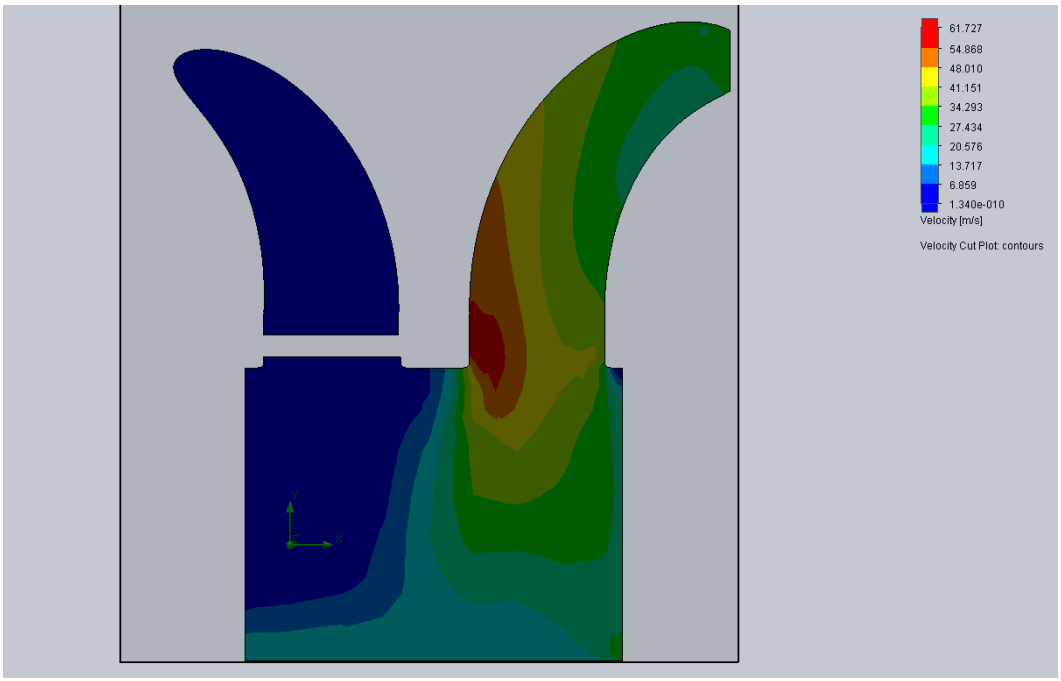

Maximum Intake Port Opening – 100°

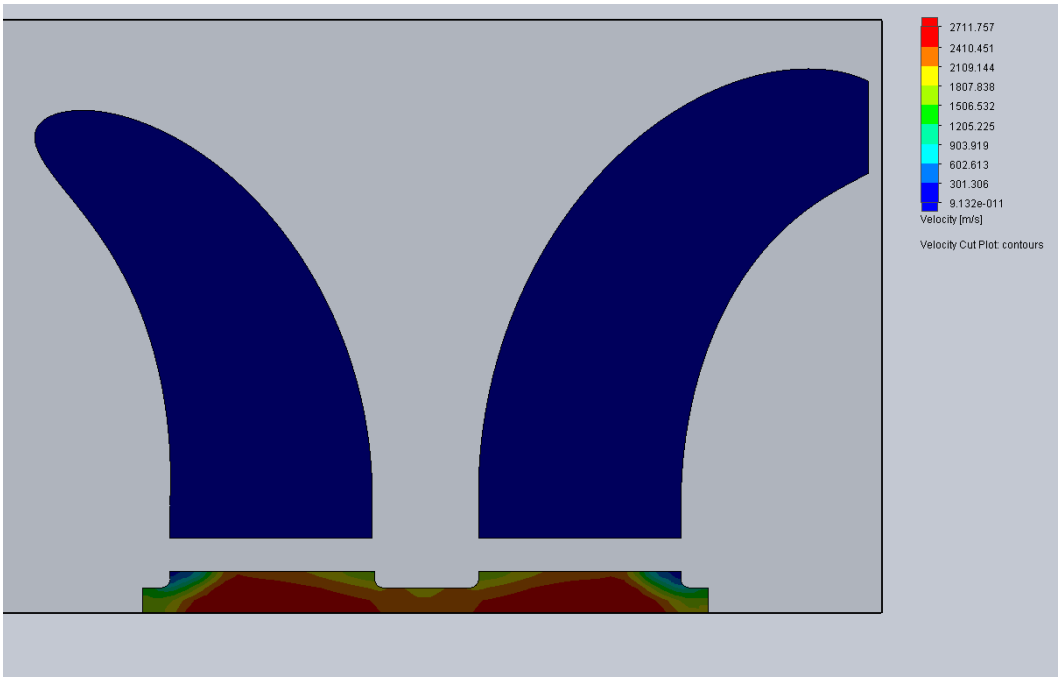

Combustion Begins – 360°

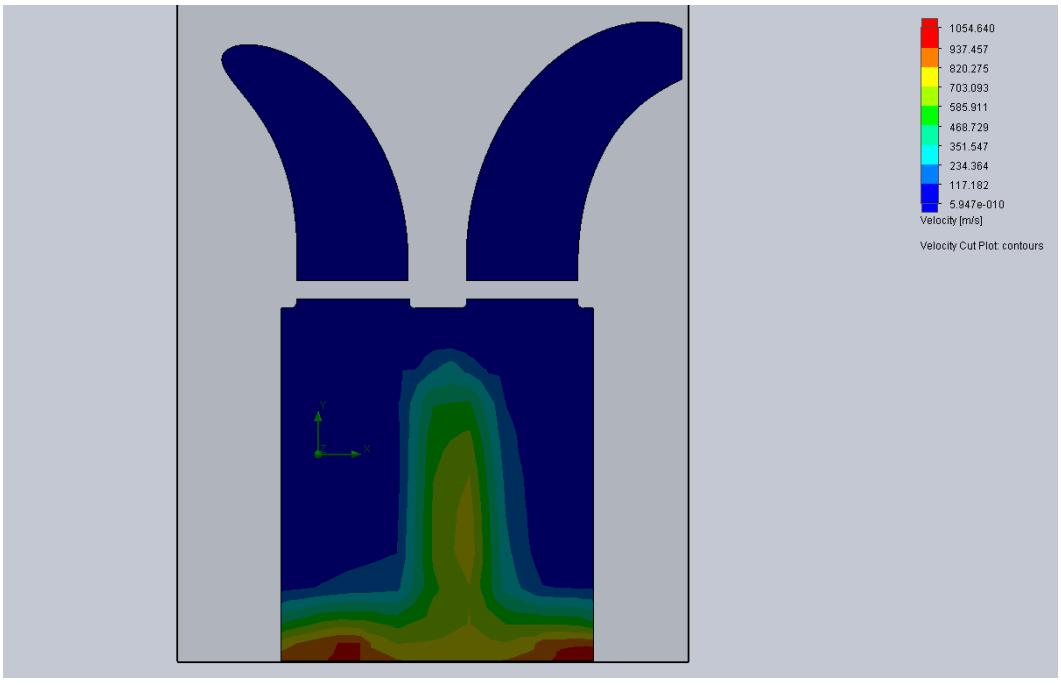

Combustion Concludes – 540°

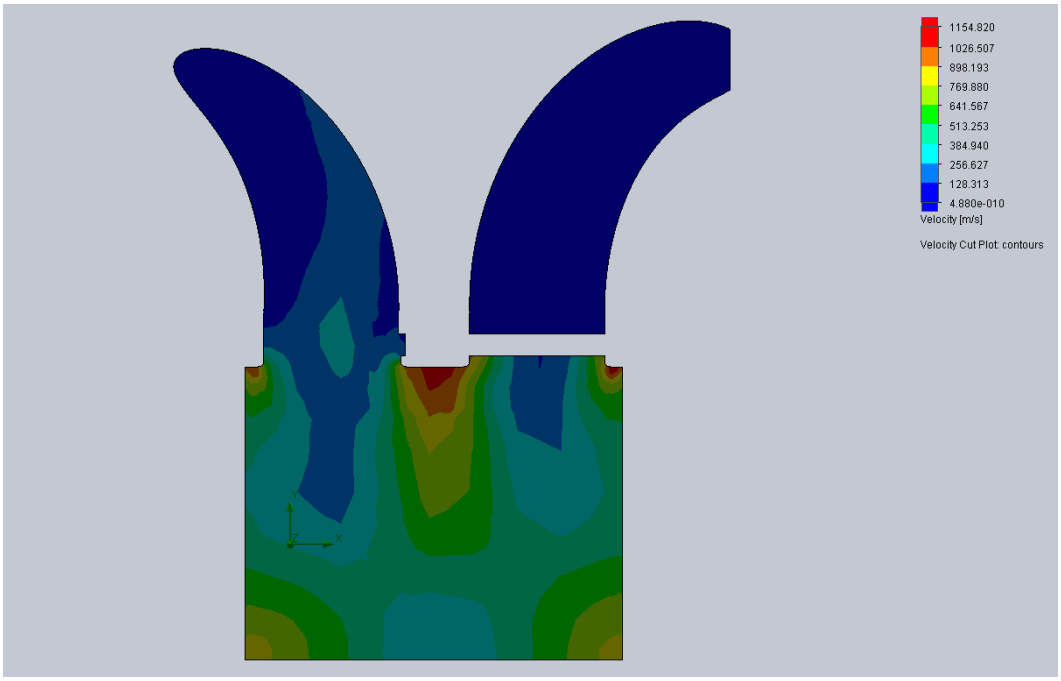

Maximum Exhaust Port Opening – 620°

Appendix P: Traditional Combustion Pressure Cut Plots

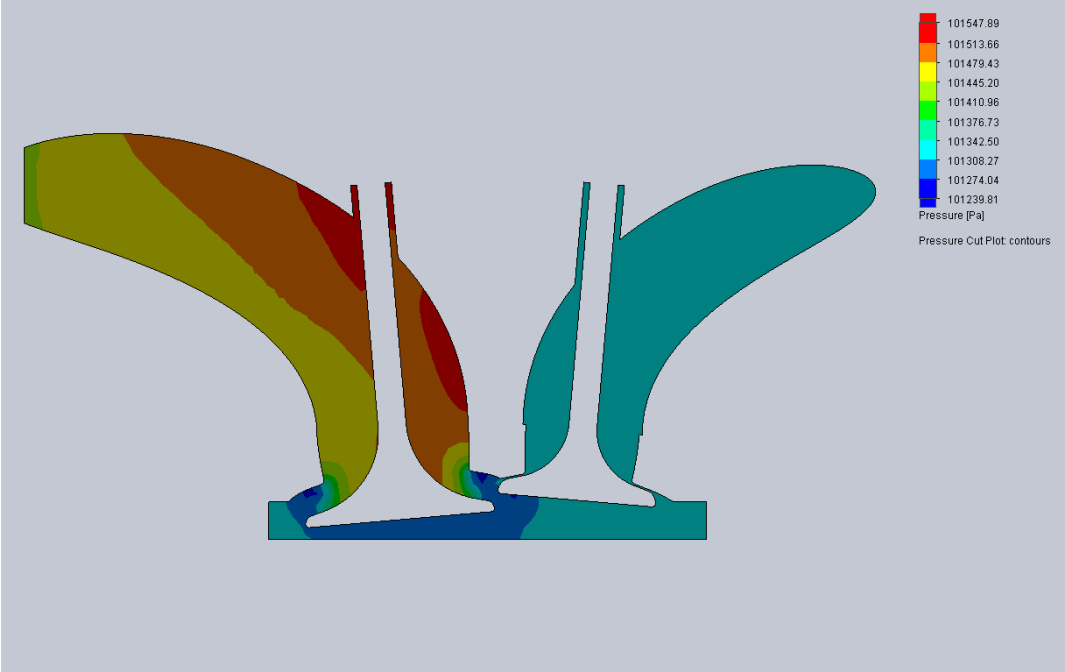

Intake Valve Opens – 20°

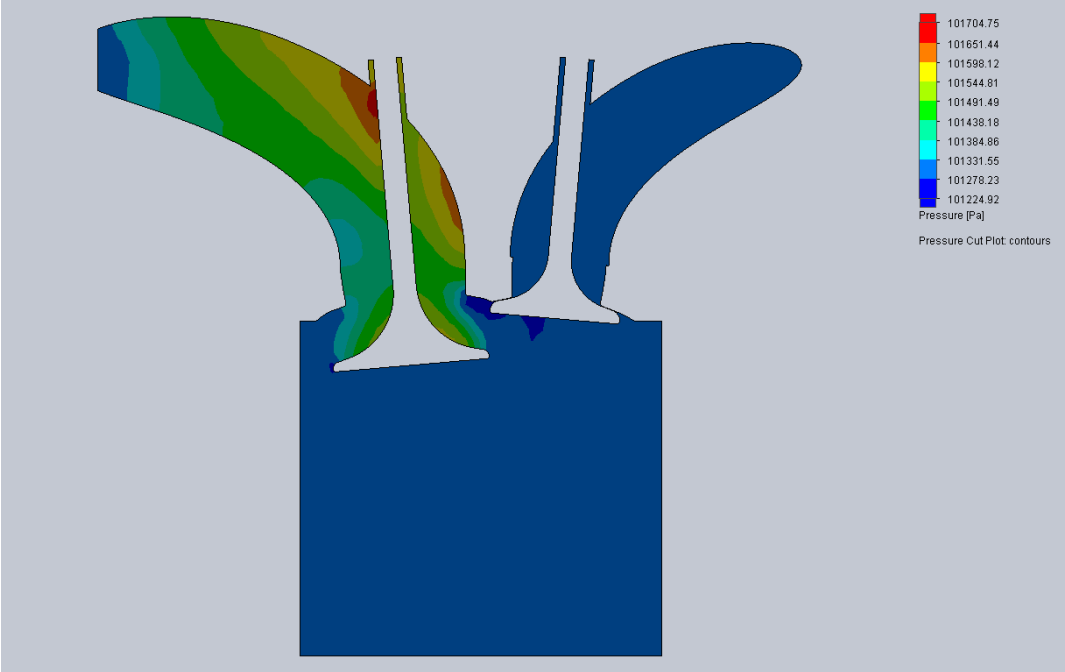

Maximum Intake Valve Opening – 120°

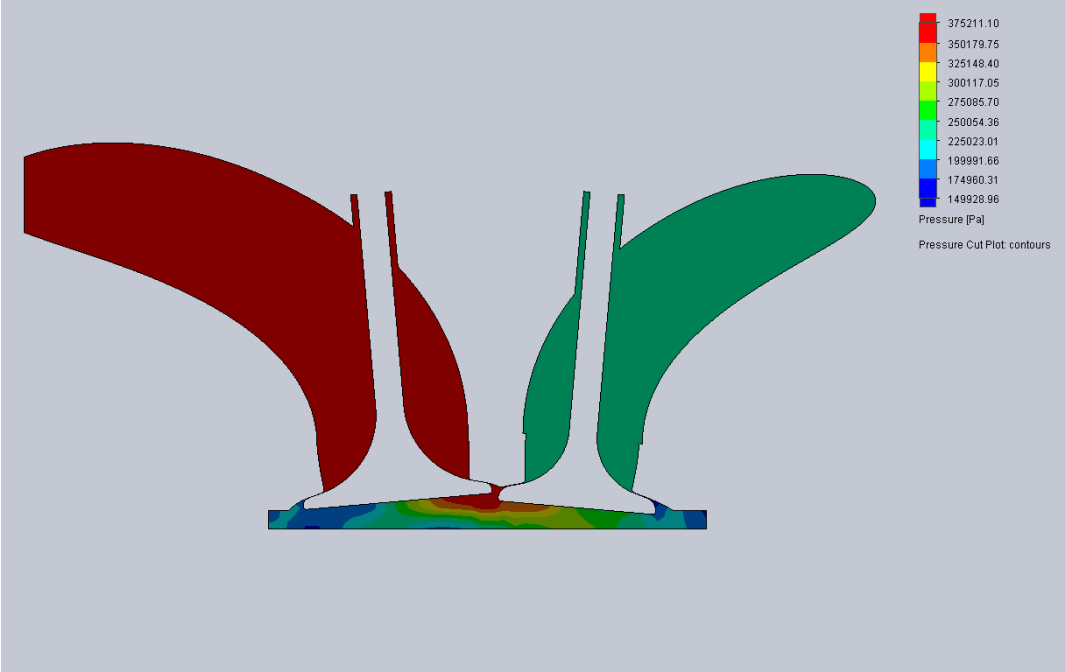

Combustion Begins – 360°

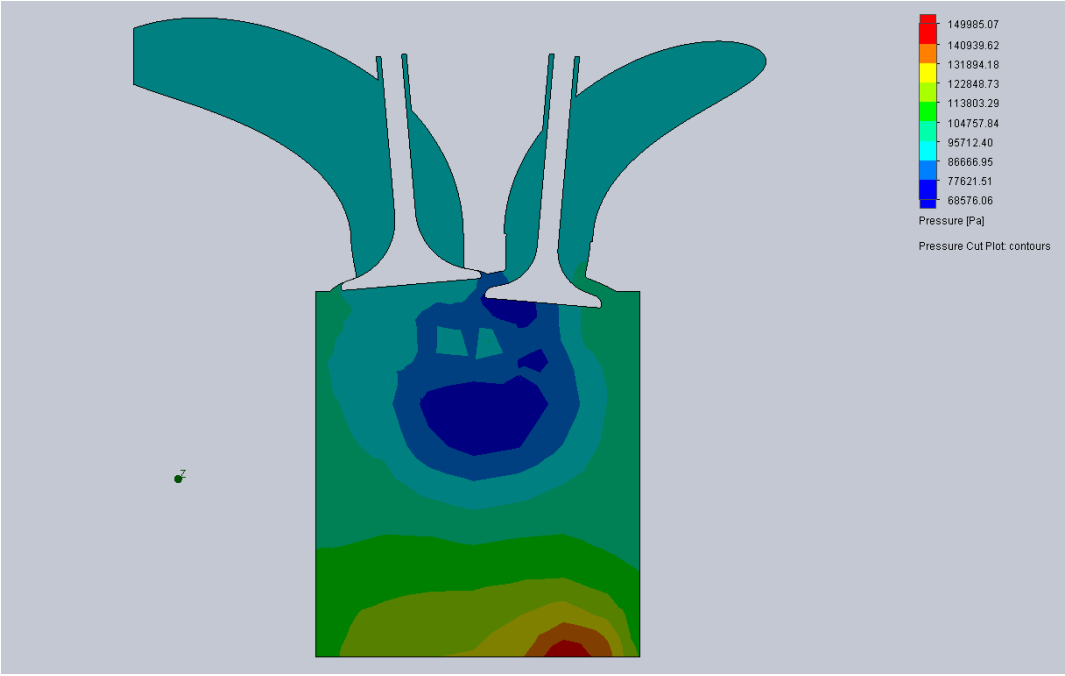

Combustion Concludes – 540°

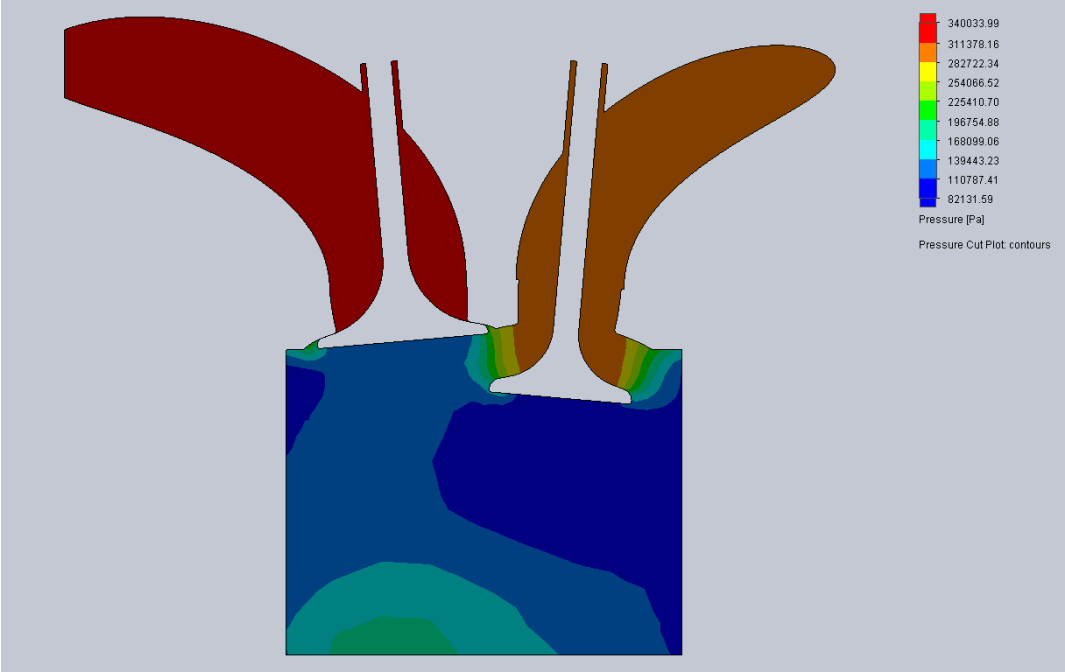

Maximum Exhaust Valve Opening – 620°

Appendix Q: RVS Combustion Pressure Cut Plots

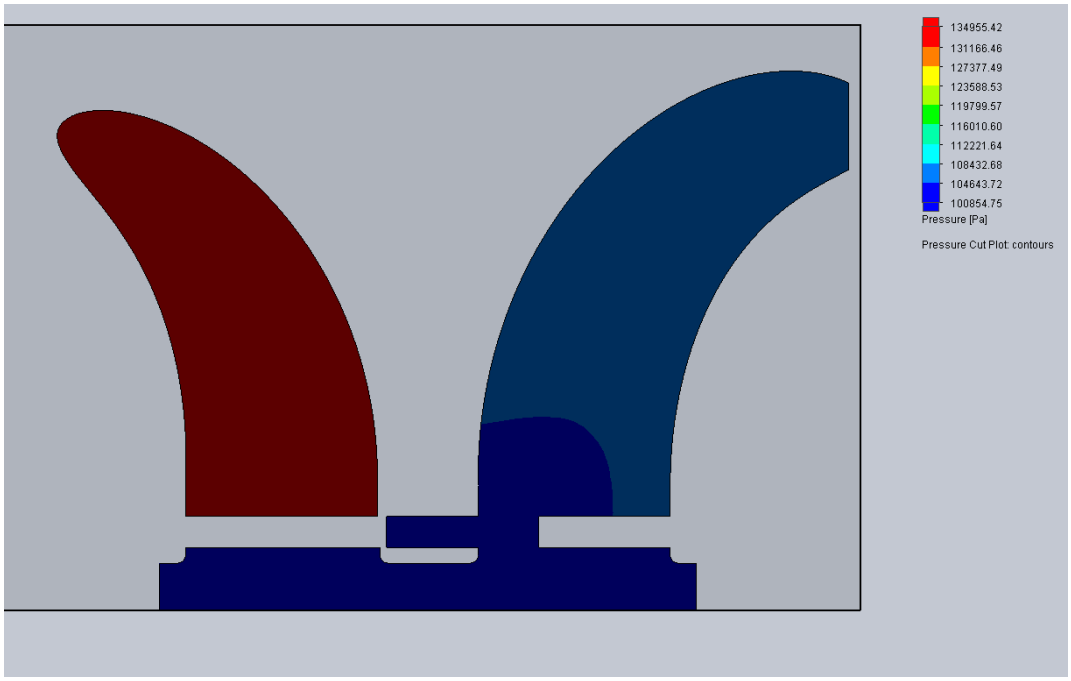

Intake Port Opens – 20°

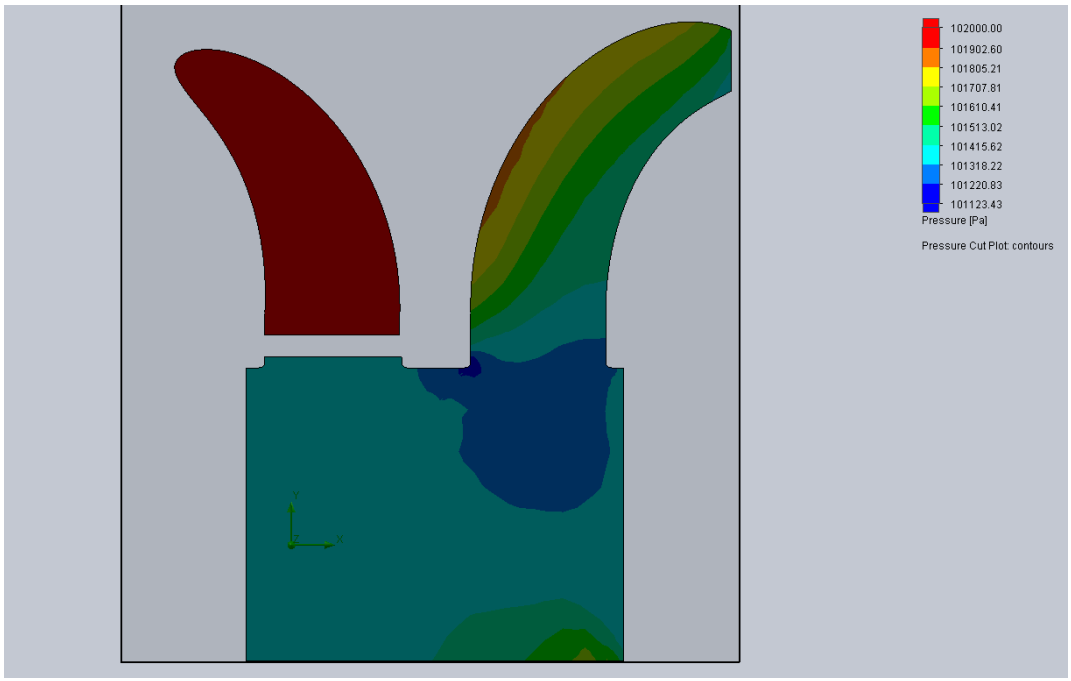

Maximum Intake Port Opening – 100°

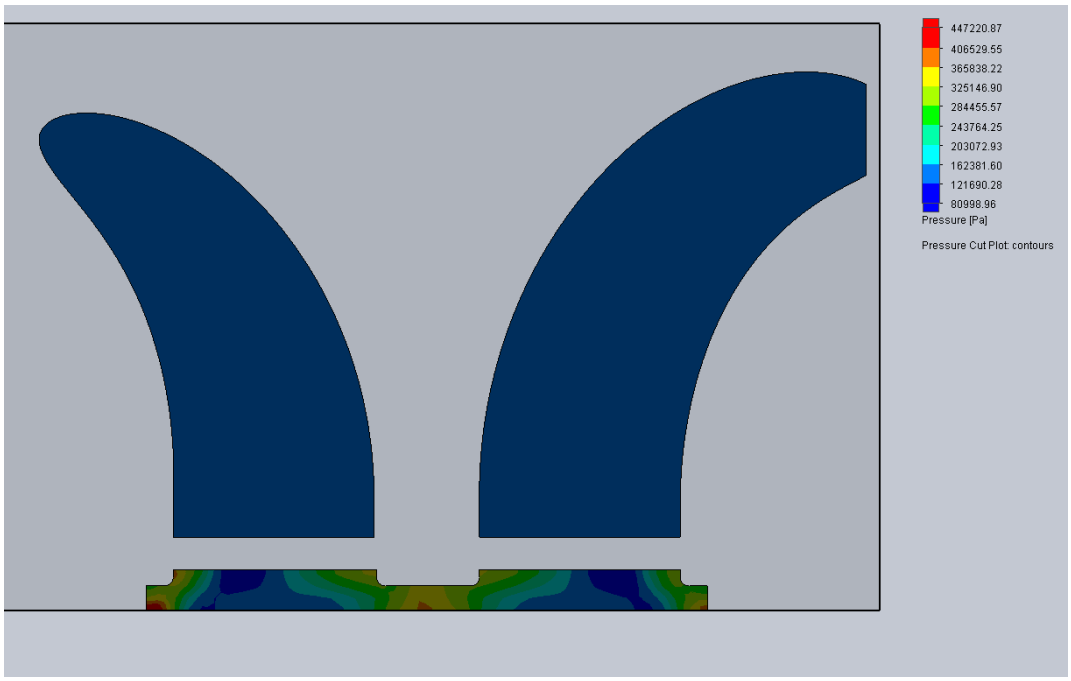

Combustion Begins – 360°

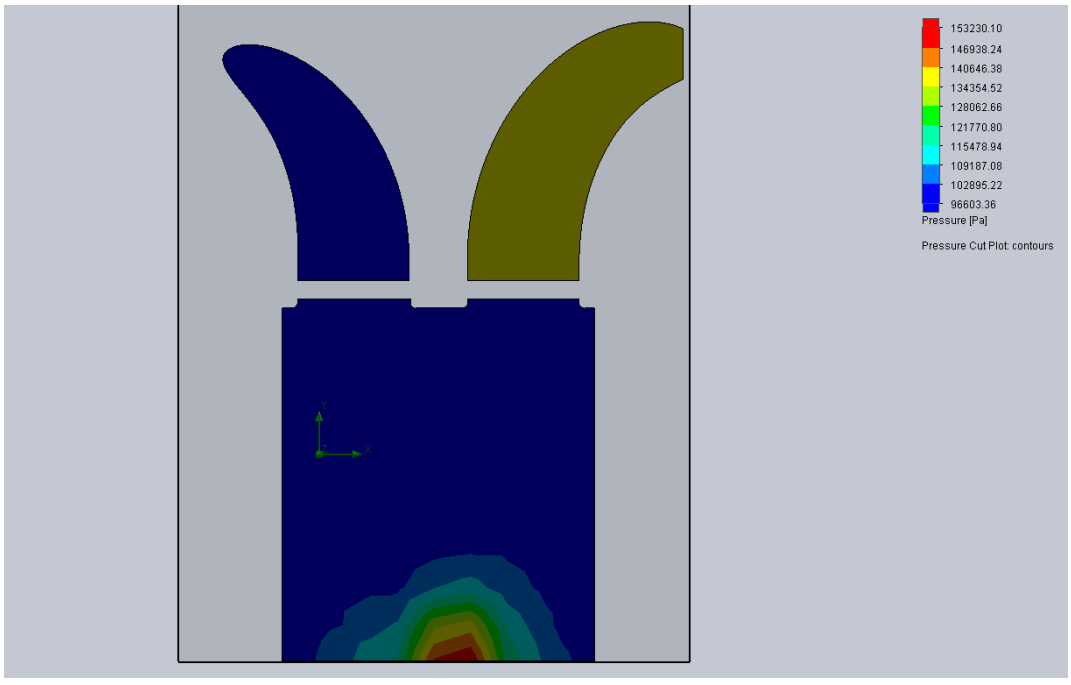

Combustion Concludes – 540°

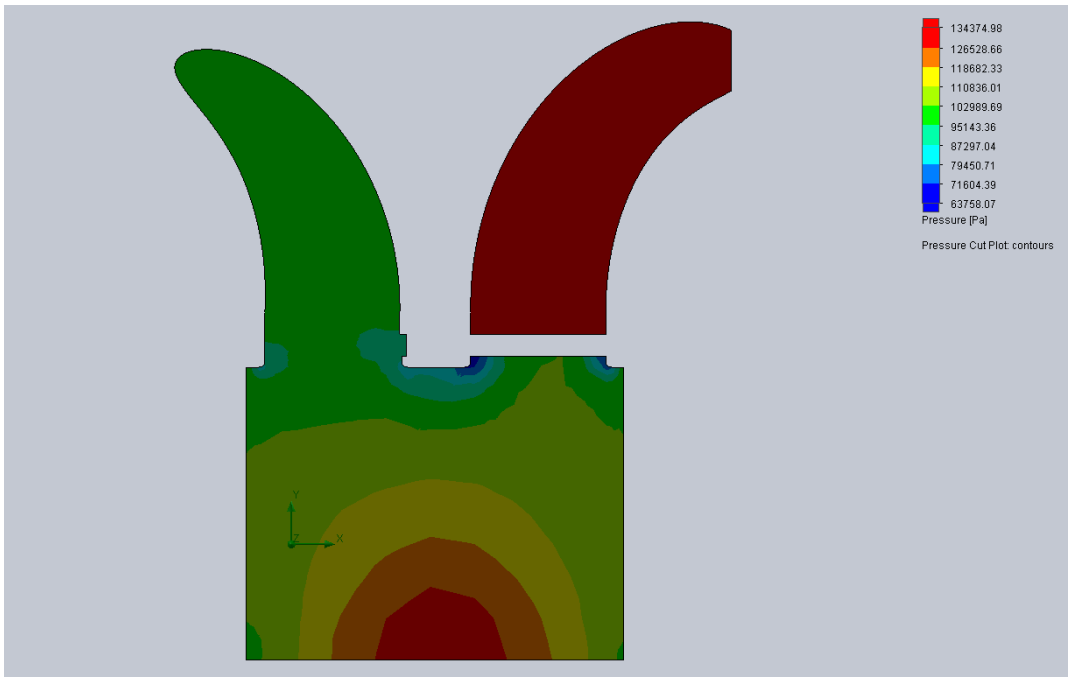

Maximum Exhaust Port Opening – 620°

Appendix R: Curvefit coefficients for k, μ, and C_p

Table B.3 Curvefit coefficients for fuel vapor thermal conductivity, viscosity, and specific heat[a]

$$\left.\begin{matrix} k(\text{W/m-K}) \\ \mu(\text{N-s/m}^2)\cdot 10^6 \\ c_p(\text{J/kg-K}) \end{matrix}\right\} = a_1 + a_2T + a_3T^2 + a_4T^3 + a_5T^4 + a_6T^5 + a_7T^6$$

Formula	Fuel	T-range (K)	Property	a_1	a_2	a_3	a_4	a_5	a_6	a_7
CH_4	Methane	100–1000	k	−1.34014990E−2	3.66307060E−4	−1.82248608E−6	5.93987998E−9	−9.14055050E−12	6.78968890E−15	−1.95048736E−18
		70–1000	μ	2.96826700E−1	3.71120100E−2	1.21829800E−5	−7.02426000E−8	7.54326900E−11	−2.72371660E−14	0
			c_p	See Table B.2						
C_3H_8	Propane	200–500	k	−1.07682209E−2	8.38590325E−5	4.22059864E−8	0	0	0	0
		270–600	μ	−3.54371100E−1	3.08009600E−2	−6.99723000E−6	0	0	0	0
			c_p	See Table B.2						
C_6H_{14}	*n*-Hexane	150–1000	k	1.28775700E−3	−2.00499443E−5	2.37858831E−7	−1.60944555E−10	7.71027290E−14	0	0
		270–900	μ	1.54541200E+0	1.15080900E−2	2.72216500E−5	−3.26900000E−8	1.24545900E−11	0	0
			c_p	See Table B.2						
C_7H_{16}	*n*-Heptane	250–1000	k	−4.60614700E−2	5.95652224E−4	−2.98893153E−6	8.44612876E−9	−1.22927E−11	9.0127E−15	−2.62961E−18
		270–580	μ	1.54009700E+0	1.09515700E−2	1.80066400E−5	−1.36379000E−8	0	0	0
		300–755	c_p	9.46260000E+1	5.86099700E+0	−1.98231320E−3	−6.88699300E−8	−1.93795260E−10	0	0
		755–1365	c_p	−7.40308000E+2	1.08935370E+1	1.26512400E−2	9.84376300E−6	−4.32282960E−9	7.86366500E−13	0
C_8H_{18}	*n*-Octane	250–500	k	−4.01391940E−3	3.38796092E−5	8.19291819E−8	0	0	0	0
		300–650	μ	8.32435400E−1	1.40045000E−2	8.79376500E−6	−6.84030000E−9	0	0	0
		275–755	c_p	2.14419800E+2	5.35690500E+0	−1.17497000E−3	−6.99115500E−7	0	0	0
		755–1365	c_p	2.43596860E+3	−4.46819470E+0	1.66843290E−2	−1.78856050E−5	8.64282020E−9	−1.61426500E−12	0
$C_{10}H_{22}$	*n*-Decane	250–500	k	−5.88274000E−3	3.72449646E−5	7.55109624E−8	0	0	0	0
			μ	Not available						
		300–700	c_p	2.40717800E+2	5.09965000E+0	−6.29026000E−4	−1.07155000E−6	0	0	0
		700–1365	c_p	−1.35345890E+4	9.14879000E+1	−2.20700000E−1	2.91406000E−4	−2.15307400E−7	8.38600000E−11	−1.34404000E−14
CH_3OH	Methanol	300–550	k	−2.02986750E−2	1.21910927E−4	−2.23748473E−8	0	0	0	0
		250–650	μ	1.19790000E+0	2.45028000E−2	1.86162740E−5	−1.30674820E−8	0	0	0
			c_p	See Table B.2						
C_2H_5OH	Ethanol	250–550	k	−2.46663000E−2	1.55892550E−4	−8.22954822E−8	0	0	0	0
		270–600	μ	−6.33595000E−2	3.20713470E−2	−6.25079576E−6	0	0	0	0
			c_p	See Table B.2						

[a]SOURCE: Andrews, J. R., and Biblarz, O., "Temperature Dependence of Gas Properties in Polynomial Form," Naval Postgraduate School, NPS67-81-001, January 1981.

Appendix S: Characteristics of Heptane

Table B.1 Selected properties of hydrocarbon fuels: enthalpy of formation,[a] Gibbs function of formation,[a] entropy,[a] and higher and lower heating values all at 298.15 K and 1 atm; boiling points[b] and latent heat of vaporization[c] at 1 atm; constant-pressure adiabatic flame temperature at 1 atm;[d] liquid density[e]

Formula	Fuel	MW (kg/kmol)	$\bar{h}_f^o$ (kJ/kmol)	$\bar{g}_f^o$ (kJ/kmol)	$\bar{s}^o$ (kJ/kmol-K)	HHV† (kJ/kg)	LHV† (kJ/kg)	Boiling pt. (°C)	h_{fg} (kJ/kg)	$T_{ad}^{\ddagger}$ (K)	ρ_{liq}^{*} (kg/m³)
CH_4	Methane	16.043	−74,831	−50,794	186.188	55,528	50,016	−164	509	2226	300
C_2H_2	Acetylene	26.038	226,748	209,200	200.819	49,923	48,225	−84	—	2539	—
C_2H_4	Ethene	28.054	52,283	68,124	219.827	50,313	47,161	−103.7	—	2369	—
C_2H_6	Ethane	30.069	−84,667	−32,886	229.492	51,901	47,489	−88.6	488	2259	370
C_3H_6	Propene	42.080	20,414	62,718	266.939	48,936	45,784	−47.4	437	2334	514
C_3H_8	Propane	44.096	−103,847	−23,489	269.910	50,368	46,357	−42.1	425	2267	500
C_4H_8	1-Butene	56.107	1,172	72,036	307.440	48,471	45,319	−63	391	2322	595
C_4H_{10}	*n*-Butane	58.123	−124,733	−15,707	310.034	49,546	45,742	−0.5	386	2270	579
C_5H_{10}	1-Pentene	70.134	−20,920	78,605	347.607	48,152	45,000	30	358	2314	641
C_5H_{12}	*n*-Pentane	72.150	−146,440	−8,201	348.402	49,032	45,355	36.1	358	2272	626
C_6H_6	Benzene	78.113	82,927	129,658	269.199	42,277	40,579	80.1	393	2342	879
C_6H_{12}	1-Hexene	84.161	−41,673	87,027	385.974	47,955	44,803	63.4	335	2308	673
C_6H_{14}	*n*-Hexane	86.177	−167,193	209	386.811	48,696	45,105	69	335	2273	659
C_7H_{14}	1-Heptene	98.188	−62,132	95,563	424.383	47,817	44,665	93.6	—	2305	—
C_7H_{16}	*n*-Heptane	100.203	−187,820	8,745	425.262	48,456	44,926	98.4	316	2274	684
C_8H_{16}	1-Octene	112.214	−82,927	104,140	462.792	47,712	44,560	121.3	—	2302	—
C_8H_{18}	*n*-Octane	114.230	−208,447	17,322	463.671	48,275	44,791	125.7	300	2275	703
C_9H_{18}	1-Nonene	126.241	−103,512	112,717	501.243	47,631	44,478	—	—	2300	—
C_9H_{20}	*n*-Nonane	128.257	−229,032	25,857	502.080	48,134	44,686	150.8	295	2276	718
$C_{10}H_{20}$	1-Decene	140.268	−124,139	121,294	539.652	47,565	44,413	170.6	—	2298	—
$C_{10}H_{22}$	*n*-Decane	142.284	−249,659	34,434	540.531	48,020	44,602	174.1	277	2277	730
$C_{11}H_{22}$	1-Undecene	154.295	−144,766	129,830	578.061	47,512	44,360	—	—	2296	—
$C_{11}H_{24}$	*n*-Undecane	156.311	−270,286	43,012	578.940	47,926	44,532	195.9	265	2277	740
$C_{12}H_{24}$	1-Dodecene	168.322	−165,352	138,407	616.471	47,468	44,316	213.4	—	2295	—
$C_{12}H_{26}$	*n*-Dodecane	170.337	−292,162	—	—	47,841	44,467	216.3	256	2277	749

†Based on gaseous fuel.

‡For stoichiometric combustion with air (79 percent N_2, 21 percent O_2).

*For liquids at 20°C or for gases at the boiling point of the liquefied gas.

SOURCES:

[a]Rossini, F. D., *et al., Selected Values of Physical and Thermodynamic Properties of Hydrocarbons and Related Compounds,* Carnegie Press, Pittsburgh, PA, 1953.

[b]Weast, R. C. (ed.), *Handbook of Chemistry and Physics,* 56th Ed., CRC Press, Cleveland, OH, 1976.

[c]Obert, E. F., *Internal Combustion Engines and Air Pollution,* Harper & Row, New York, 1973.

[d]Calculated using HPFLAME (Appendix F).

Appendix T: Characteristics of O_2

Table A.11 Oxygen (O_2), MW = 31.999, enthalpy of formation @ 298 K (kJ/kmol) = 0

T(K)	$\bar{c}_p$ (kJ/kmol-K)	$(\bar{h}^o(T)-\bar{h}_f^o(298))$ (kJ/kmol)	$\bar{h}_f^o(T)$ (kJ/kmol)	$\bar{s}^o(T)$ (kJ/kmol-K)	$\bar{g}_f^o(T)$ (kJ/kmol)
200	28.473	−2,836	0	193.518	0
298	29.315	0	0	205.043	0
300	29.331	54	0	205.224	0
400	30.210	3,031	0	213.782	0
500	31.114	6,097	0	220.620	0
600	32.030	9,254	0	226.374	0
700	32.927	12,503	0	231.379	0
800	33.757	15,838	0	235.831	0
900	34.454	19,250	0	239.849	0
1000	34.936	22,721	0	243.507	0
1100	35.270	26,232	0	246.852	0
1200	35.593	29,775	0	249.935	0
1300	35.903	33,350	0	252.796	0
1400	36.202	36,955	0	255.468	0
1500	36.490	40,590	0	257.976	0
1600	36.768	44,253	0	260.339	0
1700	37.036	47,943	0	262.577	0
1800	37.296	51,660	0	264.701	0
1900	37.546	55,402	0	266.724	0
2000	37.788	59,169	0	268.656	0
2100	38.023	62,959	0	270.506	0
2200	38.250	66,773	0	272.280	0
2300	38.470	70,609	0	273.985	0
2400	38.684	74,467	0	275.627	0
2500	38.891	78,346	0	277.210	0
2600	39.093	82,245	0	278.739	0
2700	39.289	86,164	0	280.218	0
2800	39.480	90,103	0	281.651	0
2900	39.665	94,060	0	283.039	0
3000	39.846	98,036	0	284.387	0
3100	40.023	102,029	0	285.697	0
3200	40.195	106,040	0	286.970	0
3300	40.362	110,068	0	288.209	0
3400	40.526	114,112	0	289.417	0
3500	40.686	118,173	0	290.594	0
3600	40.842	122,249	0	291.742	0
3700	40.994	126,341	0	292.863	0
3800	41.143	130,448	0	293.959	0
3900	41.287	134,570	0	295.029	0
4000	41.429	138,705	0	296.076	0
4100	41.566	142,855	0	297.101	0
4200	41.700	147,019	0	298.104	0
4300	41.830	151,195	0	299.087	0
4400	41.957	155,384	0	300.050	0
4500	42.079	159,586	0	300.994	0
4600	42.197	163,800	0	301.921	0
4700	42.312	168,026	0	302.829	0
4800	42.421	172,262	0	303.721	0
4900	42.527	176,510	0	304.597	0
5000	42.627	180,767	0	305.457	0

Appendix U: Characteristics of N_2

Table A.7 Nitrogen (N_2), $MW = 28.013$, enthalpy of formation @ 298 K (kJ/kmol) = 0

T(K)	$\bar{c}_p$ (kJ/kmol-K)	$(\bar{h}^o(T) - \bar{h}^o_f(298))$ (kJ/kmol)	$\bar{h}^o_f(T)$ (kJ/kmol)	$\bar{s}^o(T)$ (kJ/kmol-K)	$\bar{g}^o_f(T)$ (kJ/kmol)
200	28.793	−2,841	0	179.959	0
298	29.071	0	0	191.511	0
300	29.075	54	0	191.691	0
400	29.319	2,973	0	200.088	0
500	29.636	5,920	0	206.662	0
600	30.086	8,905	0	212.103	0
700	30.684	11,942	0	216.784	0
800	31.394	15,046	0	220.927	0
900	32.131	18,222	0	224.667	0
1000	32.762	21,468	0	228.087	0
1100	33.258	24,770	0	231.233	0
1200	33.707	28,118	0	234.146	0
1300	34.113	31,510	0	236.861	0
1400	34.477	34,939	0	239,402	0
1500	34.805	38,404	0	241.792	0
1600	35.099	41,899	0	244.048	0
1700	35.361	45,423	0	246.184	0
1800	35.595	48,971	0	248.212	0
1900	35.803	52,541	0	250.142	0
2000	35.988	56,130	0	251.983	0
2100	36.152	59,738	0	253.743	0
2200	36.298	63,360	0	255.429	0
2300	36.428	66,997	0	257.045	0
2400	36.543	70,645	0	258.598	0
2500	36.645	74,305	0	260.092	0
2600	36.737	77,974	0	261.531	0
2700	36.820	81,652	0	262.919	0
2800	36.895	85,338	0	264.259	0
2900	36.964	89,031	0	265.555	0
3000	37.028	92,730	0	266.810	0
3100	37.088	96,436	0	268.025	0
3200	37.144	100,148	0	269.203	0
3300	37.198	103,865	0	270.347	0
3400	37.251	107,587	0	271.458	0
3500	37.302	111,315	0	272.539	0
3600	37.352	115,048	0	273.590	0
3700	37.402	118,786	0	274.614	0
3800	37.452	122,528	0	275.612	0
3900	37.501	126,276	0	276.586	0
4000	37.549	130,028	0	277.536	0
4100	37.597	133,786	0	278.464	0
4200	37.643	137,548	0	279.370	0
4300	37.688	141,314	0	280.257	0
4400	37.730	145,085	0	281.123	0
4500	37.768	148,860	0	281.972	0
4600	37.803	152,639	0	282.802	0
4700	37.832	156,420	0	283.616	0
4800	37.854	160,205	0	284.412	0
4900	37.868	163,991	0	285.193	0
5000	37.873	167,778	0	285.958	0

Appendix V: Characteristics of H_2O

Table A.6 Water (H_2O), MW = 18.016, enthalpy of formation @ 298 K (kJ/kmol) = −241,845, enthalpy of vaporization (kJ/kmol) = 44,010

T (K)	$\bar{c}_p$ (kJ/kmol-K)	$(\bar{h}^o(T) - \bar{h}_f^o(298))$ (kJ/kmol)	$\bar{h}_f^o(T)$ (kJ/kmol)	$\bar{s}^o(T)$ (kJ/kmol-K)	$\bar{g}_f^o(T)$ (kJ/kmol)
200	32.255	−3,227	−240,838	175.602	−232,779
298	33.448	0	−241,845	188.715	−228,608
300	33.468	62	−241,865	188.922	−228,526
400	34.437	3,458	−242,858	198.686	−223,929
500	35.337	6,947	−243,822	206.467	−219,085
600	36.288	10,528	−244,753	212.992	−214,049
700	37.364	14,209	−245,638	218.665	−208,861
800	38.587	18,005	−246,461	223.733	−203,550
900	39.930	21,930	−247,209	228.354	−198,141
1000	41.315	25,993	−247,879	232.633	−192,652
1100	42.638	30,191	−248,475	236.634	−187,100
1200	43.874	34,518	−249,005	240.397	−181,497
1300	45.027	38,963	−249,477	243.955	−175,852
1400	46.102	43,520	−249,895	247.332	−170,172
1500	47.103	48,181	−250,267	250.547	−164,464
1600	48.035	52,939	−250,597	253.617	−158,733
1700	48.901	57,786	−250,890	256.556	−152,983
1800	49.705	62,717	−251,151	259.374	−147,216
1900	50.451	67,725	−251,384	262.081	−141,435
2000	51.143	72,805	−251,594	264.687	−135,643
2100	51.784	77,952	−251,783	267.198	−129,841
2200	52.378	83,160	−251,955	269.621	−124,030
2300	52.927	88,426	−252,113	271.961	−118,211
2400	53.435	93,744	−252,261	274.225	−112,386
2500	53.905	99,112	−252,399	276.416	−106,555
2600	54.340	104,524	−252,532	278.539	−100,719
2700	54.742	109,979	−252,659	280.597	−94,878
2800	55.115	115,472	−252,785	282.595	−89,031
2900	55.459	121,001	−252,909	284.535	−83,181
3000	55.779	126,563	−253,034	286.420	−77,326
3100	56.076	132,156	−253,161	288.254	−71,467
3200	56.353	137,777	−253,290	290.039	−65,604
3300	56.610	143,426	−253,423	291.777	−59,737
3400	56.851	149,099	−253,561	293.471	−53,865
3500	57.076	154,795	−253,704	295.122	−47,990
3600	57.288	160,514	−253,852	296.733	−42,110
3700	57.488	166,252	−254,007	298.305	−36,226
3800	57.676	172,011	−254,169	299.841	−30,338
3900	57.856	177,787	−254,338	301.341	−24,446
4000	58.026	183,582	−254,515	302.808	−18,549
4100	58.190	189,392	−254,699	304.243	−12,648
4200	58.346	195,219	−254,892	305.647	−6,742
4300	58.496	201,061	−255,093	307.022	−833
4400	58.641	206,918	−255,303	308.368	5,085
4500	58.781	212,790	−255,522	309.688	11,005
4600	58.916	218,674	−255,751	310.981	16,930
4700	59.047	224,573	−255,990	312.250	22,861
4800	59.173	230,484	−256,239	313.494	28,796
4900	59.295	236,407	−256,501	314.716	34,737
5000	59.412	242,343	−256,774	315.915	40,684

Appendix W: Characteristics of CO_2

Table A.2 Carbon dioxide (CO_2), $MW = 44.011$, enthalpy of formation @ 298 K (kJ/kmol) = –393,546

T(K)	$\bar{c}_p$ (kJ/kmol-K)	$(\bar{h}^o(T) - \bar{h}^o_f(298))$ (kJ/kmol)	$\bar{h}^o_f(T)$ (kJ/kmol)	$\bar{s}^o(T)$ (kJ/kmol-K)	$\bar{g}^o_f(T)$ (kJ/kmol)
200	32.387	–3,423	–393,483	199.876	–394,126
298	37.198	0	–393,546	213.736	–394,428
300	37.280	69	–393,547	213.966	–394,433
400	41.276	4,003	–393,617	225.257	–394,718
500	44.569	8,301	–393,712	234.833	–394,983
600	47.313	12,899	–393,844	243.209	–395,226
700	49.617	17,749	–394,013	250.680	–395,443
800	51.550	22,810	–394,213	257.436	–395,635
900	53.136	28,047	–394,433	263.603	–395,799
1000	54.360	33,425	–394,659	269.268	–395,939
1100	55.333	38,911	–394,875	274.495	–396,056
1200	56.205	44,488	–395,083	279.348	–396,155
1300	56.984	50,149	–395,287	283.878	–396,236
1400	57.677	55,882	–395,488	288.127	–396,300
1500	58.292	61,681	–395,691	292.128	–396,352
1600	58.836	67,538	–395,897	295.908	–396,389
1700	59.316	73,446	–396,110	299.489	–396,414
1800	59.738	79,399	–396,332	302.892	–396,425
1900	60.108	85,392	–396,564	306.132	–396,424
2000	60.433	91,420	–396,808	309.223	–396,410
2100	60.717	97,477	–397,065	312.179	–396,384
2200	60.966	103,562	–397,338	315.009	–396,346
2300	61.185	109,670	–397,626	317.724	–396,294
2400	61.378	115,798	–397,931	320.333	–396,230
2500	61.548	121,944	–398,253	322.842	–396,152
2600	61.701	128,107	–398,594	325.259	–396,061
2700	61.839	134,284	–398,952	327.590	–395,957
2800	61.965	140,474	–399,329	329.841	–395,840
2900	62.083	146,677	–399,725	332.018	–395,709
3000	62.194	152,891	–400,140	334.124	–395,562
3100	62.301	159,116	–400,573	336.165	–395,401
3200	62.406	165,351	–401,025	338.145	–395,226
3300	62.510	171,597	–401,495	340.067	–395,040
3400	62.614	177,853	–401,983	341.935	–394,839
3500	62.718	184,120	–402,489	343.751	–394,627
3600	62.825	190,397	–403,013	345.519	–394,398
3700	62.932	196,685	–403,553	347.242	–394,160
3800	63.041	202,983	–404,110	348.922	–393,909
3900	63.151	209,293	–404,684	350.561	–393,652
4000	63.261	215,613	–405,273	353.161	–393,388
4100	63.369	221,945	–405,878	353.725	–393,114
4200	63.474	228,287	–406,499	355.253	–392,833
4300	63.575	234,640	–407,135	356.748	–392,546
4400	63.669	241,002	–407,785	358.210	–392,251
4500	63.753	247,373	–408,451	359.642	–391,950
4600	63.825	253,752	–409,132	361.044	–391,643
4700	63.881	260,138	–409,828	362.417	–391,330
4800	63.918	266,528	–410,539	363.763	–391,011
4900	63.932	272,920	–411,267	365.081	–390,686
5000	63.919	279,313	–412,010	366.372	–390,355